Visualization and Characterization of Ribonucleoproteins in Plants

DISSERTATION ZUR ERLANGUNG DES DOKTORGRADES
DER NATURWISSENSCHAFTEN (DR. RER. NAT.)
DER FAKULTÄT FÜR BIOLOGIE UND VORKLINISCHE MEDIZIN
DER UNIVERSITÄT REGENSBURG

Vorgelegt von

Johannes Klaus Schönberger

aus

Roding

im Oktober 2012

Das Promotionsgesuch wurde eingereicht am:
22.10.2012

Die Arbeit wurde angeleitet von:
Dr. Ulrich Hammes

Unterschrift:
Johannes Schönberger

Table of Contents

1. Introduction

1.1. Polarity and differential inheritance

When evolution drove cells from unicellular towards multicellular organisms it had to cope with a very challenging problem: How can two distinct cell types derive from one common mother cell? The answer to that was asymmetric cell division. This can be achieved at the molecular level, with the differential inheritance of specific determinants or even cell organelles. Furthermore the derived daughter cells can take on different fates, resulting in the formation of morphologically distinct cell types and tissues. Since those early beginnings of polarity, nature has come up with a lot of different ways in establishing asymmetric cell division.

But though higher developed organisms have almost perfected dealing with polarity, even single cells, which on the first glance look symmetric, do in fact have established polarity at the molecular level.

In *E. coli*, for example, division takes place by longitudinal growth and separation by a newly forming septum. This means that the daughter cell inherits an old pole and a newly created pole. Over generations this "old" pole is always inherited by only one cell. Recent studies showed, that the cell, which inherits this old one ages over time, which manifests itself by reduced growth rate and offspring production and interestingly a higher chance of death (Stewart *et al.,* 2005).

But what is the purpose or reason of this aging? Recent studies found out, that protein aggregates and oxidized proteins are accumulating in the "older" daughter cell, giving the other offspring a rejuvenated start (Lindner *et al.,* 2008).

Given this knowledge, the very philosophical question arises, what was first: Was aging of cells a consequence of polarly dividing cells? Or was the differential inheritance of cellular components the answer on how to deal with fitness problems over the timespan? While recent studies seem to favor the latter (Ackermann *et al.,* 2007), this questions remains to be solved.

In unicellular organisms, the main drive for the establishment of differential cell division seems to be the circumvention of aging cells, which would lead to extinction at some point.

In multicellular organisms on the other hand, the maintenance of stem cells as well as the generation of different tissues are the main reasons for polarity.

A very well studied example for stem cell maintenance is the germ line of *Drosophila melanogaster*. Depending on the position in their distinct niche, those cells adopt different

fates. The stem cells stick to somatic hub cells and divide in a perpendicular orientation to those, generating one daughter that remains in touch with them and one daughter that loses direct contact. The latter start to differentiate whilst those, which are still in touch with the hub cells, keep their stem cell character (Yamashita *et al.*, 2008).

But much more important considering the aim of this work is the differentiation of different cell types.

All higher organisms start with one fertilized egg cell and end up with producing hundreds of different cell types forming all kinds of tissues. This wouldn't be possible without unequal cell division, resulting in two distinct daughter cells.

The question remains, how the different fates are established. They can be achieved by the differential segregation of internal factors. Another possibility is the effect of external cues that are secreted by an adjacent cell. Those signal molecules drive one cell to adopt another fate than its neighboring cells. The latter case is an important developmental process in the maintenance of stem cell niches, where the destiny of a cell is often decided by its position within the surrounding tissue.

Figure 1-1 depicts those two main mechanisms.

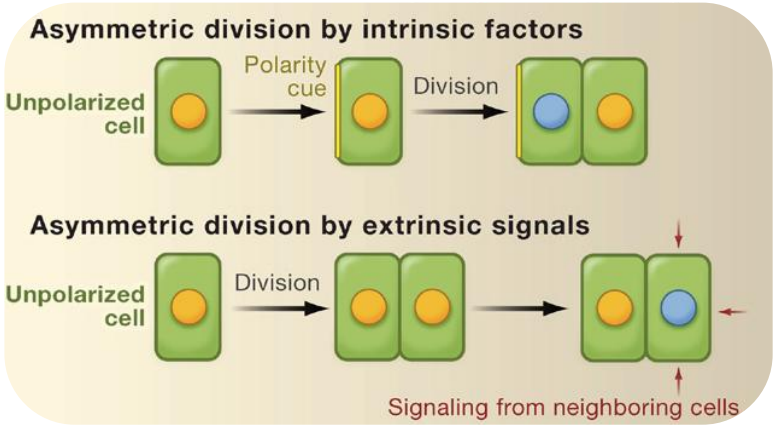

Figure 1-1 Schematic illustration of the two main principles, which determine cell fates.

An initially unpolarized cell can adopt two different fates upon cell division by the expression or differential segregation of an intrinsic cue. Furthermore, two primarily equal daughter cells can opt for different developmental paths by an extrinsic cue, which decides the fate of a cell depending on its position within the surrounding tissue. Picture taken from (Menke *et al.*, 2009).

Both mechanisms are present and described in plants.

An example for the first mechanism is the stomata formation in the leaf epidermis of Arabidopsis, which starts with the division of the meristem mother cell, resulting in the meristemoid and the stomatal lineage ground cell (SLGC). The first one undergoes several

rounds of division before differentiating into the guard cells of the stomata, whilst the latter one differentiates into a pavement cell. Interestingly, the protein BASL (**B**reaking of **A**symmetry in the **S**tomatal **L**ineage) is already polarly localized to the periphery of the meristem mother cell. The daughter cell, which inherits this peripheral BASL, will become the SLGC while the meristemoid only contains nuclear localized BASL, which triggers further cell divisions. The importance of this internal factor becomes obvious in loss-of-function mutants, where both daughter cells of the mother cell immediately differentiate into guard cells (Dong *et al.*, 2009).

The maintenance of the stem cell niche of the shoot apical meristem (SAM) is a well-described example of the effect on an extrinsic factor on cell fate. WUSCHEL (WUS) is key regulator for stem cell maintenance in the SAM of Arabidopsis (Laux *et al.,* 1996). Cells that are embedded within the niche retain their stem cell character, whereas cells that lose contact to that niche undergo differentiation. Since the SAM is a small region, the expression of WUS obviously has to be tightly controlled. The small, secreted peptide Clavata 3, which inhibits WUS via a downstream cascade, is a key factor in the regulatory feedback loop, which restricts the influence of WUS (Fletcher *et al.,* 1999; Lenhard *et al.,* 1999). Via this extrinsic cue, the expression of WUS is controlled thus enabling the differentiation of the cells that have left the stem cell niche.

So what arrangements do have to take place within the cell to form two distinct daughters?

One typical answer to this question is the differential segregation of so called cell fate determinants, which can be proteins as well as RNA.

A very well examined example is the differentiation of neurons in Drosophila. The crucial step in a progenitor cell division is the differential inheritance of a transcription factor called Prospero in combination with an adaptor called Numb, acting in the Notch pathway (Knoblich 2008). But what keeps those factors restricted to a certain pole? A set of conserved proteins, PAR, co-operate in restricting the mentioned determinants to certain poles of the cell and help to orientate the spindle axis in its designated position (Knoblich 2008). How this is achieved is not clear yet, although some mechanisms suggest, that proteins are anchored at the plasma membrane and kept from diffusing away by forming large oligomers (Feng *et al.,* 2007). But although homologs to the PAR proteins are found from Drosophila up to mammals, they are not present in plants and fungi, indicating, that those organisms have come up with other ways to establish polar cell division (Goldstein *et al.,* 2007).

Nevertheless this is only a small fraction of a large variety of components, which are differentially distributed to the daughter cells, which range from extra-chromosomal DNA, Centrosomes, and ER to Vesicle trafficking.
But most important in the context of this work is the differential distribution of RNA. This will be further highlighted in Chapter 1.3.
Also in plants, a lot of tissues are the result of polar development, e.g. roots, stomata and of course the embryo. A closer look on the development of the first two examples would go far beyond the scope of this work especially since they are fairly well characterized.
Therefore an emphasis is put on the early development of the Arabidopsis plant, starting from the egg cell, which is already a highly polarized cell towards the embryo.

1.2. Development of the embryo

In Arabidopsis, the result of the highly complex development of the female gametophyte is an embryo sac consisting of two synergid cells, one egg, one central cell and three antipodal cells which was previously extensively reviewed by Sprunck *et al.* (Sprunck *et al.*, 2011). A schematic picture and a DIC image, showing a mature embryo sac from Arabidopsis is given in Figure 1-2.

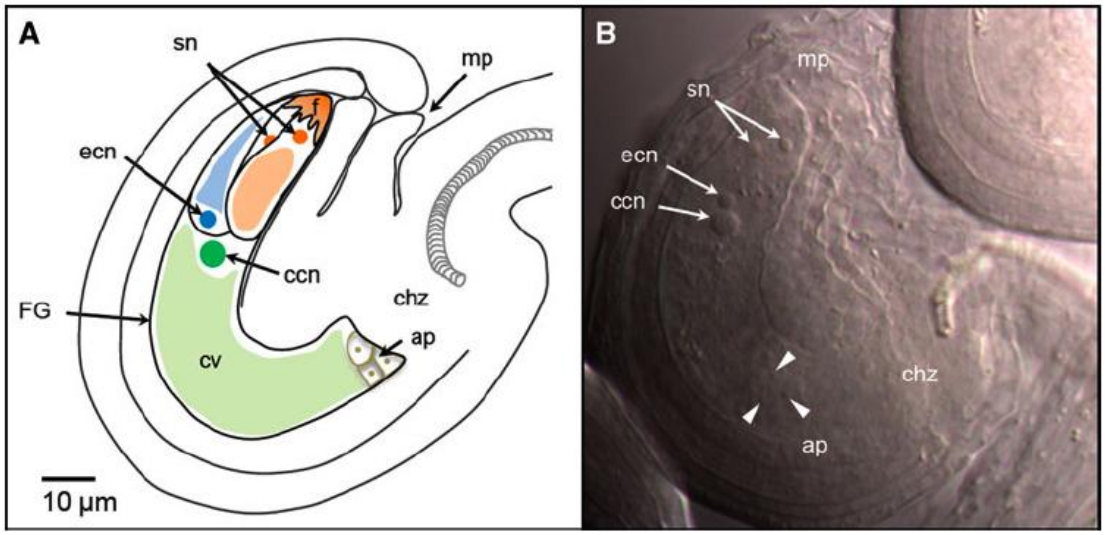

Figure 1-2 Schematic and microscopic view of a mature Arabidopsis embryo sac.

(A) Cartoon of an embryo sac, showing the position of the female gamteophyte (FG) within the embedding tissue. The egg cell already is a highly assymetric cell. Within its stretched morphology the nucleus (ecn) is always oriented towards the nucleus of the much larger central cell (ccn). This orientation always is opposite of the micropylar region (mp), the entry site of the pollen tube. The large vacuole of the egg cell is also prominent. Next to the egg cell rest the two synergids (sn, synergid nuclei), which undergo cell death upon fertilization. On the chalazal pole lie the three antipodal cells (ap) which are a result of the cell divisions starting from the megaspore mother cell.
(B) DIC picture of an embryo sac showing the same cells as in (A). Picture taken from (Sprunck *et al.*, 2011).

When fertilization takes place, the pollen tube, which enters through the micropylar region, releases its two sperm cells, one of which fertilizes the egg cell and the other one the central cell. The newly formed cells give rise to the embryo, and the endosperm, respectively. Here, the emphasis will be put on the development of the embryo.

In Arabidopsis, the zygote elongates about two- to three-fold (Faure *et al.*, 2002) before it divides unequally into an apical and a basal cell. The small apical cell undergoes two rounds of longitudinal cell divisions followed by a transverse one, resulting in the 8-cell pro-embryo. The larger basal daughter on the other side only divides transversally, forming a filamentous structure. From those cells, only the uppermost, the hypophysis, will become part of the root meristems. The other cells form the suspensor, which pushes the embryo into the lumen of the seed (Jeong *et al.*, 2011; Zhang *et al.*, 2011).

Recent studies found some cues, which determine the polar development of the zygote and the first divisions of the embryo. The members of the transcription factor family WUSCHEL-related Homeobox Protein (WOX) (Haecker *et al.*, 2004), a signaling cascade, including the Yoda (yda) kinase (Lukowitz *et al.*, 2004) and the plant hormone auxin (Friml *et al.*, 2003) all

are important factors in early embryogenesis. Their roles and interplays of those early determinants of embryogenesis remain to be elucidated. A schematic overview of the expression and distribution pattern of some of the mentioned key players is shown in Figure 1-3.

Essential in triggering zygote elongation and suspensor fate is the mitogen-activated protein (MAP) kinase cascade filed around the MAP kinase kinase kinase YODA (YDA) and its MAP kinases MPK3 and MPK6 (Lukowitz *et al.,* 2004). Loss-of function mutants in this cascade show zygotes, which fail to elongate and produce a smaller sized basal cell. This results in abnormally shaped suspensors.

Furthermore, meristemoid cells, which are progenitors in stomata development, lose the ability for differential cell division in loss-of-function mutants of *yda*. This results in the formation of two guard cells instead of one pavement and one guard cell (Bergmann *et al.,* 2004).

In contrast, overexpression of *yda* leads to hyper-elongated zygotes, larger basal cells and longer suspensor, which disturbs the formation of the proembryo.

Recent findings revealed a protein called SHORT SUSPENSOR (SSP) that activates YDA. This protein is anchored to the plasma membrane and probably acts on YDA by mediating protein-protein interactions. In regard of this work, however, the most intriguing fact about SSP is, that its RNA is present in the pollen but not translated. Only upon fertilization, when the RNA is delivered into the egg cell, it gets translated and the protein can be detected (see 1.3) (Bayer *et al.,* 2009).

Another important player, as in almost all developmental processes in plants, is auxin. It was reported, that auxin accumulates in the apical cell after the first cell division, as a result of its export from the basal cell by PIN7. Pin7 mutants seem to support this theory, since either auxin is accumulated in the basal cell or the formation of the apical cell is severely disturbed (Friml *et al.,* 2003).

The last factors, triggering the polar division of the egg cell, which are highlighted here, are the WOX genes, which are a plant-specific family of transcription factors. In the zygote, the transcripts of both WOX2 and WOX8 are present. While WOX2 is restricted to the apical cell after the first division, WOX8 is only present in the basal cell and the suspensor from the 1-cell stage on. Additionally, WOX9 is initially formed in the basal daughter before it is restricted to the uppermost cell of the suspensor (Haecker *et al.,* 2004). Interestingly, the maize orthologs are expressed in a similar pattern, indicating conservation (Chandler *et al.,* 2008).

Wox8 or wox9 mutants show no or at least not penetrant phenotypes (Wu *et al.,* 2007). Double mutants, however, show irregular cell divisions and misshaped cells in the basal lineage. Furthermore, also the apical cell divisions are disturbed and auxin distribution becomes uniformly. This indicates an influence of WOX8/9 on the apical lineage as well (Breuninger *et al.,* 2008).

Surprisingly, neither combinations of wox2, 8 and 9 mutants, including the triple mutant had an effect on the zygote itself. Since at least WOX2 and 8 are present as transcripts, the question arises, if they are only stored and sequestered after the first division, or if the balanced expression of those transcription factors is necessary for triggering the asymmetric division of the zygote. The latter hypothesis is supported by the introduction of WOX2 into the wox8wox9 mutant background, which leads to the division of the zygote into two monomorphous cells (Breuninger *et al.,* 2008).

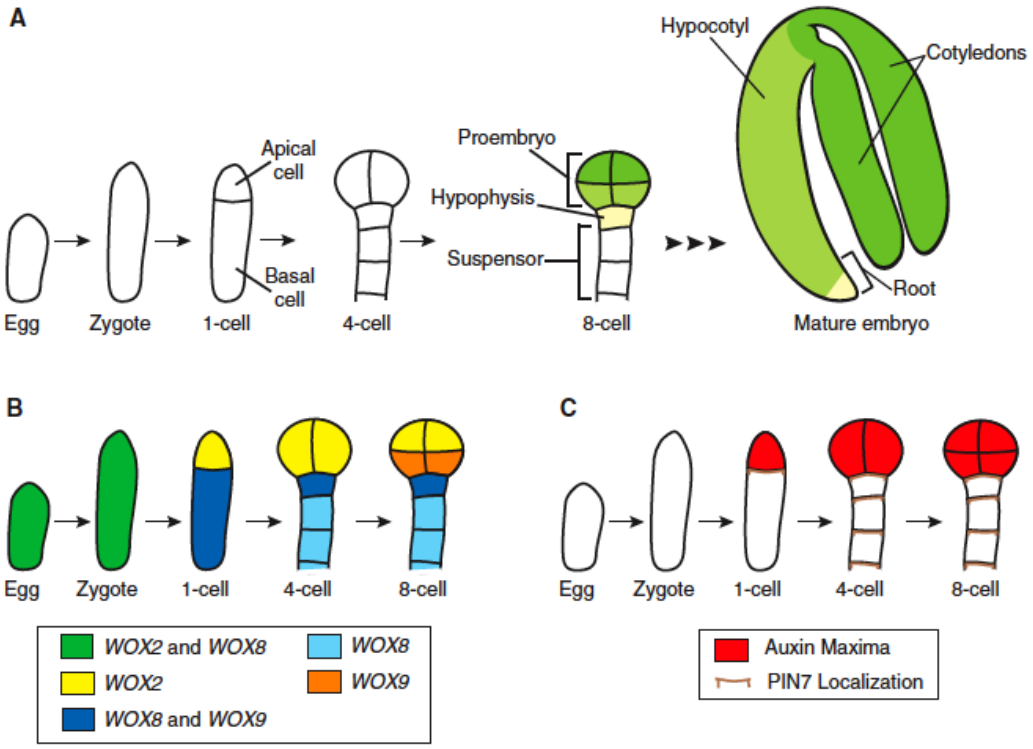

Figure 1-3 Embryo development and asymmetric distribution of key factors in *Arabidopsis thaliana.*

(A) Schematic scheme of the first divisions in the embryo. After fertilization the zygote stretches and divides asymmetrically, giving rise to the 1-cell embryo. The numbers are referring to the number of cells in the apical, thus the embryonic region only. The apical cell undergoes several rounds of cell division resulting in the 8-cell proembryo. The basal cell exclusively undergoes transversal cell divisions, forming a filamentous structure, of which only the uppermost cell, the hypophysis, will be incorporated into the embryo. At that stage (8-cell), four different tissues can be distinguished: the upper (green) and lower (light-green) tiers of the proembryo, the hypophysis (yellow) and the suspensor (white). Upon maturation of the embryo, the tissue will take on the fate corresponding to colors assigned in the 8-cell stage.

(B) Schematic distribution of the expression of *WOX* genes in the proembryo. Noteworthy is the strict asymmetric distribution of *WOX2* and *WOX8* between apical and basal cell after first cell division. At the 8-cell stage, the *WOX* pattern coincides with the four distinct cell types (see A).

(C) Image of the auxin maxima and localization of PIN7 in the proembryo. The auxin flow from basal to apical cell is facilitated by the localization of PIN7 to the upper membrane of the basal cell, thus generating a maximum in the apical domain.

Picture from (Petricka *et al.*, 2009).

The results above show, that some factors of the first division of the zygote have been revealed but still a lot of details remain elusive. In regards to the aims to this work, the question still remains of how is the polar division of the zygote triggered? Is it solely a paternal factor like the *SSP* RNA? Or are also maternal factors involved, like in animals where maternally inherited RNAs are stored in the egg cell? It is still unclear if such a maternal-zygotic shift happens in plants.

1.3. RNA localization as a key factor in development

During the last years a new perception of RNA has found its way into research. While in the beginnings of molecular biology, RNA was thought to be only the message bearer on the way from gene to protein, nowadays a lot of regulatory and developmental key processes are attributed to RNA. This is not only the case for small and non-coding RNAs but also for messenger RNA (mRNA).

There is a whole set of mRNAs in all different species which is involved in spatial control of protein expression, thus increasing its concentration at a certain position of the cell, where they function mainly in differential cell division. An overview of well-studied examples is given in Figure 1-4.

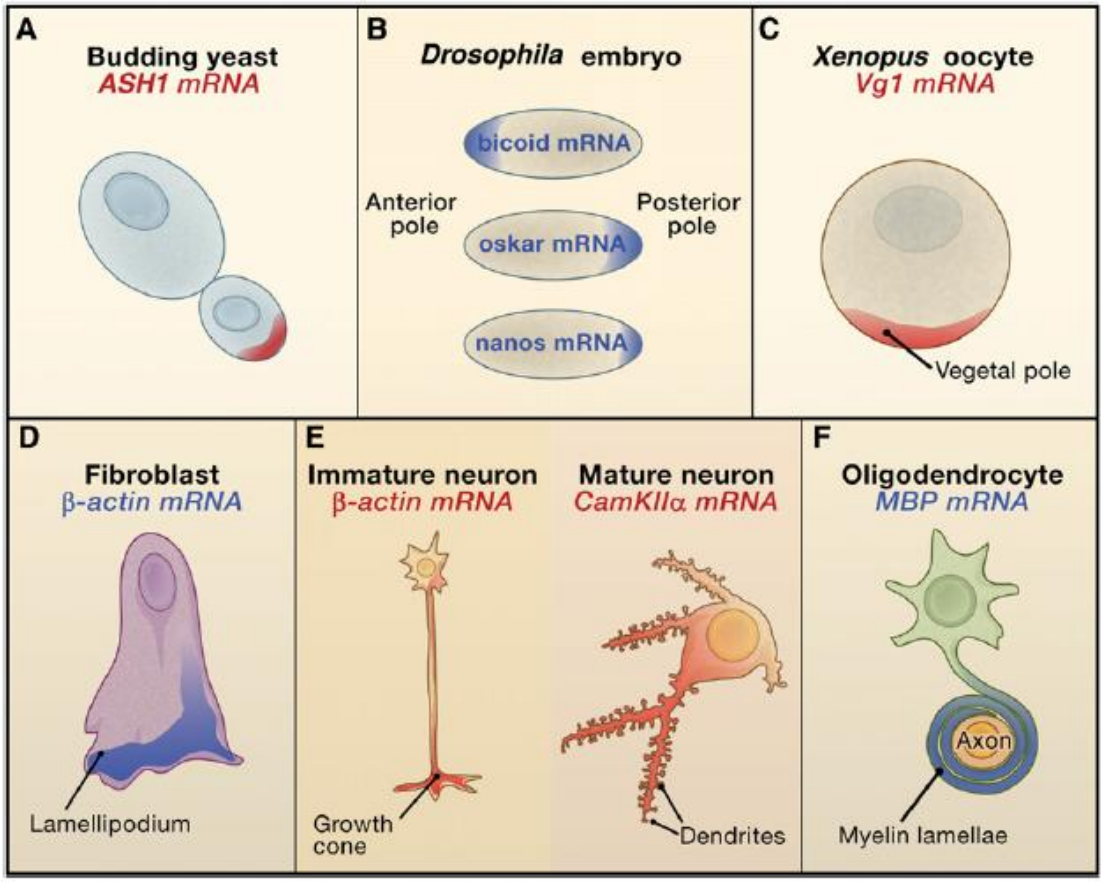

Figure 1-4 Examples for polarly localized mRNAs.

(A) *Ash1* mRNA in budding yeast is localized towards the tip of the newly formed bud, preventing mating type switching.

(B) In *Drosophila melanogaster* embryos *bicoid* localizes at the anterior pole, whereas *oskar* and *nanos* can be found at the posterior pole.

(C) In *Xenopus* oocytes, the mRNA of Vegetalizing factor 1 (Vg1)localizes to the vegetal pole of the cells.

(D) *β-actin* mRNA can be found in the protruding ends of lamellopodia in chicken and mammalian fibroblasts.

(E) *β-actin* mRNA can also be found at the distal growth cones in immature mammalian neurons. The mRNA of *CamKIIα* localizes to the distal dendrites in fully developed pyramidal neurons.

(F) In mammalian oligodendrocytes, *MBP* mRNA encodes for the myelin basic protein, thus localizing to myelination processes, which are required for ensheathing neuronal axons.

Picture taken from (Martin *et al.*, 2009).

While Figure 1-4 gives just a snapshot, recent studies have shown that in Drosophila embryos about 70% of 3000 studied transcripts had a distinct localization (Lecuyer *et al.*, 2007). This number gives rise to the speculation that mRNA localization might be of much larger significance than previously thought. But what is most eye-catching is the fact, that one domain is not present in the figure shown above: Plants. So far, no distinct RNA localization in a plant cell has been described (Shav-Tal *et al.*, 2005; Martin *et al.*, 2009).

The importance of localization manifests itself in the occurrence of such a mechanism even in prokaryotes (Nevo-Dinur *et al.*, 2011).

But what is the purpose of a cell to distribute RNA? The first reason is definitely the spatial control of protein expression translation. Another reason, which is related to the first one, is the temporal resolution, so that a local signal can trigger the translation of RNA. Additional reasons could be the efficiency, the establishment of protein gradients as well as the protection of some cell compartments from otherwise toxic proteins (Martin *et al.,* 2009).
There are three main mechanisms for a cell to concentrate RNA locally.

1.3.1. Trapping of freely diffusing RNA

One method is the local trapping of otherwise freely diffusing RNA. A well-studied example is *nanos* in Drosophila. This RNA is localized to the posterior pole in late oogenesis where it interacts with the germ plasm. It was shown, that this anchoring requires the actin cytoskeleton. This way of building up an RNA gradient, however is not very efficient and needs the aim of other mechanisms, like the one described in the next chapter (Forrest *et al.,* 2003).

1.3.2. Local stabilization/degradation

Another way of generating a locally increased concentration of RNA is the interplay between stabilization and degradation. To cite again the example mentioned above, *nanos* RNA is localized by this mechanism. Although the majority of RNA is delivered elsewhere, it is stable only at the posterior pole of the early embryo, whereas everywhere else, it is bound by Smaug (Smg), which triggers deadenylation and thus degradation of *nanos* (Zaessinger *et al.,* 2006).

1.3.3. Directed transport of RNA

But probably the most important way is the localization via Ribonucleoparticles (RNPs), which guide the RNA to its destination and in which the RNA is kept in a translational repression state.
In mammals the RNA itself often possesses so-called “zip codes” mainly found in the 3’ UTR, which form secondary structures. Those are recognized by RNA binding proteins

(RBPs), which form multimeric RNPs that are transported to their destination within the cell along the cytoskeleton.

So far, no consensus sequence for a zip code could be identified. Furthermore it is likely that the stem loops, which those regions form, are more crucial for the localization. This strongly indicates the importance of the secondary structure of RNA in general. In Drosophila, the best-studied systems about RNA localization so far, the RNA of *bicoid* is localized at the anterior pole of the oocyte. For this, a *cis*-acting zip code is responsible, which resides in the 3' UTR and contains several BLE (bicoid localization elements) (Macdonald *et al.,* 1993). It could be shown, that if the primary structure of those BLEs was altered in a way that kept the secondary stem loop structure, the localization still was performed correctly (Ferrandon *et al.,* 1997).

A very well characterized example for a large RNP is the locasome in yeast. In Budding yeast, the RNA *ash1* is localized to the emerging daughter cell to prevent mating type switching (see Figure 1-4). When *ash1* RNA is transcribed, She2p binds the nascent mRNA and recruits Puf6p. After export from the nucleus this complex binds to She3p, which mediates the binding to Myo4p, a motor protein connected with actin fibers. Together with other co-associated proteins, this complex is transported along the actin cable towards the tip. During the transport, the bound Puf6p and Khd1p ensure the translational repression of *ash1* mRNA until it is anchored at the bud tip where translation is activated (Paquin *et al.,* 2008; Muller *et al.,*).

What is indeed interesting is the fact, that the binding of the single proteins to the RNA seems to happen with low affinity but when binding in a concerted manner, all RBPs together show a great affinity to their bound RNA (Muller *et al.,*). Furthermore, *ash1* is not the exclusive target of this locasome, since many different transcripts have been identified within this RNP (Shepard *et al.,* 2003).

Taken together, the formation of RNPs seems to be a concerted interaction of several RBPs together with several RNAs to form a fairly big complex for RNA transport.

In general, there are four major types of RNP granules, which differ in number and size: (i) germ-line granules; (ii) stress or stored granules (SGs); (iii) Processing bodies (P-bodies); and (iv) transport granules (Moser *et al.,* 2010).

The SGs and the PBs are microscopically visible foci, about 300 nm in size and they are mainly involved in RNA sorting, storage and degradation (Kedersha *et al.,* 2005; Anderson *et al.,* 2008).

So far little is known about the assembly and localization of RNPs in plants. This might be due to the accessibility of plant systems but also to the set of RBPs, which is unique in plants and doesn't show any homology to metazoan proteins (Lorkovic *et al.*, 2002).
The probably best-studied system of localizing RNA in plants so far is the assembly of plant viruses, like the tobacco mosaic virus (Sambade *et al.*, 2008).
Until now there is only one example of a transported RNA in early Arabidopsis development: The interleukin-1 receptor-associated kinase IRAK/Pelle-like kinase SHORT SUSPENSOR (SSP), which was previously described to be transported in the pollen and delivered into the egg upon fertilization (see Chapter 1.2). It could be shown, that only the RNA is present in the pollen tube but not the corresponding protein, whereas there is no expression at all in the egg cell. After fertilization, the SSP protein became visible both in the newly formed zygote and central cell (Bayer *et al.*, 2009). There it acts in the yoda pathway to trigger embryogenesis as described above.

1.4. Visualizing RNA in plants

To further elucidate the pathways and developmental processes mentioned in Chapter 1.3 the methods in monitoring the subcellular distribution of RNA need to be improved. In general, *in situ* hybridization techniques work in fixed and sectioned plant cells but due to the special requirements of plant tissues, this is only very labor-intensive and time consuming. Furthermore, due to the fixation no dynamic structures or transport processes can be monitored.
To overcome this obstacle, a number of *in vivo* RNA imaging systems has been established, of which most have been shown to work in plants (Christensen *et al.*, 2010).
One method, which results in a good signal to noise ratio are the injection of directly labeled RNA. It takes advantage of the incorporation of fluorescently labeled nucleotides, while the RNA is transcribed *in vitro*. The invasive delivery of directly labeled RNA could recently show the visualization of viral RNA particles in plants *in vivo* (Christensen *et al.*, 2009). Nevertheless, this method requires the direct injection of RNA into cells, thus damaging the surrounding tissue leading to stress or damage responses. Since the Arabidopsis egg cell is deeply embedded in its surrounding tissue, the direct delivery of RNA seems not only technically difficult, if not impossible, but could also lead to an artificial RNA distribution due to the disruption of the tissue. Furthermore, this method is very time consuming and requires high technical skills and is therefore not suitable for high throughput studies.

Another system is based on the Pumilio family of RNA binding proteins in connection with bimolecular fluorescence complementation (Pumilio-BiFC) (Ozawa *et al.,* 2007). In this method, a specific Pumilio protein is randomly fused with one of two fragment of a fluorescent protein. When two proteins with the complementary fragments bind the same RNA in close proximity, the fluorescent protein becomes restored, thus emitting a signal. An advantage of this method is, that the sequence of the RNA to be investigated remains unaltered, since the Pumilio protein is genetically engineered to recognize specific stem loop structures within this RNA (Cheong *et al.,* 2006). This already represents the drawback of this method: The successive optimization of the RNA-binding affinity by mutational variation is very time consuming and labor intensive. Additionally, one Pumilio is optimized for only one RNA molecule, thus making it unsuitable for high-throughput studies. Nevertheless, it has been successfully applied for the detection of viral RNA in plants (Tilsner *et al.,* 2009).

The mimicking of GFP by RNA, as previously reported by Paige et al. (Paige *et al.,* 2011), seems also very promising. In this study, they found an RNA which specifically binds an organic molecule, which resembles the cyclic fluorophore within GFP. When bound, the RNA-fluorophore complex emits a light, which has similar properties, as the natural fluorescent protein. This method, however, is still at its beginnings.

Apparently the best systems for high-throughput screening of RNA visualization are based on the capability of certain RBPs to bind to specific stem loops. Two systems have been previously described and will be the subject of this work.

The MS2 coat protein (MS2CP), which is derived from the MS2 phage, binds its corresponding 19-nucleotide stem loops with high affinity (K_d= 6.2 nM) and specificity (LeCuyer *et al.,* 1995). The MS2CP can be functionally fused to a fluorescent tag, thus making it suitable to track RNA in the living cell (Bertrand *et al.,* 1998). So far, this system has been used several times successfully to study RNA transport dynamics in plants (Hamada *et al.,* 2003; Sambade *et al.,* 2008).

Another system, which was introduced by Daigle and Ellenberg, uses a 22-aminoacid peptide fragment of the N protein from the lambda-phage giving it the name λN_{22} (Daigle *et al.,* 2007). This peptide binds its corresponding stem-loops, called boxB (15 nucleotides), with a lower affinity (K_d= 22 nM) than MS2CP. Before this work, this method proofed to work in animal cells and fungi (Lange *et al.,* 2008; Konig *et al.,* 2009) but not in plants. One great advantage of those two visualization methods in comparison with the direct labeling of RNA is the genomic integration of the target loops. This ensures, that the RNA is fully processed, including splicing. Recent studies showed the importance of correct splicing of *oskar* RNA in

Drosophila, where the formation of the so-called spliced oskar localization element (SOLE) is essential for the localization of the RNA to the posterior pole of the oocyte (Ghosh *et al.*, 2012).

1.5. Aims of this work

This work aims to unravel the fundamental mechanisms in the development of the Arabidopsis egg cell and embryo and if such processes are triggered by the polar localization of RNA.

The utilization of two RNA visualization systems, MS2 and λN_{22}, will be tested in plants. This will be performed by transient expression assays in *N. benthamiana*.

Afterwards a versatile GATEWAY™ compatible vector series will be generated, enabling the high-throughput screen of RNA distribution in the Arabidopsis egg cell. As a basis for this screen, a candidate list of putatively polarized RNAs will be compiled of microarray data, available for the gametophytic and embryonic tissue.

Subsequently, transgenic reporter plants for all candidate genes will be generated and their RNA localization will be monitored in the Arabidopsis egg cell and the embryo.

Furthermore, the protein composition of RNPs, which transport the putatively polar RNA towards its destination, will be investigated by biochemical studies.

All this together will unravel the mysteries of the polar development of the Arabidopsis embryo in combination with its molecular and biochemical elements.

2. Results

2.1. Visualizing RNA in plants

For the general approach to study the localization of RNA *in vivo*, different methods have been described (see Chapter 1.4). In this work, the principle of an RNA binding domain fused to a fluorescent protein in combination with specifically recognized RNA stem loops was applied.

2.1.1. A versatile Gateway™ based vector series for RNA visualization in plants

For visualization, both the MS2 system (LeCuyer *et al.*, 1995) and the λN_{22} system (Daigle *et al.*, 2007) were used, as introduced in Chapter 1.4. So far, only the MS2 system had been shown to work in plants (Hamada *et al.*, 2003; Sambade *et al.*, 2008) but not the λN_{22} system.
In order to check the use of both systems *in planta*, a vector series for both was created.
Generally, both detection systems consist of two separate parts, which have to be introduced into plants simultaneously.
One half of the system is the so-called marker, which consists of the binding protein (BP), namely MS2CP or λN_{22}, respectively. Both BP were C-terminally fused with the different fluorescence proteins (FP) CFP, GFP, mVenus and mCherry, respectively (Schönberger *et al.*, 2012). Furthermore, the construct contains the Nuclear-localization sequence (NLS) from the Simian Vacuolating Virus 40 large T antigen (SV40 Tag) (Kalderon *et al.*, 1984) In the absence of target RNA (see below), the BP-FP-NLS fusion protein should remain in the nucleus, resulting in a fluorescence-free cytosol, thus reducing background signals. Additionally, the marker vectors were cloned under control of the ubiquitin 10 promoter from Arabidopsis (*UBQ10*) which has a high expression rate in transient experiments (Grefen *et al.*, 2010).
The other half is made up by the target RNAs. It contains the transcriptional fusion of the investigated RNA with the specific stem-loops, MS2, which is recognized by the MS2 coat protein (MS2CP, see below) or boxB, which is bound by λN_{22}. In this case, a Gateway™ based vector series was engineered, enabling the study of any number of transcripts with little cloning effort. In order to rule out any steric effects of the attached loops, six repeats of MS2 and 16 repeats of boxB were each cloned either in 5' or 3' position of the Gateway™ cassette.

These transcripts are expressed under the control of the strong *35S* promoter from cauliflower mosaic virus (Benfey *et al.*, 1989).

Figure 2-1 shows a schematic representation of the two-component visualization system.

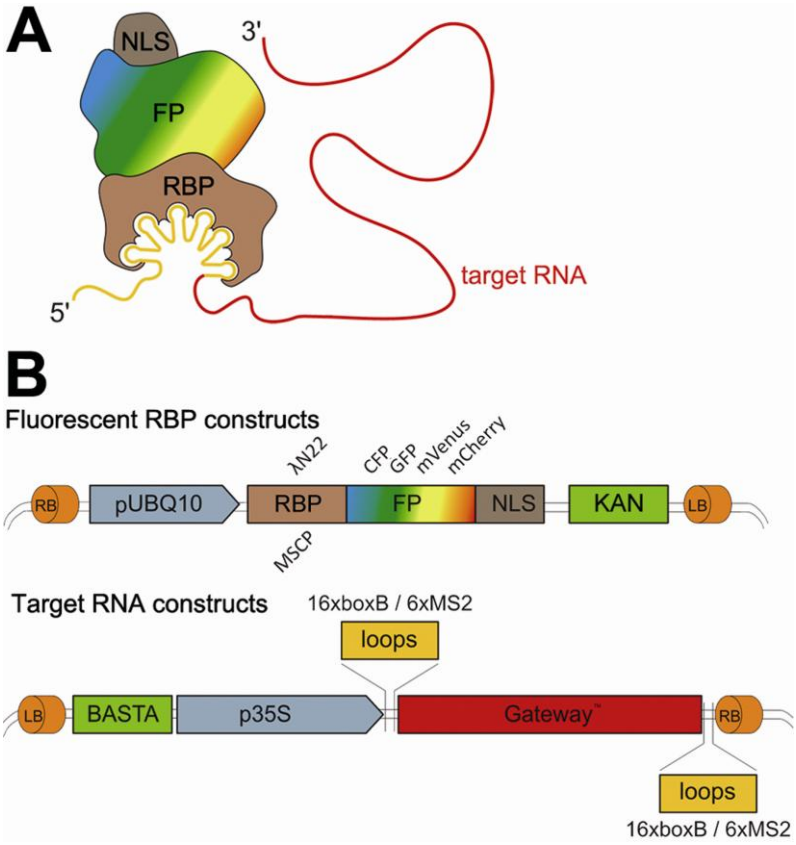

Figure 2-1 Schematic illustration of the two component RNA visualization system.

(A) Cartoon of the two-part RNA visualization system. A phage derived binding protein (BP, brown), MS2CP or λN_{22}, specifically binds hair-loop structures, termed MS2 and boxB, respectively, which are attached as multiple repeats to RNA. Here the fusion to the 5' end is depicted. The BP is fused to a fluorescent protein (FP: CFP, GFP, mVenus and mCherry) and to an NLS.

(B) Illustration of the vector series. The T-DNA of the vectors between the left and right border is depicted. BP-FP-NLS is driven by the *UBQ10* promoter. Selection of stable transformands can be performed with kanamycin. The target RNA, which is expressed under control of the *35S* promoter, can be inserted in 3' or 5' position of the stem-loops via Gateway™ recombination. For enhancement of signal, the sequence of six repeats of MS2 and 16 repeats of boxB are used respectively. Stable transformands can be identified by BASTA selection. Illustration taken from (Schönberger *et al.*, 2012).

2.1.2. The MS2 and the λN_{22} systems are both suitable for RNA monitoring in planta

To test the functionality of the vectors in plants, transient expression assays were performed by infiltration into *Nicotiana benthamiana* leafs and subsequent confocal microscopic

analysis (see Chapters 6.4.3. and 6.4.4.). Primarily, the vectors encoding the λN_{22}-GFP-NLS and MS2CP-mVenus-NLS were tested.

Both constructs showed a nuclear localization without any background in the cytosol. There was even a higher accumulation in the nucleolus (Figure 2-2 A, B, E and F).

When co-infiltration was performed with bacterial strains, carrying vectors encoding a target RNA, the signal remained strongest in the nucleus, but there was also a clear redistribution of fluorescent signal into the cytosol indicating the export and cytosolic localization of the target RNA (Figure 2-2 C, D, G and H) (Schönberger *et al.*, 2012).

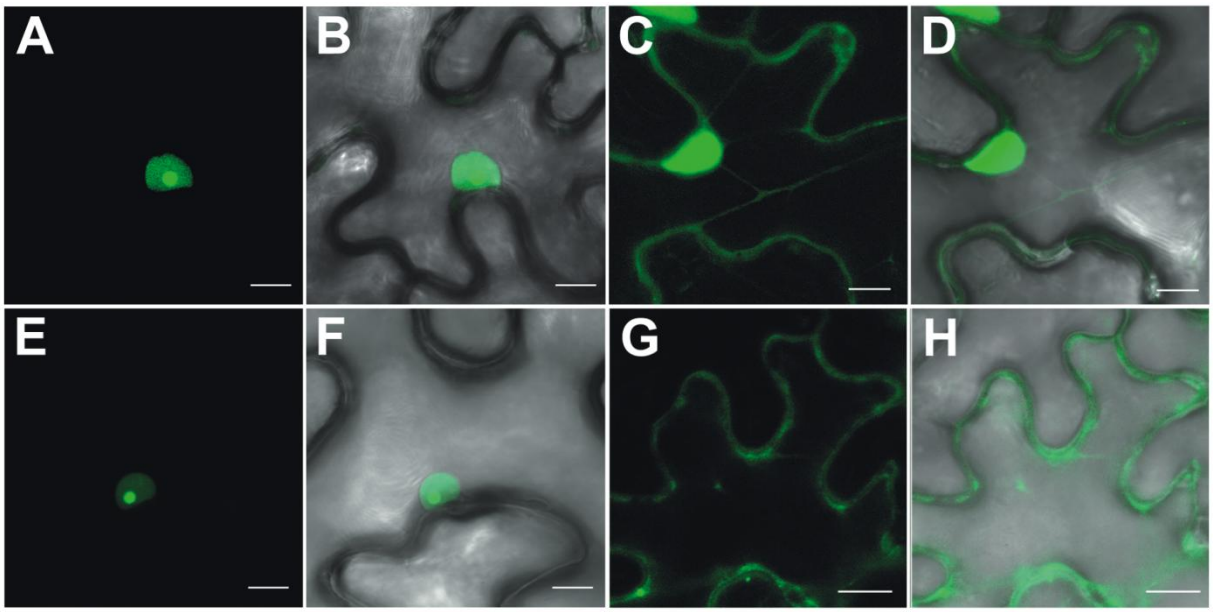

Figure 2-2 Transient expression of both RNA visualization systems in *N. benthamiana*.
(A-D) λN_{22}-GFP-NLS. (E-H) MS2CP-mVenus-NLS. (A, B, E and F) In the presence of only the BP-FP-NLS constructs, the signal remained solely in the nucleus of the epidermis cells. Upon co-infiltration with a target RNA fused to the corresponding stem loops, fluorescence can also be observed in the cytosol (C, D, G and H). A, C, E and G are fluorescent light images. B, D, F and H each are overlays of the fluorescent and its corresponding bright light channel to depict the typical jigsaw shape of tobacco epidermis cells. Scale bars depict 10 µm each. Pictures were taken from (Schönberger *et al.*, 2012).

To rule out any unspecific binding of either of the binding proteins to any RNA, controls were performed. On one hand, λN_{22}-GFP-NLS was either co-infiltrated with RNA without stem-loops (Figure 2-3 A, B and C) or RNA fused to MS2 loops (Figure 2-3 D, E and F). On the other hand, MS2CP-mVenus-NLS was also co-infiltrated together with RNA without loops (Figure 2-3 G, H and I) or with boxB loops (Figure 2-3 J, K and L). To identify double-infiltrated cells, this RNA was coding for tagRFP in all experiments as a scorable marker.

None of the binding proteins shows neither unspecific binding to any RNA nor binding to the corresponding stem-loops derived from the other system based on the lack of cytoplasmic fluorescence (Figure 2-3) (Schönberger *et al.*, 2012).

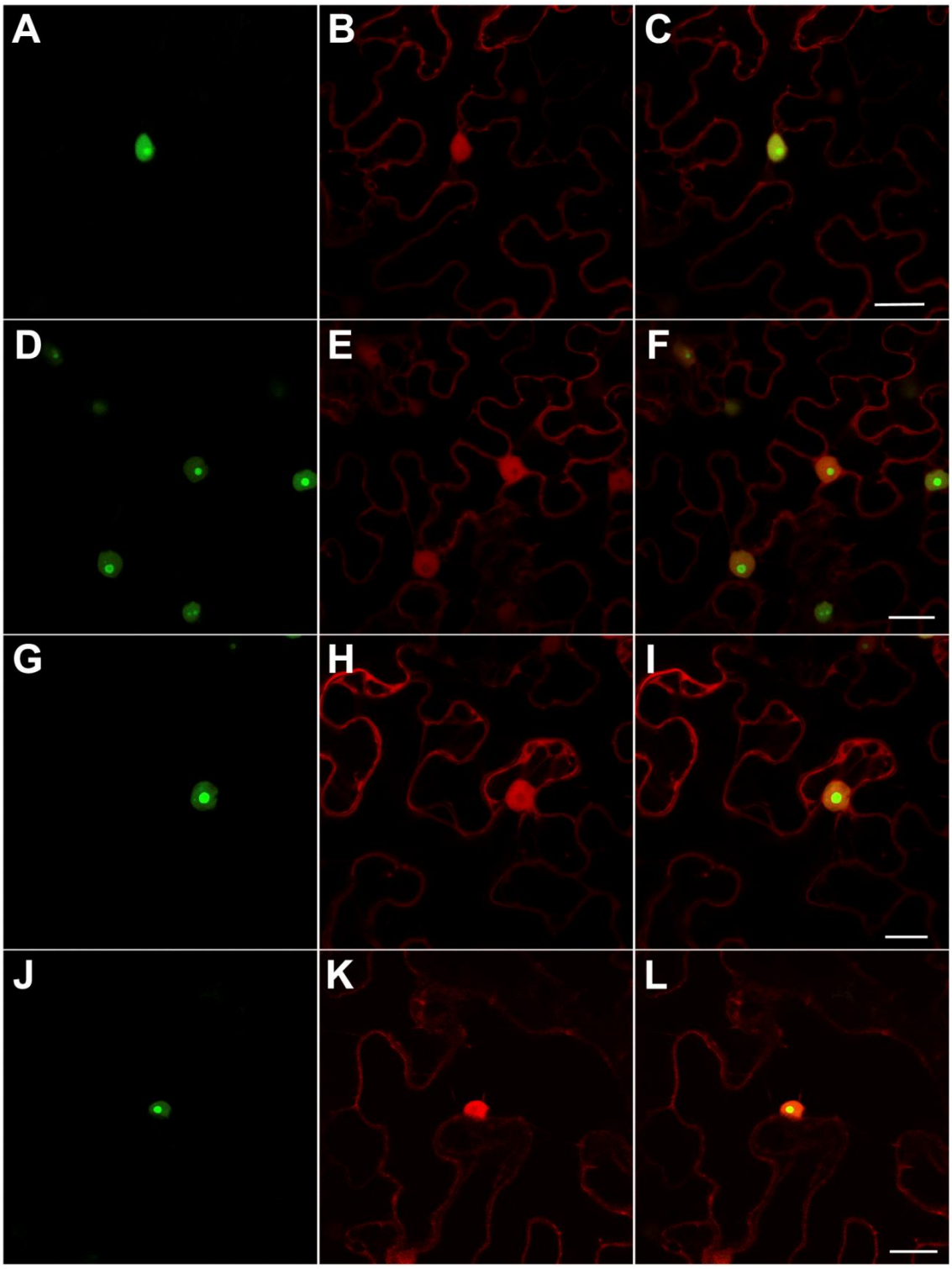

Figure 2-3 Co-expression of the BP-FP fusions with non-target RNAs.

(A-C) Co-expression of λN_{22}-GFP-NLS with a *tagRFP*-RNA containing no target stem-loops. (D-F) Co-expression of λN_{22}-GFP-NLS with *tagRFP*-6x-MS2-RNA (G-I) Co-expression of MS2-CP with a *tagRFP*-RNA containing no target stem-loops. (J-L) Co-expression of MS2-CP with *tagRFP*-16x-boxB-RNA.

The nuclear localisation of the markers protein remained unaffected in all cases. Scale bars represent 10µm. Pictures and legend taken from (Schönberger *et al.*, 2012).

In order to rule out, that the redistribution of fluorescence upon co-infiltration resulted from degradation of BP-FP fusions, a Western Blot analysis of total protein extract of infiltrated leafs was performed using an anti-GFP antibody.(Figure 2-4). It could be clearly seen, that the λN_{22}-GFP-NLS only gave one signal at its expected size (31kDa) for both extracts, whereas the MS2CP-mVenus-NLS showed an additional band at the size of free GFP, when a target RNA was present. This indicates that fluorescent signals visible in the cytosol are a mixture of free mVenus and the intact BP-FP fusions. Furthermore, next to the expected size (43kDa) an additional band at about 90kDa was visible, which would correspond to the size of the dimer (Schönberger *et al.*, 2012).

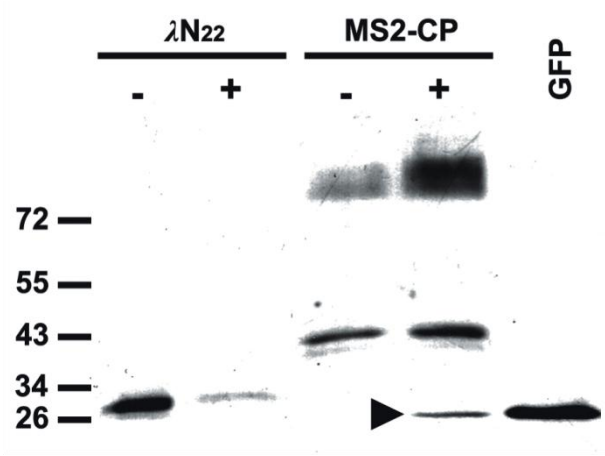

Figure 2-4 Western Blot of λN_{22}-GFP-NLS and MS2CP-mVenus-NLS.
Protein extract of infiltrated leafs as shown in Figure 2-2 was isolated in the absence (-) and presence (+) of target RNA labeled with corresponding loops. λN_{22}-GFP-NLS could be detected in both cases as single band at the expected size of 31 kDa. MS2CP-mVenus-NLS showed the expected band at 43 kDa but also an additional band, which corresponds to the size of free mVenus (arrowhead), when stem-loop RNA was present. Furthermore, a band could be detected in both cases at the size of the expected dimer (~90 kDa). GFP: positive control cytosolic GFP. Picture taken from (Schönberger *et al.*, 2012).

Taken together, this indicates the general applicability of both systems in plants. For the λN_{22} system this is the first proof of its applicability in plants. Additionally, the λN_{22}-GFP-NLS seems to be more stable, since no aberrant bands were visible on the Western Blot when target RNA is present, whereas MS2CP seems to undergo proteolytic degradation upon co-infiltration with target RNA.

2.1.3. Further characterization of the viability of the λN_{22} and the MS2 system and the influence of the position of the stem loops

To further characterize the two systems as versatile tools for studying RNA distribution in plants *in vivo*, the influence of the position of the loops with respect to the RNA on its distribution and subsequent translation was analyzed. Therefore, co-infiltration experiments were performed with λN_{22}-GFP-NLS and MS2CP-mVenus-NLS and their corresponding stem loops in 5' as well as in 3' position of the tagRFP-RNA.

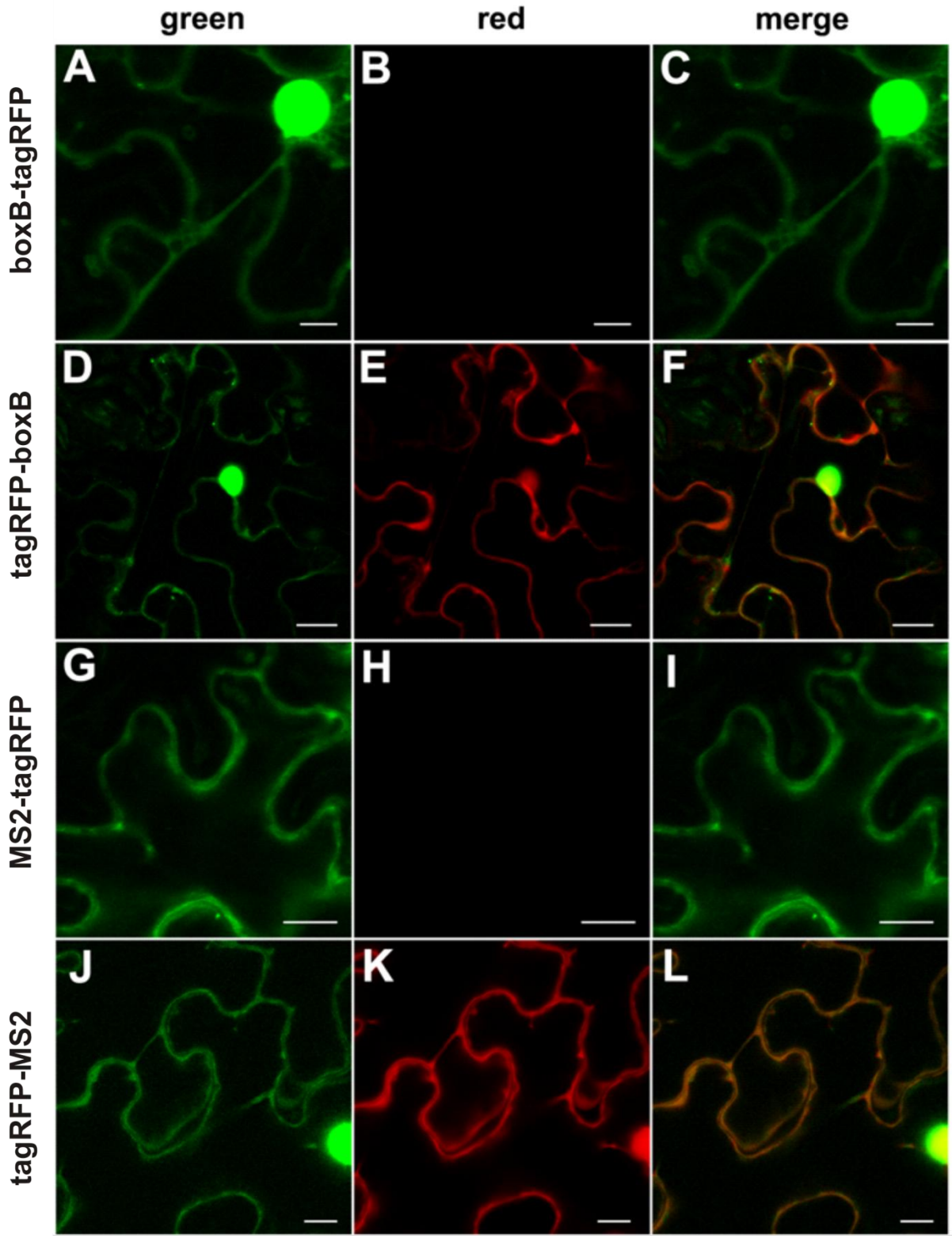

Figure 2-5 Co-infiltration of λN_{22}-GFP-NLS or MS2CP-mVenus-NLS together with tagRFP RNA containing the corresponding stem loops either in 5' or in 3' position to investigate the influence of the loop structure on translation. (A-C) λN_{22}-GFP-NLS with 16x-boxB-tagRFP. (D-F) λN_{22}-GFP-NLS and tagRFP-16x-boxB. (G-I) MS2CP-mVenus-NLS with 6x-MS2-tagRFP. (J-L) MS2CP-mVenus-NLS and tagRFP-6x-MS2. Co-expression of BP-FP with stem-loop RNA led to distribution of the marker protein to the nucleus and cytosol (A, D, G and J). Translation of the tagRFP reporter was only detectable with the loops in 3' position of the ORF (E and K). Scale bars represent 20 µm (D-F and J-L) and 10 µm (A-C and G-I), respectively. Pictures taken from (Schönberger *et al.*, 2012).

As shown in Figure 2-5, signals of BP-FP constructs could always be detected in the cytosol, indicating export of RNA from nucleus independent of the position of the stem-loops (Figure 2-5 A, D, G and J). Intriguingly, red fluorescence, indicating translation of the reporter *tagRFP*-RNA could only be detected, when the stem-loops were fused in 3' position indicating a disturbing effect of the stem loops on protein translation (Schönberger *et al.*, 2012).

In order to proof the presence of the target RNA, RT-PCR analysis of infiltrated leaf sections was performed (Figure 2-6). As can be seen, target RNA was present in all four assays. Furthermore, the actin controls show the purity of the isolated RNA proving the absence of contaminating genomic DNA (Schönberger *et al.*, 2012).

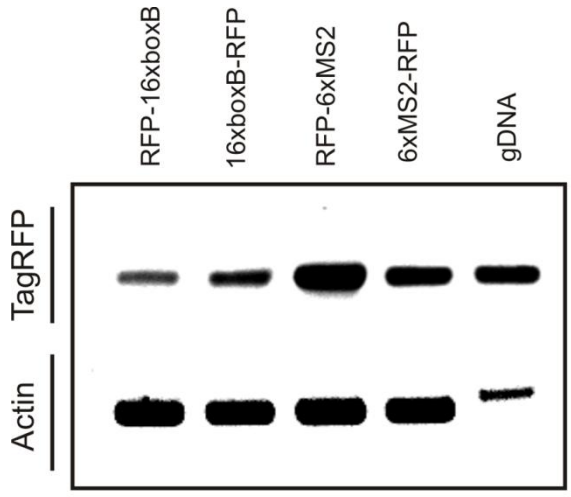

Figure 2-6 RT-PCR on the presence of *tagRFP*-RNA.

mRNA from infiltrated leaf sections as shown in Figure 2-5 was isolated, followed by subsequent oligo-dT primed RT-PCR. *tagRFP*-RNA could be detected in all tissues isolated, independent from the position of the loops. gDNA: genomic DNA was taken as positive control; Actin controls show the exclusive presence of RNA only by size-shift vs. genomic actin. Picture taken from (Schönberger *et al.*, 2012).

Additionally, generated λN_{22}-FP-NLS constructs, e.g. fusions with CFP, mVenus and mCherry were tested. The experimental procedure was the same as described above. As expected, all generated fusion proteins were suitable for localizing RNA within the cytosol, thus allowing *in vivo* monitoring of the RNA transport (Figure 2-7).

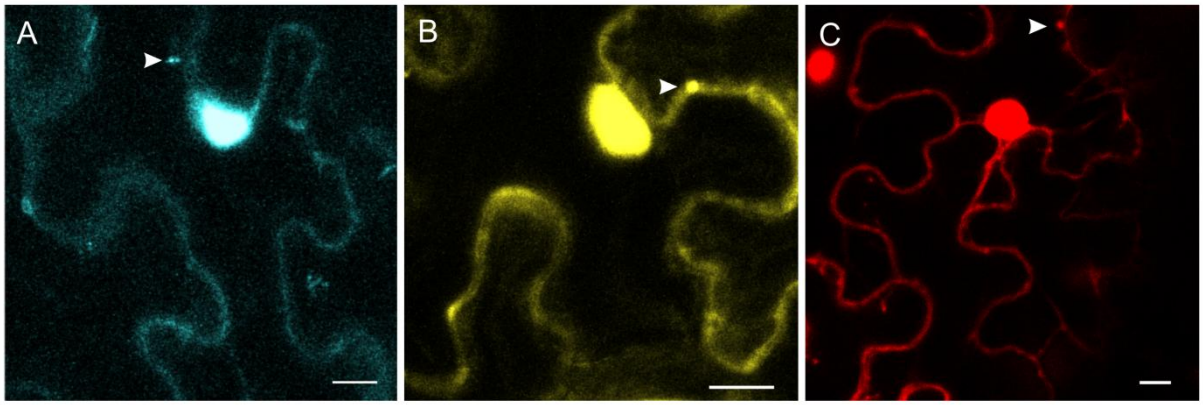

Figure 2-7 Fluorescence light images of λN_{22}-FP-NLS constructs in transiently transformed *N. benthamiana* cells.
(A) λN_{22}-CFP-NLS. (B) λN_{22}-mVenus-NLS. (C) λN_{22}-mCherry-NLS. All constructs were co-infiltrated with the 5' boxB constructs of the genomic region of At1g60030. The pattern resembled the observed one for λN_{22}-GFP-NLS together with a target RNA. The nuclear signal remained the strongest, but a clear fluorescence signal could be monitored within the cytosol. Arrowheads in (A - C) indicate putative RNP particles. Scale bars are 10 µm.

2.1.4. RNA is transported within microscopically visible RNA transport granules

Interestingly, the signal of the binding protein often accumulated in cytoplasmic foci throughout all experiment. This was previously reported for RNA granules (Thomas *et al.*, 2011). However, there were clear differences in abundance and signal strength of those foci. Whereas for GFP and mVenus the detection was possible in almost every transformed cell, only few of those putative RNPs could be monitored when using the mCherry or CFP fusions. Whether this is due to signal strength or molecular preferences of the fluorescent proteins remains to be determined. Therefore, the further characterization of those foci was mainly performed with the λN_{22}-GFP and the MS2CP-mVenus constructs.

Figure 2-8 shows a detailed section of a cell that was co-infiltrated with λN_{22}-GFP-NLS and *tagRFP*-16xboxB. Plotting the intensities of each pixel of the green channel against the intensities of the red channel resulted in the scatter blot in Figure 2-8 B. The highlighted pixels correspond to the marked foci in Figure 2-8 A (arrowheads). This shows, that the marked foci were comprised exclusively of binding protein and probably tagRFP-RNA (Schönberger *et al.*, 2012).

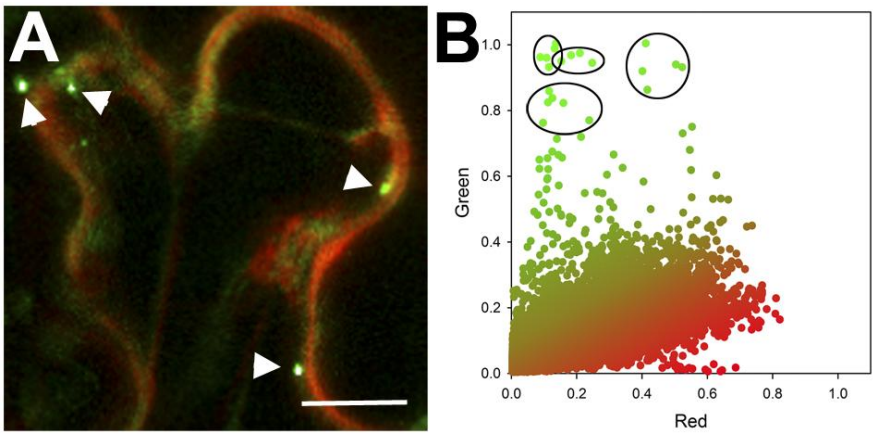

Figure 2-8 Co-expression of λN_{22}-GFP-NLS and *tagRFP*-16xboxB.

(A) Close-up of a representative picture, showing λN_{22}-GFP-NLS and tagRFP. Mostly, the two fluorescent signals co-localized but the presence of distinct foci, comprised of GFP only could be detected (arrowheads). Those foci probably depict RNA transport granules.

(B) Intensities of both channels were plotted against each other. The encircled pixels were very intense green and almost free of red signals. They corresponded to the marked granules in (A). Those data indicate that the granules consist exclusively of λN_{22}-GFP-NLS and probably *tagRFP*-RNA. Scale bars are 20 µm. Pictures taken from (Schönberger *et al.*, 2012).

Additionally, the appearance of those foci was independent of the kind of RNA. Tests with RNA coding for tagRFP, for a secreted protein (At1g60030, Nucleobase-ascorbate transporter 7) or a nuclear protein (At3g04610, Flowering locus KH domain RNA binding protein) revealed no differences.

To further rule out the possibility, that the monitored foci were the result of stress due to the over expression of λN_{22} or MS2CP, respectively, agrobacteria, hosting a vector encoding for DCP2-GFP were infiltrated into tobacco leafs. This decapping enzyme was previously reported to be involved in RNA degradation and part of processing bodies (Xu *et al.*, 2006). The visualization of DCP2-GFP however revealed a totally different picture of cytoplasmic foci (see Figure 2-9) differing relatively much more in size than the λN_{22} or MS2CP foci, respectively (400 ± 200 µm vs. 1000 ± 200µm). Furthermore, the DCP2 foci hardly moved.

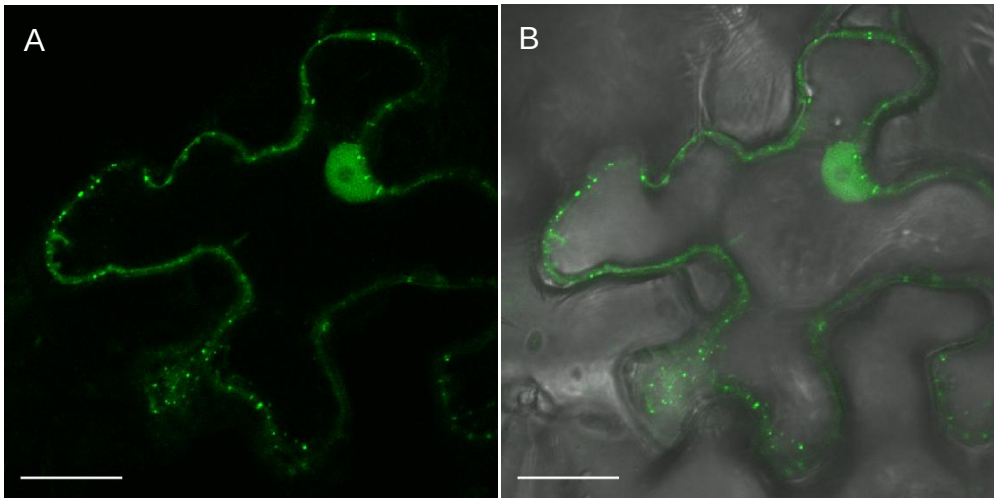

Figure 2-9 Transient expression of DCP2-GFP in *N. benthamiana*.

The C-terminal fusion of GFP with DCP2 driven by the *35S* promoter was expressed in tobacco epidermis cells. (A) Fluorescent light image. (B) Corresponding overlay of fluorescent image and bright-field image. The appearance and number of the DCP2 particles, involved in mRNA degradation, differed to the observed λN_{22} and MS2CP particles. During all taken time series, the DCP2 granules remained stationary. Scale bars: 20 µm.

Obviously, the foci formed by the BP-FP constructs, were uniformly sized and highly motile. Due to the large size of the fluorescent protein (i.e. λN_{22} to GFP ratio 1:7) and the limitations of the available confocal microscope system, the true size of the particles was hard to determine, but given the pictures it could be estimated within a range of 800-1200 nm. This size is in accordance with previously reported mRNPs, indicating that those granules are mRNPs (Schönberger *et al.*, 2012). The movement of the particles was directional but appeared to happen in rather a stop-and-go fashion, which suggests a transport along the cytoskeleton, as was previously reported. Short clips, showing the movement of the putative RNPs can be seen on the attached CD.

Figure 2-10 shows representative traces of the movement of two RNP granules, containing either MS2CP-mVenus-NLS or λN_{22}-GFP-NLS.

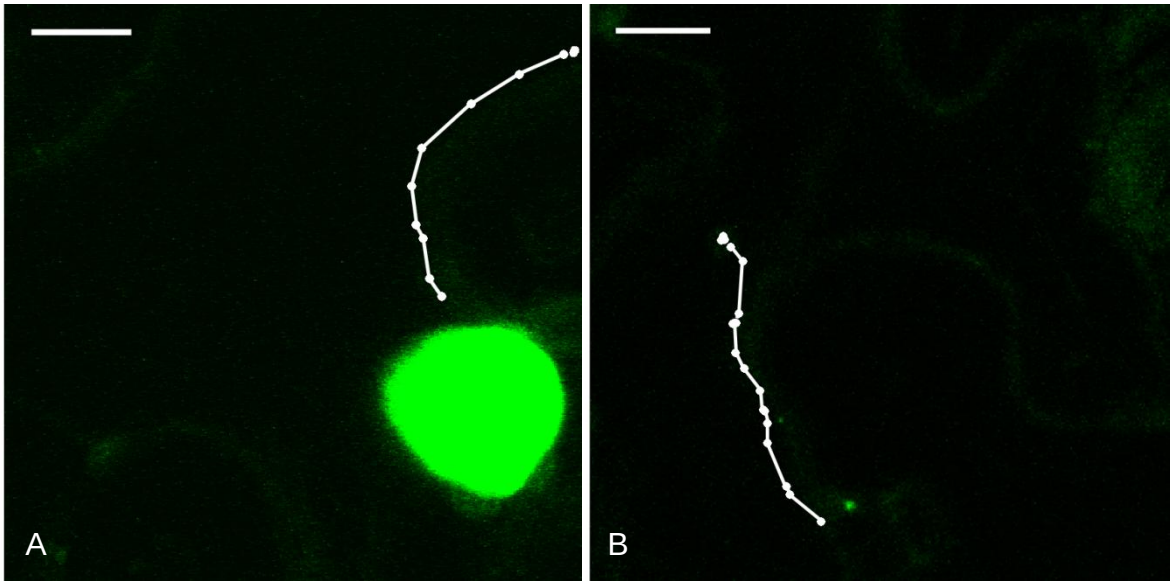

Figure 2-10 Visualization of the stop-and-go fashion movement of RNP granules.
(A) Series of eleven frames, showing the movement of a RNP granule, containing MS2CP-mVenus-NLS, was analyzed for the motility of the particles. Each dot represents the position of the granule in a single frame. (B) Analysis of a series of 18 pictures showing the trace of a particle, containing λN_{22}-GFP-NLS. Each dot represents the position of the granule in a single frame. The accumulation of dots at a static position depicts the pausing of the particle during its directional movement. The frames were taken every two seconds. A video of the two series can be seen on the attached CD. Scale bars represent 10 µm.

The velocities of the particles were determined by measuring the covered distance and elapsed time of five individual RNPs for each system. For λN_{22}-GFP-NLS the pace was determined as 0.98 ± 0.1 µm s^{-1}, while for MS2CP-mVenus-NLS it was measured as 0.31 ± 0.05 µm s^{-1} (n = 5 each, time series taken in different cells) (Schönberger *et al.*, 2012).

2.1.5. Dual application of both systems

As both systems seemed to work in plants, they were both applied simultaneously in order to monitor two different RNAs simultaneously. With regard of the previous results we infiltrated *N. benthamiana* leafs with four constructs: λN_{22}-CFP-NLS, MS2CP-mVenus-NLS and two different RNAs fused to the corresponding stem-loops. In order to increase the chance for the formation of distinct pools of RNPs, target RNAs were chosen with the premise of different translation sites. This was supposed to promote differential localization of the RNA within the highly differentiated and non-polar epidermis cells from tobacco. For λN_{22} the genomic region, including 5' and 3' UTRs as well as introns, of a membrane localized protein

(At1g60030, Nucleobase-ascorbate Transporter 7) was used as a target RNA, which should be translated by ribosomes associated with the rough ER. For the MS2CP, a nuclear protein was chosen (At3g04610, Flowering Locus KH domain RNA binding protein). This should be translated at free ribosomes. Figure 2-11 clearly shows the simultaneous visualization of two distinct RNP foci within one cell (Schönberger *et al.*, 2012).

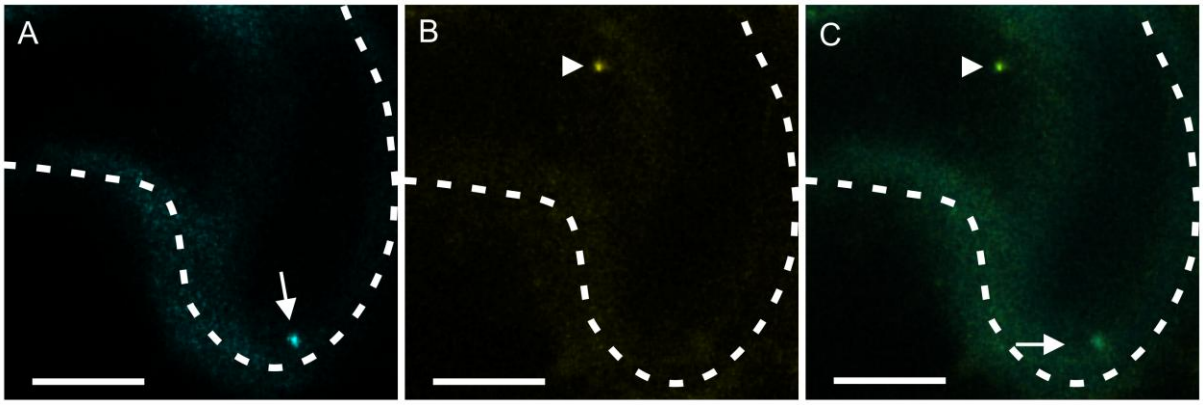

Figure 2-11 Transient co-expression of λN_{22}-CFP-NLS and MS2CP-mVenus-NLS with target RNAs fused to the corresponding stem-loops in *Nicotiana benthamiana*.

(A) λN_{22}-CFP-NLS. (B) MS2CP-mVenus-NLS. (C) Merge of both channels. An arrow in A and C marks a transport granule exclusively containing λN_{22}-CFP-NLS. A second particle, consisting solely of MS2CP-mVenus-NLS is highlighted by an arrowhead in B and C. The outline of the epidermis cell is indicated by the dotted line. Scale bars represent 10 µm. Pictures taken from (Schönberger *et al.*, 2012).

2.2. Elucidating the role of polarly distributed RNA in the Arabidopsis egg cell

It was introduced in Chapter 1.3 that polarly distributed RNAs play crucial roles in the developmental processes throughout all kingdoms of life. Furthermore, the polar division of plant cells by the asymmetric division of internal clues has been shown in the development of stomata. As was described in Chapter 1.1, BASL is segregated differentially when a certain precursor cell divides, thus determining the fate of the different daughter cells. So far, no mechanism, involving the polar distribution of RNA in plant cells has been described in plants. This is surprising, especially as the Arabidopsis egg cell and further the zygote represent highly polarized cells. All those indications together, led to the hypothesis, that the highly polar development of the Arabidopsis embryo might be determined by the establishment of RNA gradients within the egg cell of *Arabidopsis thaliana*.
To address this issue, a high-throughput screen was planned in order to visualize a list of potentially polarly localized RNAs.

2.2.1. Setting up the vector system for RNA visualization in the egg cell

First, a versatile marker system had to be set up. For visualization, again both the MS2 system (LeCuyer *et al.*, 1995) and the λN_{22} system (Daigle *et al.*, 2007) should be used, as it was introduced in Chapter 1.4.
Therefore, derivates of the vectors described in Chapter 2.1.1 were cloned for constitutive expression. A schematic illustration of the vectors can be seen in Figure 2-1 in Chapter 2.1.1, just that for this experimental setup the *EC1.1* promoter was used instead of the *UBQ10* and *35S* promoters.
The marker system was fused to only one fluorescent protein this time. For MS2CP the mVenus fusion was used whereas for λN_{22} the GFP fusion was used. Those were chosen for their applicability in downstream experiments measuring FRET efficiencies in order to elucidate potential interaction partners in RNA binding and transport and they will be referred to as markers or BP-FP fusions.
On the RNA side, six repeats of the MS2 loops in 5' and 16 repeats of the boxB loops in 3' position of the Gateway™ cassette were used (see Chapter 2.1.1).
For the visualization of RNA in the Arabidopsis egg cell, a very strong egg cell specific promoter, *EC1.1*, was used, which is shut off immediately after fertilization (Sprunck *et al.*, accepted). This ensures that detected RNAs originated from transcription in the egg cell and

are not a product of the zygote or even paternally delivered, as previously reported for short suspensor (SSP) (Bayer *et al.*, 2009). Both sides of the system, the markers and the target vectors contain this specific promoter.
In order to obtain stably transformed Arabidopsis plants, the marker vectors were cloned with a resistance for kanamycin while the target vectors can be selected with BASTA.

2.2.2. A list of putative polar RNAs was generated for high-throughput screening

To start with the high-throughput screen, a list of potentially polarly localized RNAs in the egg cell and later on the zygote was defined, based on microarray data from gamteophytic and embryonic single cells.
On the one hand, this list was based on expression data of isolated egg, central and synergid cells (Šoljić et al., in preparation) from Arabidopsis. From the raw data of this array, those genes were filtered, which showed an exceptional high as well as an exclusive expression in the Arabidopsis egg cell. Furthermore, the expression levels from dissected and isolated apical and basal cells from maize embryos were added to the analysis (Krohn et al., in preparation). A second independent list was created, in which certain genes showed either a high expression in the apical or basal cell of the maize embryo, respectively. The orthologues in Arabidopsis were found via Blast on the TAIR homepage (www.arabidopsis.org).
Afterwards the lists were combined. A validation and adaption was performed by a comparison with the data, available at the e-FP browser (http://bar.utoronto.ca/efp_arabidopsis/cgi-bin/efpWeb.cgi) (Winter *et al.*, 2007). These publicly available expression values were obtained by isolating single cells via laser capturing followed by microarray analysis (Casson *et al.*, 2005). In the end, four candidates were added as a result from literature research, including PIN1 and some putative RNA binding proteins, which also showed high expression in the egg cell (see Table 2-1). On the basis of recently published data, which showed the expression of two plant specific transcription factors, WOX2 and WOX8 that are differentially segregated onto the apical and basal cell after the first division (Breuninger *et al.*, 2008), those two genes were included as putative positive controls. All those genes will be referred as candidate RNAs throughout this work.
Finally a list, containing 27 genes, was defined, which is shown in Table 2-1. Known zip codes, which localize RNA within a cell, can be predominantly found in the 3' UTR, as for example in *nanos* in Drosophila (Macdonald *et al.*, 1988), but they can also be found in the 5' UTR (Saunders *et al.*, 1999). Furthermore, it has been reported, that the processing of the pre-

mRNA can be crucial for the correct localization (Giorgi *et al.*, 2007). Therefore, the whole genomic DNA of the constructs was cloned for the study, including the 5' and 3' UTR as well as all the introns. Basis for this data were the annotations on TAIR.

Table 2-1 Target mRNAs currently under investigation. All RNAs are fused to boxB or MS2 target sequences either 5' or 3'.

The table is showing the accession numbers and (predicted) protein products of the candidate genes, investigated for generating an RNA gradient in the Arabidopsis egg cell, sorted by putative functions. A stands for apical expression, B for basal expression and "equal" for non-polar expression based on either the Maize data set (Krohn *et al.*, unpublished) or the online available data set provided by the eFP browser (Casson *et al.*, 2005).

AGI Identifier	Annotation	Maize Data	eFP Set
Transcription factors			
At5g04340	Cold Induced Zinc Finger (C2H2 type)	---	B
At2g17410	ARID/BRIGHT DNA-binding Protein;	A	B
At3g61830	ARF18	---	B
At2g20130	LCV1 (LIKE COV 1)	A	B
At2g40750	WRKY 54	---	Equal
At3g28920	Zinc Finger Homeodomain 9	---	A
At1g60280	ANAC023	---	B
At2g40220	ABI4	---	A
At1g72220	Ring/U-box Superfamily Protein	---	A
At1g14350	MYB124	---	B
RNA binding proteins			
At4g17520	Hyaluronan/mRNA Binding Protein Family (RBP1)	---	B
At3g04610	Flowering Locus KH Domain	---	A
At1g60650	Zinc Finger-containing Glycine-rich RNA-binding Proteins	---	A
At1g22910	RRM containing protein	---	A
Literature cured			
At1g73590	PIN1	(Galweiler *et al.*, 1998); Plasmamembrane	
At5g59340	WOX2	(Haecker *et al.*, 2004); Nucleus	
At5g45980	WOX8	(Haecker *et al.*, 2004); Nucleus	
At1g19850	Monopteros (ARF5)	(Hardtke *et al.*, 1998); Nucleus	
At1g04550	Bodenlos (IAA12)	(Hamann *et al.*, 1999); Nucleus	
Other			
At1g31450	Aspartylprotease	---	A
At1g24510	TCP-1/cpn60 Chaperonin Family Protein	A	B
At5g65620	Zincin-like Metalloproteases Family Protein	B	A
At1g60030	Nucleobase-Ascorbate Transporter 7	---	B
At1g63010	SPX domain-containing protein	A	B
At4g17770	TPS5	A	A
At5g51720	AT-NEET	A	A
At5g59120	Subtilase 4. 13	---	A

2.2.3. Stably transformed MS2CP- and λN22-plants show different patterns of expression and localization

After cloning and introduction of the BP-FP constructs into Arabidopsis Col-0 background, plants were selected for the marker gene.
This resulted in 30 independent lines each for each marker. Those were controlled for correct expression via confocal microscopy two days after emasculation.
Figure 2-12 shows a representative ovule of a plant, expressing the pEC1.1:MS2CP-mVenus-NLS construct.

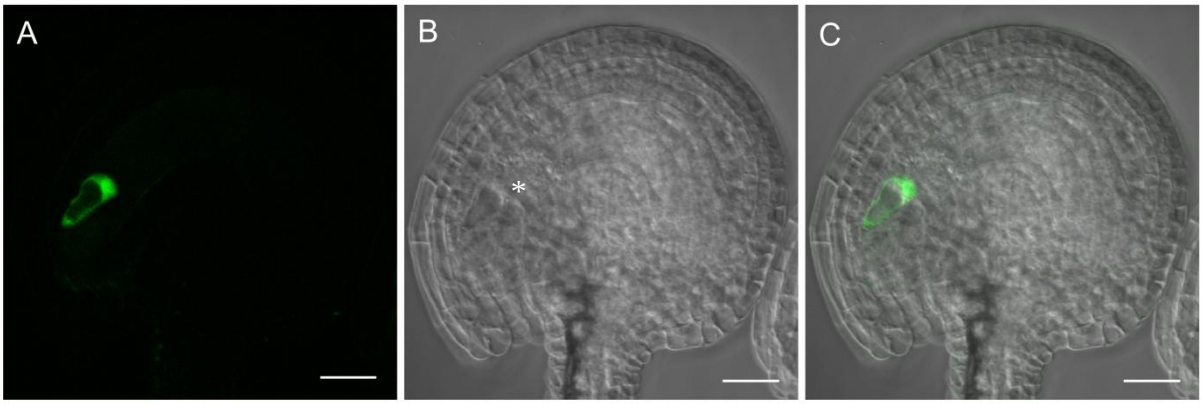

Figure 2-12 Arabidopsis ovule expressing pEC1.1:MS2CP-mVenus-NLS.
A young flower was emasculated and pistils were dissected two days after. (A) Fluorescence light image. (B) DIC image of the ovule showing the distinct outline of the vacuole of the egg cell (asterisk). (C) Merge of both channels. (A and C) clearly show the egg cell, expressing MS2CP-mVenus-NLS under the control of *EC1.1* with a clear background signal in the cytosol. The accumulation in the upper part of the cell is the nucleus and the dark space in the middle is the large vacuole of the Arabidopsis egg cell. Scale bars are 20 µm.

The exclusive expression of the protein in the egg cell of the plant can be clearly seen. However, although in the absence of target RNA, the protein localization shows a clear cytosolic background. This exacerbates the further studies, which rely on a background free cytosol, thus resulting in low noise. Furthermore, some of the studied MS2 marker plants showed not only expression in the egg cell but also in the synergids (Figure 2-13) although the reliability of the promoter had been tested copiously (Sprunck *et al.*, accepted). This leakiness of the *EC1.1* promoter, which was visible in 9 out of 30 investigated lines, states a clear disadvantage of the used MS2CP marker.

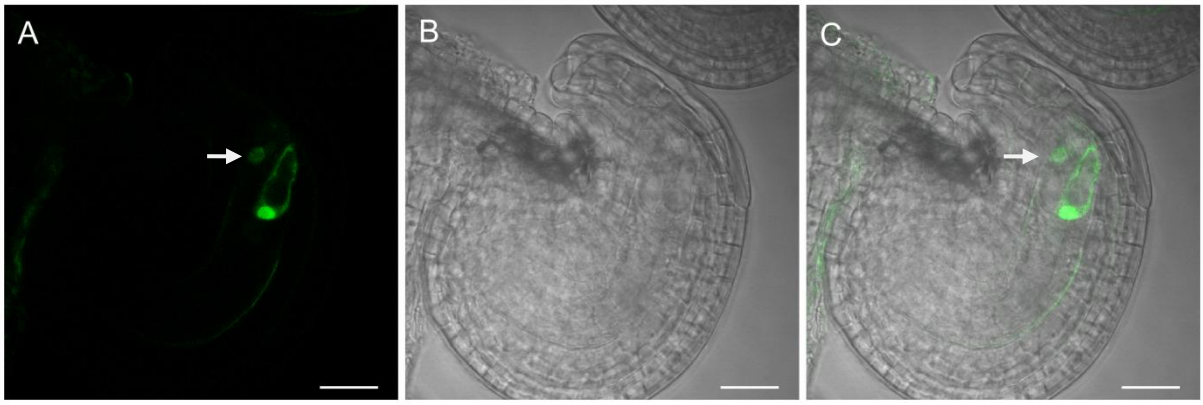

Figure 2-13 Arabidopsis ovule expressing pEC1.1:MS2CP-mVenus-NLS.
A young flower was emasculated and pistils were dissected two days after. (A) Fluorescence light image. (B) DIC image of the ovule. (C) Merge of both channels. (A and C) show the expression of MS2CP-mVenus-NLS in the egg cell with cytosolic background and also in one of the synergids (arrow). Scale bars are 20 µm.

Since both systems were set up in parallel, Arabidopsis wild type plants were also transformed with the λN_{22} constructs. As for the MS2 system, 30 plants, which were positive after selection on kanamycin, were checked for the expression of the λN_{22}-GFP.
Figure 2-14 shows a representative plant, expressing the pEC1.1:λN_{22}-GFP-NLS construct.

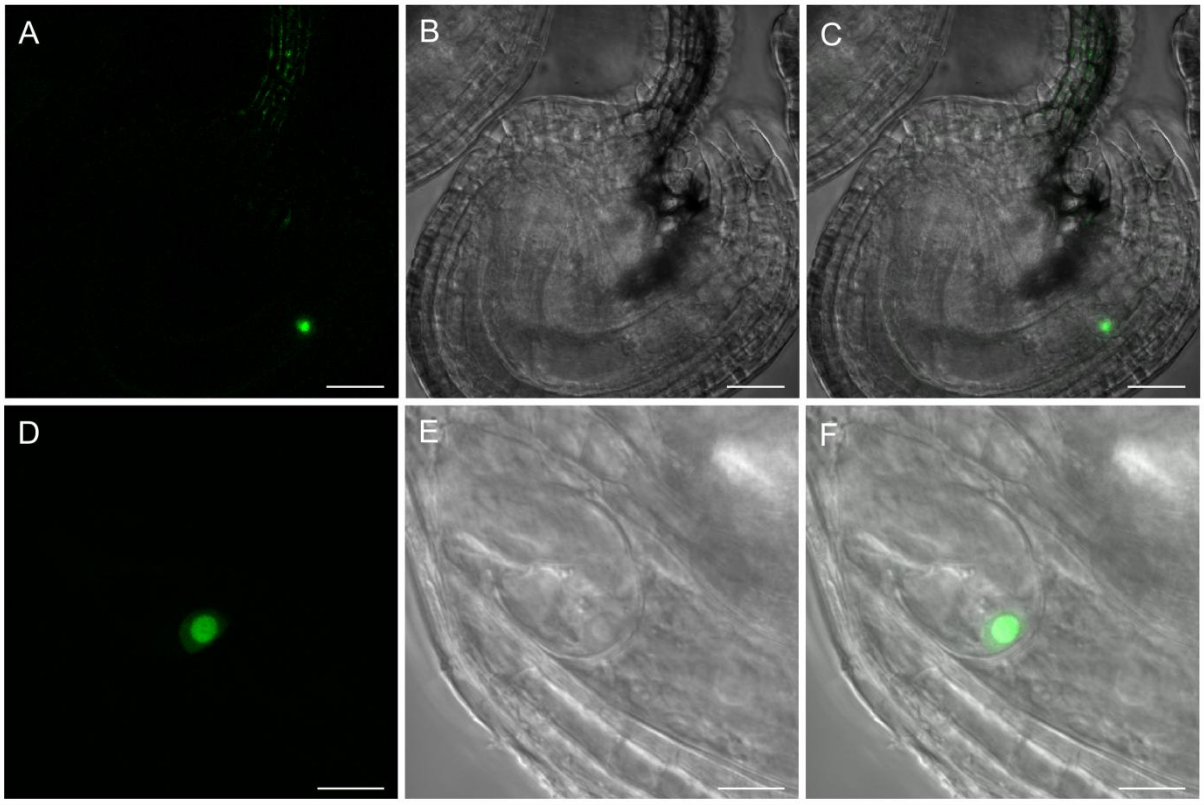

Figure 2-14 Arabidopsis ovules expressing pEC1.1:λN$_{22}$-GFP-NLS.

A young flower of a kanamycin-positive plant was emasculated and pistils were dissected two days after. (A-C) Picture of a whole Arabidopsis ovule expressing λN$_{22}$-GFP-NLS under the control of the egg cell specific *EC1.1* promoter. (D-F) are showing a close up of the egg cell of another line expressing the same construct (A and D) Fluorescence light images. (B and E) DIC images of the ovule and egg cell, respectively. (C and F) Merged pictures of bright-field and fluorescence channels.

(A and C) clearly show the expression of the λN$_{22}$-GFP fusion restricted to the egg cell. Furthermore the fluorescence signal remains located exclusively in the nucleus.

(D and F) highlight the nuclear restriction of λN$_{22}$-GFP to the nucleus with a higher concentration of protein being located in the nucleolus. This matches with the data observed for the transient experiments outlined in Chapter 2.1.2. Scale bars are 20 µm for A to C and 10 µm for D to F, respectively.

It is evident, the signal is visible in the egg cell. Furthermore, in contrast to the MS2 plants, the signal is exclusively localized in the nucleus, with an accumulation in the nucleolus. Additionally, the signal was detectable solely in the egg cell for all plants studied (n = 30).

Due to those obvious disadvantages of the MS2 system in the stable Arabidopsis lines in combination with the drawbacks, already outlined in Chapter 2.1.2, all further studies from that point on focused on the λN$_{22}$ system.

Among the selected λN$_{22}$ plants, which showed a strong and egg-exclusive expression, several were picked for segregation studies. Two lines split in a ratio of 3:1 indicating a single

integration of the construct. Subsequent selection of the successive lines resulted in a plant, homozygous for pEC1.1:λN_{22}-GFP-NLS.

2.2.4. The distribution of the λN_{22} changes upon expression of a target RNA carrying boxB stem loops

The homozygous marker plant for λN_{22} was crossed with plants, carrying a RNA-loop construct in first generation. The first double-positive plants to be analyzed were expressing the putative Flowering Locus KH Domain RNA Binding Protein, with the Accession number At3g04610, as shown in Figure 2-15. After selection for both marker genes, the plants were analyzed by confocal laser scanning microscopy two days after emasculation.

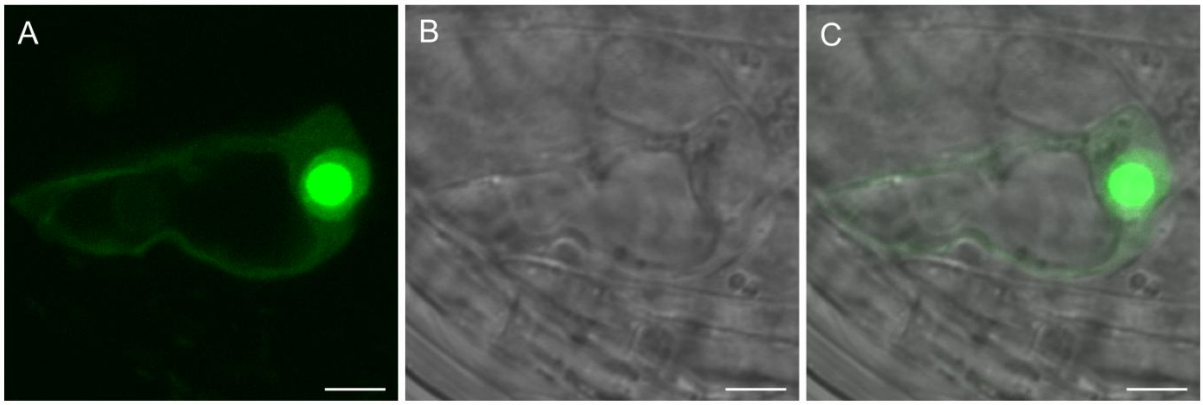

Figure 2-15 Close-up of an egg cell from an Arabidopsis plant homozygous for pEC1.1:λN_{22}-GFP-NLS and additionally expressing pEC1.1:At3g04610-16xboxB.

Young flowers were emasculated and analyzed two days later by confocal microscopy. (A) Fluorescence light image. (B) DIC image of the egg cell. (C) Merge of both channels. (A and C) show the expression of λN_{22}-GFP-NLS when a target RNA with boxB loops at the 3' position, in this case At1g04610, is present. Fluorescence is now visible in the nucleus and the cytosol, indicating an export of the tagged RNA out of the nucleus. Judged by the distribution pattern, the RNA of At1g04610 seems to be distributed homogenously throughout the egg cell. Scale bars represent 5 µm.

It can be clearly seen, that BP-FP shows a weak fluorescent signal in the cytosol in addition to the strong nuclear localization. This indicates the viability of the system in the Arabidopsis embryo. The allocation of the GFP-signal, however, looks homogenous, given the large vacuole of the cell. This indicates that the Flowering Locus KH Domain RNA is not polarly localized within the egg cell.

So far, the stem-loop vectors for 24 candidates plus WOX 2, WOX8 and PIN1 as putative positive controls (see Table 2-1) have been cloned, introduced into Arabidopsis wild-type

plants and partially crossed with the homozygous λN_{22}-GFP plants. At that point Andrea Bleckmann from the working group continued the high-throughput study.

2.2.5. Further characterization of the candidate RNAs

In addition to the genomic fragments of each candidate RNA, the coding sequences (CDS) of all of them were cloned for further subcellular studies in order to obtain more information about the protein product of the transcript. Therefore, the CDSs were fused to GFP N- and C-terminally, respectively, using the vectors published by Karimi et al (Karimi *et al.*, 2005). This was again performed by Gateway™ cloning. Afterwards, the constructs were analyzed by transient expression in *N. benthamiana*. Table 2-2 shows the candidate list with the corresponding proteins, their predicted (TAIR) and determined subcellular localization.

Table 2-2 List of candidates tested for subcellular localization in transient expression assays in *N. benthamiana*

The list includes the predicted localizations, according to TAIR (Lamesch *et al.*, 2010)(if available) and the experimentally determined subcellular localizations. TBD: To be determined (no data available); N.D. Not determined (no amplification of CDS possible); PM: Plasma membrane; PD: Plasmodesmata; ER: Endoplasmatic Reticulum;

Annotation	**Predicted localization (TAIR)**	**Subcellular localization in *N. benthamiana***
Transcription factors		
Cold Induced Zinc Finger (C2H2 type)	Intracellular	Nucleus
ARID/BRIGHT DNA-binding Protein;	TBD	Nucleus
ARF18	N	Nucleus
LCV1 (LIKE COV 1)	TBD	Cytosol/Granules
WRKY 54	TBD	Nucleus
Zinc Finger Homeodomain 9	TBD	Nucleus
ANAC023	TBD	N.D.
ABI4	published: Nucleus	Nucleus
Ring/U-box Superfamily Protein	TBD	N.D.
MYB124	TBD	Nucleus
RNA binding proteins		
Hyaluronan/mRNA Binding Protein Family (RBP1)	Cytosol, Nucleus and Peroxisomes	Cytosol, RNPs
Flowering Locus KH Domain	Nucleus	Nucleus
Zinc Finger-containing Glycine-rich RNA-binding Proteins	Nucleus	Nucleus
RRM containing protein	TBD	N.D.
Other		
Aspartylprotease	ER	ER
TCP-1/cpn60 Chaperonin Family Protein	Cytosol/ PM/PD	Cytosol
Zincin-like Metalloproteases Family Protein	Chloroplasts/Stroma/ Cytosol	Chloroplasts and Mitochondria
Nucleobase-Ascorbate Transporter 7	PM/PD	PM
SPX domain-containing protein	Vacuole	Vacuole
TPS5	TBD	ER
AT-NEET	Chloroplasts	Chloroplasts
Subtilase 4. 13	ER/Cell wall	ER/Golgi

Strikingly, there is no obvious contradiction between predictions and experimental data. Most of the not yet determined transcription factors localized to the nucleus, which is not surprising. The pictures of all subcellular localizations can be seen in Chapter 8.3 within the appendix. In order to visualize the high-throughput study of subcellular localizations, one example is mentioned here to finish this chapter. For this purpose, the Nucleobase-Ascorbate Transporter 7 (At1g60030) is chosen because its RNA was already used in the dual tracking experiment in Chapter 2.1.5. The protein of this gene is predicted to localize to the plasma membrane. This prediction could be confirmed, as is depicted in Figure 2-16.

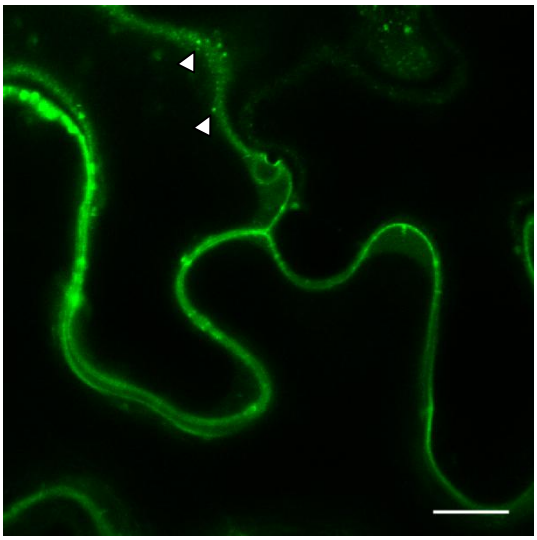

Figure 2-16 Transient expression of GFP-At1g60030 in *N. benthamiana* epidermis cells.
The N-terminal GFP fusion with the CDS of At1g60030 under the control of the *35S* promoter shows a clear localization to the plasma membrane of the cell. Interestingly, vesicles transporting the fusion protein to its destination can be observed (arrowheads). Scale bar is 10 µm.

2.3. Characterization of an endogenous RNA binding protein

2.3.1. RBP1 and its intriguing subcellular localization

One subset of the candidates of putatively polarized RNA is constituted of proteins encoding for RNA binding domains (see Chapter 2.2.2). The candidate with the accession number At4g17520, which will be referred to as RBP1 (RNA Binding Protein 1) throughout this work, was also subject to subcellular localization studies via infiltration into *N. benthamiana* leafs. At4g17520 is a member of the Hyaluronan mRNA binding family and has two very close homologues in Arabidopsis, At4g16830 and At5g47210, which are highly conserved within their RNA binding motifs. Those will be referred to as RGGA and RBPX, respectively throughout this work.

Those proteins are predicted to be members of the Hyaluronan/mRNA binding protein family. In 2000, this class of protein was described for the first time in animals. It contained a conserved Arginine rich motif and had a strong binding affinity to Hyaluronan and a weak affinity towards RNA (Huang *et al.*, 2000). Shortly afterwards, the protein could be co-immunoprecipitated with the mRNA encoding for the plasminogen-activator inhibitor (PAI) type I. Based on data from those experiments, the protein, which was termed intracellular Hyaluronan Binding protein (IHABP) 4, was supposed to stabilize the RNA of PAI, thus providing a function for the protein (Heaton *et al.*, 2001). Later it was shown, that HABP4 is similar to an antigen found in Hodgkin Lymphoma, named Ki-1/57, where it is involved in chromatin remodeling and transcription regulation (Nery *et al.*, 2004). Since then, other functions were described, like the involvement in pre-mRNA splicing (Bressan *et al.*, 2010). So far, all studies on this sort of protein have been done in animal systems like human cell culture or mouse and a clear function and structure of this or a relative homologue still remains to be resolved. The Arabidopsis orthologs, which are mentioned above, have been assigned to be members of this family because of their RGG-motifs, which are supposed to be responsible for RNA binding. This motif has been extensively studied in higher organisms (Corley *et al.*, 2008), but not in plants. Figure 2-17 highlights the most conserved region of the three RBP homologues in comparison with the HABP from mice and human.

Figure 2-17 The RGG motif is conserved through all species.

Alignment of the three members of the Hyaluronan mRNA binding protein family from *Arabidopsis thaliana* (At_RBP1, At_RGGA and At_RBPX) with the intracellular Hyaluronan binding proteins (IHABP) 4 from mouse (Mus musculus, Mm) and humans (Homo sapiens, Hs). The boxes highlight the two conserved RGG-motifs, which are conserved throughout the kingdoms of life and which are crucial for RNA binding. Conserved amino acids are depicted in red, similar residues in blue.

The expression profile of RBP1 in an Arabidopsis wild-type plant was analyzed by semi-quantitative real-time PCR. The values were normalized against the expression of the *UBQ10* gene, as was previously described (Czechowski *et al.*, 2005). Figure 2-18 shows the expression of the RBP1 gene throughout all tissues examined with a significantly higher value in the open flower.

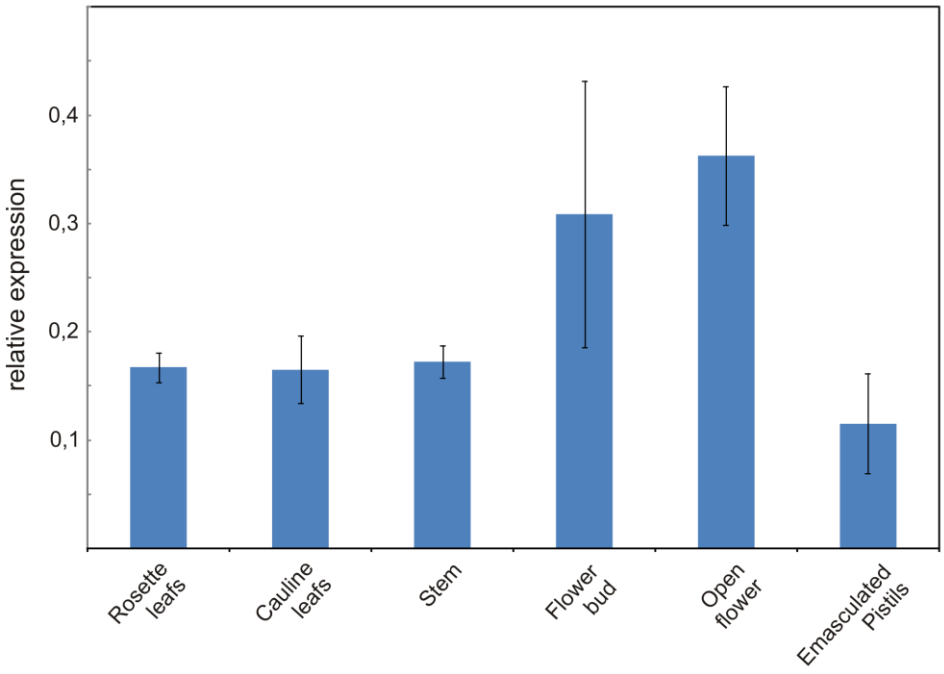

Figure 2-18 Quantitative real-time PCR analysis of different tissues from *Arabidopsis thaliana*.
The expression of RBP1 was normalized to the expression of the housekeeping gene UBQ10 (At5g25760). Emasculated pistils were collected two days after emasculation.

RBP1 clearly localized to the cytosol, with a high concentration of protein in cytosolic foci, with a size of 1000 ± 210 nm, regardless of the position of the GFP fusion (N- or C-terminal, Figure 2-19).

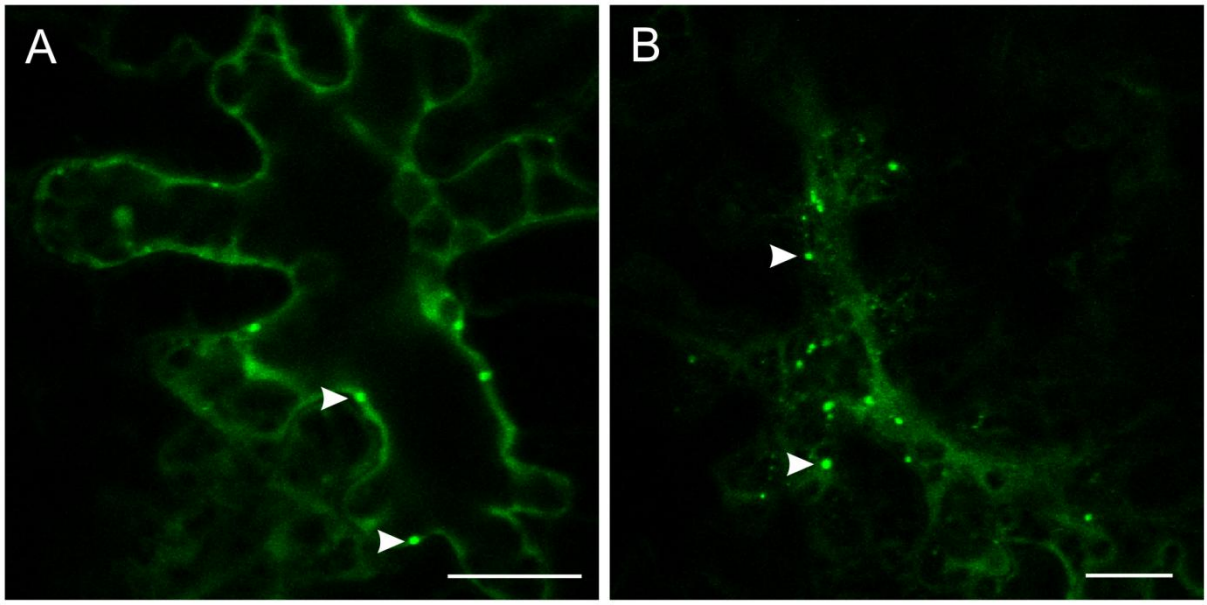

Figure 2-19 Transient Expression of C- and N-terminal GFP fusion with RBP1 (At4g17520) in *N. benthamiana*

Plant leafs were infiltrated with *Agrobacterium tumfecaiens* cells, hosting plasmids expressing RBP1-GFP (A) and GFP-RBP1 (B), respectively, under the control of the *35S* promoter. The cytosolic distribution of the protein can be clearly seen, as well as its concentration into cytoplasmic foci, presumably RNPs (arrowheads). Scale bars represent 20 µm.

Additionally, both homologues show the same subcellular localization as their relative RBP1 as is depicted in Figure 2-20.

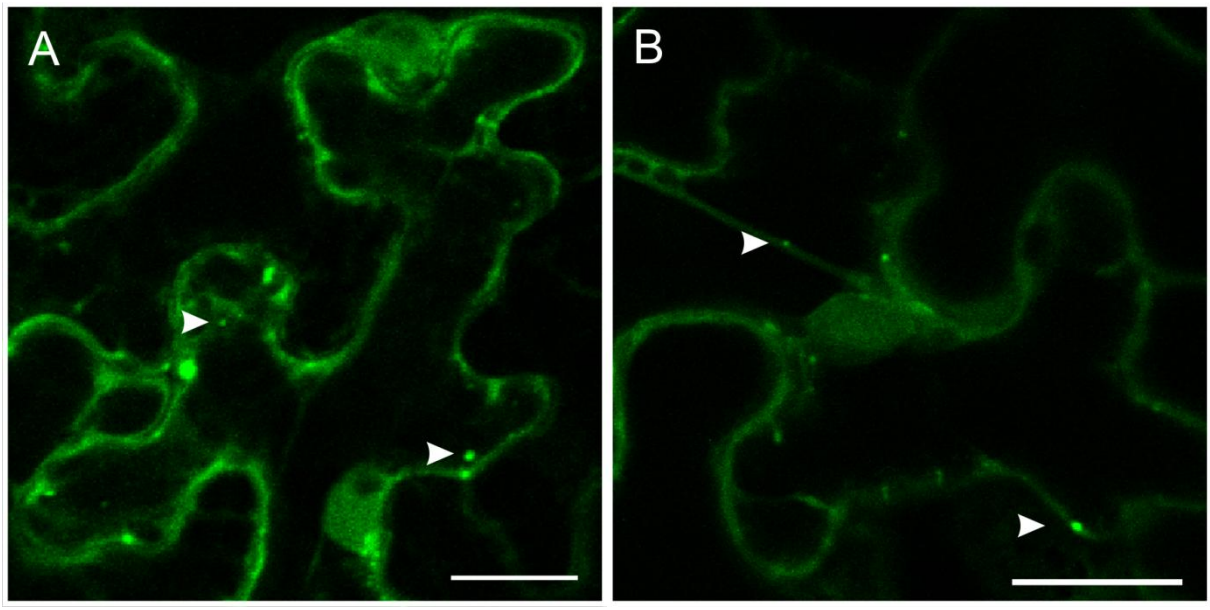

Figure 2-20 Protein localisation of RBP1 homologs

Transient expression of C-terminal GFP fusion of RGGA (A) and RBPX (B), respectively in *N. benthamiana*. The cytoplasmic distribution as well as the concentration into higher-order structures is clearly visible (compare Figure 2-19). Arrowheads indicate such foci. Scale bars = 20µm.

None of the single knockout lines of the RBPs shows an obvious phenotype. Therefore the homozygous knockout lines are currently crossed to obtain double and triple knockout mutants.

RBP1, which was a candidate on the list for differential RNA distribution (see Chapter 2.2.2) was already subjected to the polar localization experiment. It didn't show any differential localization of its RNA within the Arabidopsis egg cell (Figure 2-21).

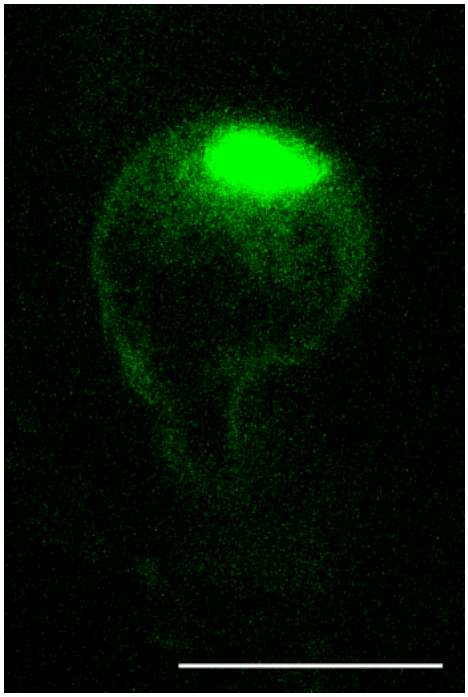

Figure 2-21 Egg cell expressing RBP1-16xboxB together with λN_{22}-GFP-NLS

Cytosolic signal could be detected, indicating binding of λN_{22}-GFP-NLS to RBP1-RNA. With respect to the distribution, no polar localization of RBP1-RNA could be monitored. Scale bar indicates 15 µm.

2.3.2. Studying RBP1 and its role in RNA transport

While monitoring the cells over a time lapse, those cytoplasmic foci moved in a similar pattern as was described for RNP particles, when using the marker systems, as mentioned in Chapter 2.1.4 and reported previously (Hamada *et al.*, 2003; Schönberger *et al.*, 2012). This is a strong indication that RBP1 and its homologues function as RNA binding proteins. Therefore they were examined more closely. This function manifested itself in a stop and go fashion whilst the directional movement of the particle. Figure 2-22 shows the track of a representative RBP1-GFP particle on its way through the cell. Each dot marks the position of the focus in a distinct frame. The velocity of the particles were measured as 1.4 ± 0.5 µm s^{-1} (n = 5, in independent cells).

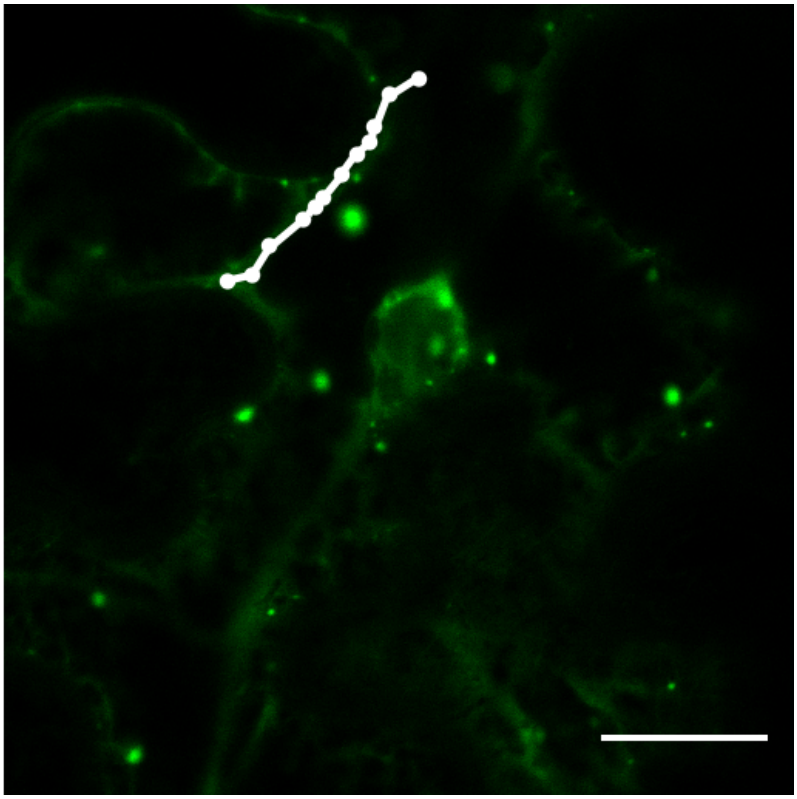

Figure 2-22 Transient expression of RBP1-GFP in *N. benthamiana* and indicated movement of granule.
A time series of the transient expression of RBP1-GFP was taken. The position of a representative granule was marked by a dot in each frame. Ten frames were taken every two seconds. Accumulation of dots indicates a pausing of the granule at certain position, followed by subsequent faster and directed movement, represented by distant marks. Scale bar = 20µm.

With RBP1 having an endogenous RNA binding protein at hands, the dual usage with one of the marker systems was tested. Therefore RBP1-GFP was co-infiltrated with λN_{22}-mCherry-NLS and a 3'-boxB-tagged RNA encoding for the membrane localized protein Nucleobase-Ascorbate Transporter 7 (At1g60030, see Chapter 2.1.5).

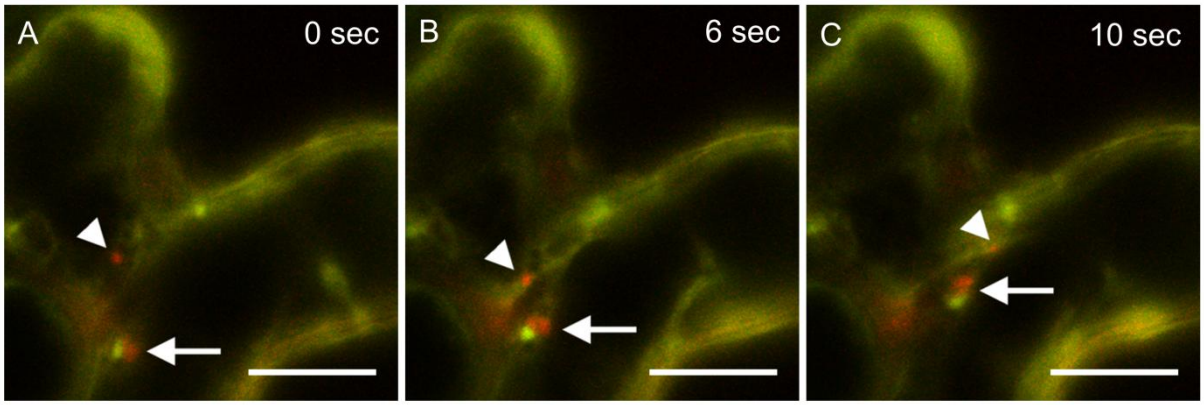

Figure 2-23 Transient expression of RBP1-GFP, λN_{22}-mCherry-NLS and a Nucleobase-Ascorbate Transporter (At1g60030)-16xboxB in *N. benthamiana.*

(A-C) Merged pictures of RBP-GFP and λN_{22}-mCherry-NLS over a time series of ten seconds. When boxB-RNA is co-expressed in the cells, red granules appear within the cytosol (arrowheads), representing particles containing only λN_{22}-mCherry-NLS, besides the abundant green RBP1-granules (not shown). Furthermore, the movement of dually labeled granules could be monitored (arrow), containing both, RBP1-GFP and λN_{22}-mCherry-NLS. Those particles moved in a coordinated manner. The single fluorescent granules circle around each other, which resembles the movement of a Slinky toy. A film, this series is derived from can be viewed on the attached CD. Scale bars represent 10 µm.

Figure 2-23 shows an exemplary picture series of those experiments. Three sorts of granules could be monitored: Green ones, which represented the overall largest fraction, red ones (arrowhead) and a few particles that clearly contained red and green fluorescent signals (arrow). Strikingly, the fluorescence in those particles did not completely colocalize but seemed distinct to each other. Nevertheless the particles moved in proximity and in the manner of a Slinky toy. The velocity of those "dual" particles was measured as 0.5 ± 0.1 µm s^{-1}, which was insignificantly lower than those of the individual red (0.9 ± 0.1 µm s^{-1}) or green (1.4 ± 0.5 µm s^{-1}) particles, which was detected during those experiments (Schönberger *et al.*, 2012).

In the absence of target RNA, the λN_{22}-mCherry remains exclusively in the nucleus whereas the RBP1-GFP doesn't show an altered behavior, which expresses itself in the formation of green RNP granules (Figure 2-24).

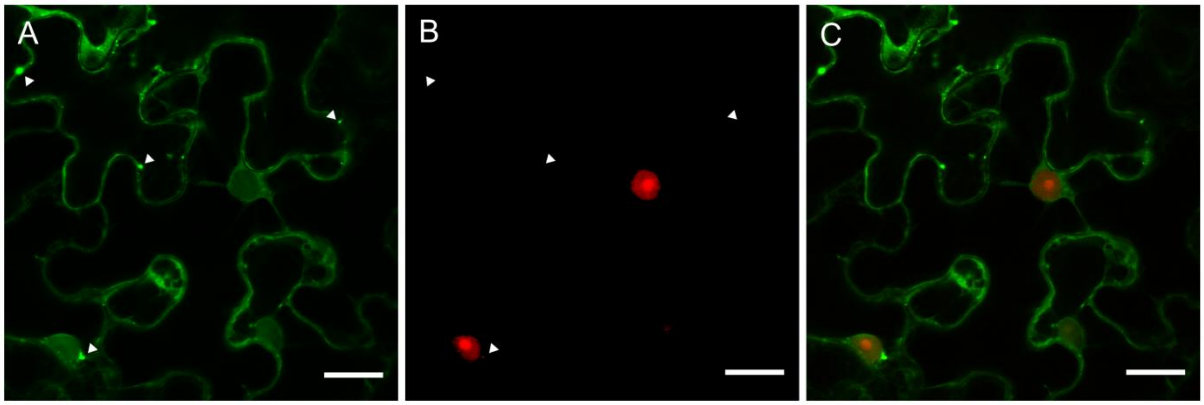

Figure 2-24 Transient expression of RBP1-GFP, λN_{22}-mCherry-NLS without corresponding boxB- in *N. benthamiana.* (A and B) show the fluorescent light images of RBP1-GFP and λN_{22}-mCherry-NLS, respectively. (C) shows the merge of both channels. The RBP1-GFP localizes normally to the cytosol with a concentration of signal in distinct foci (arrowheads in A), whereas the λN_{22}-mCherry-NLS stays within the nucleus when no specific stem-loop RNA is present. Arrowheads in B represent the position of the foci in A. Scale bars represent 20 µm.

The motility of the RBP1 granules indicates a coordinated movement along the cytoskeleton. Transport along both, microtubules and actin microfilaments, has been reported for RNA transport in yeast and animal systems (Munchow *et al.*, 1999; Vallee *et al.*, 2004; Hirokawa *et al.*, 2009). To investigate whether RBP1 associates with the actin cables it was co-infiltrated with a vector coding for Lifeact-RFP. Lifeact is a 17-amino-acid peptide, which binds specifically to F-actin, thus making it a versatile marker actin (Riedl *et al.*, 2008).

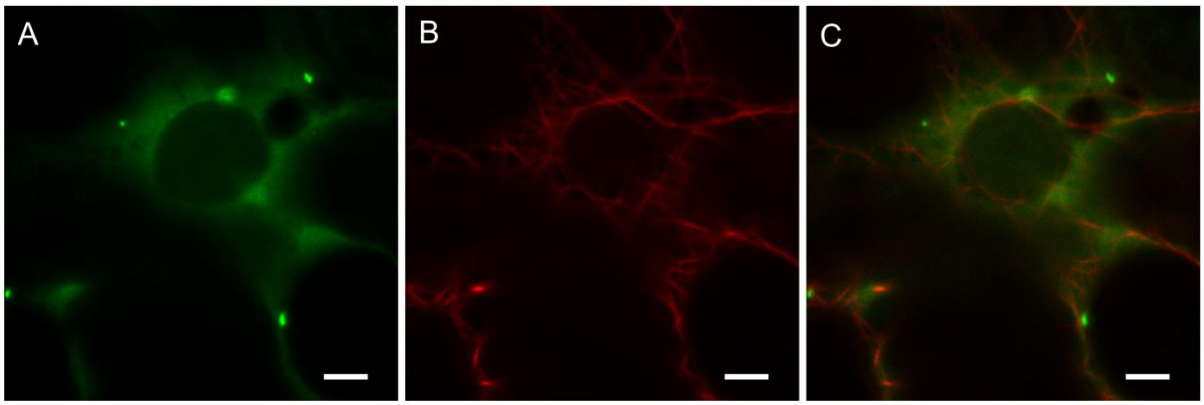

Figure 2-25 Co-expression of RBP1-GFP together with Lifeact-tagRFP in *N. benthamiana* epidermis cells.
RBP1-GFP (A) co-expressed with Lifeact-tagRFP (B). (C) shows the merged pictures. The typical distribution of RBP1-GFP in the cytosol around the nucleus with bright fluorescent signals, which accumulated in cytoplasmic granules, can be observed in (A). Lifeact-tagRFP binds the F-actin, thus revealing the cobweb-like structure of the actin cytoskeleton. The merged pictures in (C) don't allow a clear conclusion of the co-localization of RBP1 granules with actin. Scale bars are 5 µm each.

Based on Figure 2-25, which shows RBP1-GFP together with Lifeact-tagRFP, there is no clear co-localization of the cytoplasmic granule with the actin filaments. If this is really the case or if this is due to technical reasons will be discussed later. More obvious was the finding that RBP1-GFP granules stopped almost all motion when co-expressed with the Lifeact marker constructs. RNPs still formed approximately with the same frequency, as if expressed alone, but they remained more or less static throughout the monitored time. Only a little shivering movement as if moved back and forth with a covered distance of about 1 µm could be detected (see Figure 2-26).

When RBP1 infiltrated leaf sections were treated for 15h with the Myosin ATPase inhibitor 2,3-Butanedione monoxime two days after infiltration, the movement of RBP1 granules came to a full stop, whereas the control sections with buffer only weren't affected (Figure 2-6). This indicates a transport of RBP1 containing particles with a myosin motor along the actin cytoskeleton.

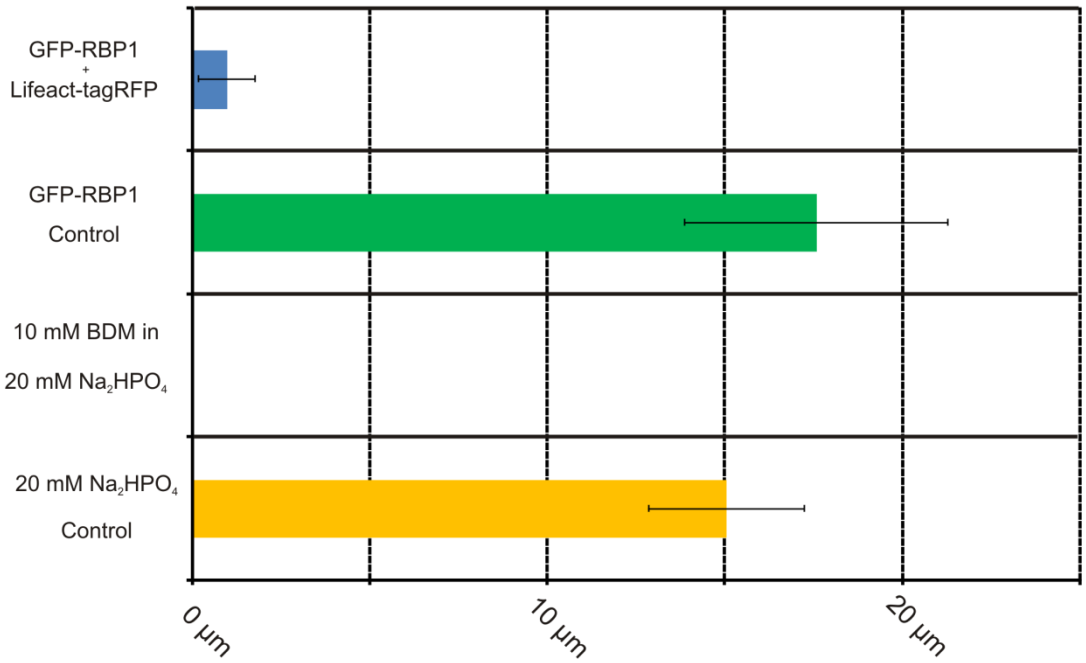

Figure 2-26 Lifeact-tagRFP and BDM affect the motility of RBP1-GFP granules.

RBP1-GFP was transiently expressed in *N. benthamiana*. 48h after infiltration, cells were observed for 80 seconds each and frames were taken every two seconds. From these data the movement of three independent RBP1-GFP granules each was monitored and the distances measured. When cells were co-expressing Lifeact-tagRFP (see Figure 2-25) the motility was almost abolished. Only a little 'shivering' of the foci could be measured, manifesting itself in distances of around 1 µm. A control, with the same time-lapse between infiltration and analysis revealed a high motility of RBP1 granules. Treatment of infiltrated leaf sections with 2,3-Butanedionemonoxim (BDM) even had a stronger effect than Lifeact. Sections were cut out 48 hours after infiltration and kept in 20mM Na_2HPO_4 buffer containing 10 mM BDM for 15h. Granules had formed in normal size and abundance but remained stationary throughout the whole experiment. Control sections kept in Na_2HPO_4 buffer for 15h showed no abnormal behaviour, indicating the viability of the leaf sections after buffer treatment.

2.3.3. Heterologous expression and affinity purification of RBP1

To give a final proof for the observed foci to be RNPs, pull-down experiments were planned to find out the protein composition of those granules on the one hand and to unravel the identity of the putatively bound RNAs. Therefore and for further investigations on RBP1 the protein was expressed in *E. coli* cells for subsequent affinity purification. Primary aims were the co-immunoprecipitation of associated proteins in RNPs, nucleotide-binding affinity studies and CLIP-Seq (Covalent Linking, Immunoprecipitation and Sequencing) to get information about the bound RNAs. Therefore, different tags for affinity purification were fused to RBP1 (Table 2-3).

Table 2-3 List of RBP1 derivatives for heterologous expression in *E. coli*, showing the different tags.

C stands for C-terminal fusion and N for N-terminal fusion, respectively. Yes and No indicating the presence and absence, respectively, of an additional GFP tag, always directly linked with RBP. RBP1 itself has a size of 31 kDa. CBD is the Chitin Binding Domain. MBP is the maltose binding protein, which was either derived from *E.* coli or *P. furiosus*, respectively. N.B. stands for 'No Binding' of protein to affinity matrix. N.E. stands for failed induction of expression.

Name	Position of Purification Tag with respect to RBP1	Size of Tag	Tag for Purification	GFP Yes/ No	Position of GFP with respect to RBP1	Overall size	Behaviour
pSCJ356	C	60 kDa	CBD	Yes	C	125 kDa	N.B.
pSCJ357	C	60 kDa	CBD	Yes	N	125 kDa	OK.
pSCJ362	N	60 kDa	CBD	Yes	N	125 kDa	N.B.
pSCJ363	C	60 kDa	CBD	No	---	100 kDa	N.B.
pSCJ364	N	60 kDa	CBD	No	---	100 kDa	N.B.
pSCJ360	C	21 kDa	GS-Tap	Yes	N	86 kDa	N.E.
pSCJ361	C	21 kDA	GS-Tap	Yes	C	86 kDa	N.E.
pSCJ365	N	26 kDa	GST	Yes	C	91 kDa	N.B.
pSCJ366	N	26 kDa	GST	Yes	N	91 kDa	N.B.
pSCJ367	N	41 kDa	MBP (*E. coli*)	Yes	C	105 kDa	N.B.
pSCJ368	N	41 kDa	MBP (*E. coli*)	Yes	N	105 kDa	N.B.
pSCJ369	N	41 kDa	MBP (*P. furiosus*)	Yes	C	105 kDa	N.B.
pSCJ370	N	41 kDa	MBP (*P. furiosus*)	Yes	N	105 kDa	N.B.

Figure 2-27 shows the crude protein extracts of *E. coli* cells, before and after induction, which were analyzed by SDS-PAGE and subsequent Coomassie staining. The extract from induced cells shows an additional band at the expected size of about 125 kDa of the fusion protein (CBD-GFP-RBP1).

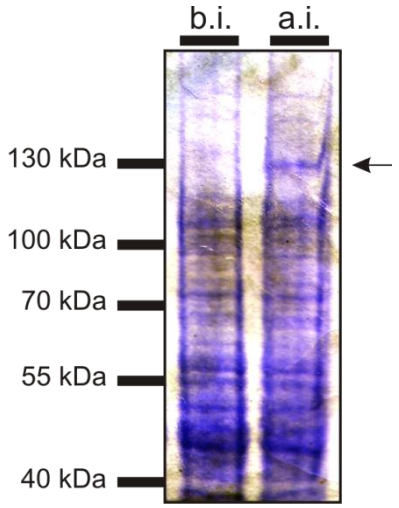

Figure 2-27 Coomassie stained SDS-PAGE Gel of crude *E. coli* extracts 24h after induction of CBD-GFP-RBP1

Coomassie stained SDS-Gel . Each lane contains the crude extract of 0.5 OD cells. The emergence of a weak band in the right lane at the expected size of ~125 kDa indicates the succesful induction of the fusion protein (arrow).

b.i. is 'before induction'; a.i. is 'after induction';

With the method described in Chapter 6.3.5, a GFP-RBP1 fusion could be successfully expressed in *E. coli* cells. In numerous trials, using different buffers (see 6.3.5.), cell breaking procedures and affinity matrices (see Table 2-3), the protein could be induced but never be bound to the affinity matrix (N.B., see Table 2-3). Finally, this could be accomplished by freezing the cells in liquid nitrogen 24 hours after induction and storing them at -80 °C overnight. Obviously, this was the necessary step to establish the binding of the tag to the column. Two prominent bands showed up on the Western Blot in the lane of the final eluate (Figure 2-28). One corresponds to the full-length fusion protein (~70 kDa) and one to free GFP (26 kDa), indicating a fairly high rate of degradation. By applying the given eluate to an Amicon (Millipore®) filter with an exclusion limit of 50 kDa, one can further purify the sample by discarding the free GFP.

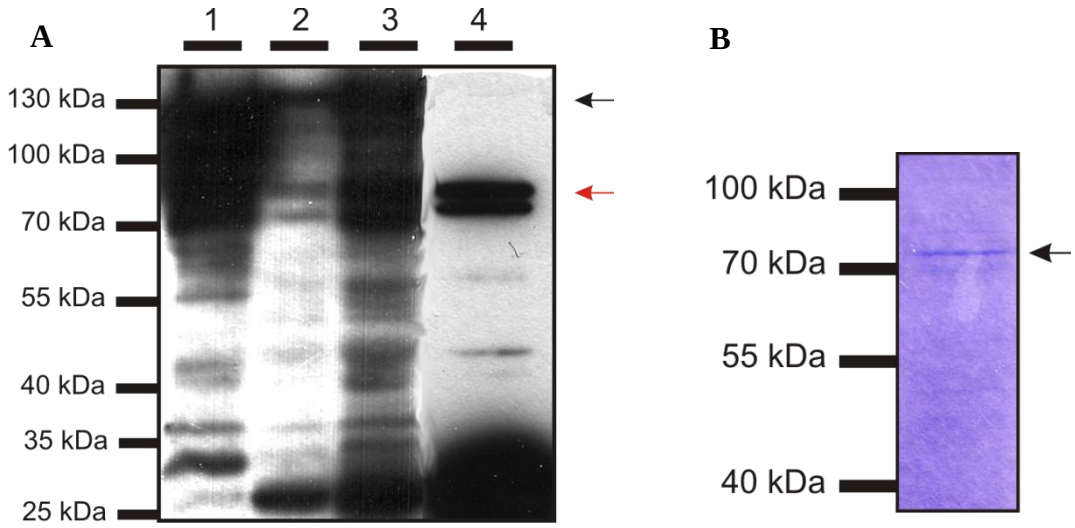

Figure 2-28 Western Blot and Coomassie stained gel of the successful expression, binding and elution.

(A) BL21 cells harboring the construct pSCJ362 were induced with IPTG for 24h at 20 °C. Afterwards, crude protein extract was centrifuged for 30 min at 20 000 g and the supernatant (1) was loaded on a chitin column. After loading (3, flowthrough) the column was washed with 100 ml wash buffer (2; first 5ml) and incubated with elution buffer for 72h at 4 °C in the dark and subsequently eluted (4). The black arrow marks the size of the fusion protein (CBD-RBP1-GFP) at ~125 kDa, which gives the strongest signal in (1-3). The shift towards the size of the RBP1-GFP (72 kDa, red arrow) can be clearly seen and indicates a successful on column cleavage. Amounts were 5 µl each for (1-3) and 1 µl for (4). Western Blot was performed with an α-GFP antibody. For buffers see Chapter 6.3.5.
(B) Coomassie stained gel of 5 µl of the eluate fraction from (A).

The marked band (Arrow, Figure 2-28 B) was analyzed by MALDI MS analysis. By spectral comparison with the Arabidopsis database on NCBI, the band had a protein score of 382 and an ion score of 223. Both scores had coverage of 100 %, meaning that all detected fragments could be annotated with a potential peptide from RBP1. Taken this together, the identity of the protein band being the RBP1-GFP fusion protein could be confirmed doubtlessly.
The hitherto obtained protein, however, was not enough to perform any of the experiments mentioned above. Nevertheless this final procedure could be reproduced and it can be easily upscaled to obtain enough protein.

3. Discussion

3.1. The *in vivo* visualization of RNA in plant cells

3.1.1. The generated vectors offer a broad spectrum for in vivo visualization of RNA

Over the past decade, the knowledge about mRNA and its function beyond being a simple message carrier between transcription and translation has tremendously increased. This was certainly also a result of the enormous improvement of the systems for *in vivo* visualization of RNA. In this thesis the establishment of a vector series for both the λN_{22}-boxB and the MS2CP-MS2 system for RNA visualization and its further application by dual use was established. The importance of this series is highlighted by the great number of request for the plasmids. Since its publication in *The Plant Journal* in January, the plasmid has been sent out to around twenty labs worldwide, which were interested in applying these versatile vectors for their own studies.

Each of the BP was fused to CFP, eGFP, mVenus or mCherry, respectively, in order to facilitate downstream experiments like e.g. protein co-localization or interaction studies via FRET quantification.

Localization of RNA depends on certain features like *cis*-acting zip codes, trans-acting proteins, potentially including the one, it is encoding for, the correct nuclear history, the correct binding of transport complexes to motor proteins and finally the anchoring at the destination site (Martin *et al.*, 2009; Medioni *et al.*, 2012).

The broad spectrum of features makes it obvious, that a lot of conditions have to be considered to leave the RNA as unaltered as possible.

To begin with, the number of repeats of the stem loops should be considered. As a rule of principle a minimum of loops should be used since this likely alters the secondary structure of the RNA least. This might be of importance since global analyses of the yeast transcriptome for example revealed the diversity and importance of the secondary structure of the mRNA for the message itself. Those experiments showed, that the open reading frame is more structured than the UTRs, thus enabling the access of the initiation machinery and localization proteins to those regions (Kertesz *et al.*, 2010; Mauger *et al.*, 2010). On the other hand, the more loops, the more protein can bind to a single molecule, increasing the signal.

For the MS2 system, commonly 24 repeats are used (comp. (Fusco *et al.*, 2003; Wu *et al.*, 2012)), but up to 64 have been reported. In our studies we introduced a six-fold repeat of the

MS2 loops, since this has been shown to be sufficient (Fusco *et al.*, 2003) and this number of MS2 repeats was readily available on a vector. Additionally, it turned out, that the ratio between signal and noise is not an issue with the applied constructs thus making the introduction of a greater number of loops obsolete. Although down to four repeats of boxB loops had been successfully tested (Daigle *et al.*, 2007), the vectors used in this work contained 16 repeats of the 15-nt sequence due to availability. Nevertheless this number was successfully applied in funghi (Konig *et al.*, 2009).

3.1.2. MS2 and λN_{22} are both suitable systems for in vivo studies of RNA distribution in plants

The experiments in Chapter 2.1.2 showed that both systems worked in transient assays. When only the BP-FP was expressed in the cells, the signal remained in the nucleus due to the fused NLS. This resulted in a background free cytosol which gave a high signal to noise ratio. Furthermore, this is crucial for the recognition of a putative RNA gradient within a cell (see Chapter 2.2).

There was even an accumulation of BP-FP in the nucleolus (see 2.1.2). If this was due to a specific pre-assembly site of future RNPs as described recently (Jellbauer *et al.*, 2008) or just a random distribution remains elusive.

Upon co-infiltration of a BP-FP together with an RNA fused to its corresponding stem loop, the fluorescence could also be found in the cytosol. This indicates the functionality of the vectors and thus the systems for the use in plants. These data are consistent with published data for the MS2 system, which had been used in plants before (Hamada *et al.*, 2003; Zhang *et al.*, 2003; Sambade *et al.*, 2008).

The λN_{22} system, however, had never been used in plants before. In this thesis its functionality in plant cells could be shown (Schönberger *et al.*, 2012). Especially due to the presented superiority over the MS2 system, this technical advance adds a new and powerful tool for studying RNA localization and transport in plants.

Also controls with stem-loop-less RNA and labeled RNA from the respectively distinct system revealed no cross-reactions, proofing the binding specificity of the BP in plant cells. This is in line with experiments, where both systems have been used in yeast before (Lange *et al.*, 2008).

A Western Blot analysis was performed to check for integrity of the BP-FP fusion proteins. The λN_{22}-GFP-NLS showed the expected size with or without corresponding RNA. This indicates that all cytosolic fluorescence represents a BP-FP/RNA complex. The MS2CP also showed the expected band in both lanes, e.g. with and without target RNA. In addition to these, however, it also exhibited a band, which corresponded to the size of free GFP, presumably by proteolytic cleavage of the fusion protein in the cytosol as soon as it leaves the nucleus when bound to target RNA. Furthermore, the Blot showed an additional band in both lanes at the size, which corresponds to the dimer. Originally, MS2CP binds its corresponding RNA as a dimer (Valegard *et al.*, 1994). Although several mutations have been introduced to minimize the multimerization by parallel keeping the RNA affinity at a high level (LeCuyer *et al.*, 1995) it is still commonly believed, that only the dimer can bind the RNA. On the contrary, recent studies showed that the dimerization of MS2CP only takes place with very low rates in the cell. Conclusions of this study link non-bound monomeric MS2CP with background signals (Wu *et al.*, 2012). This implies, that the presence of dimers would increase the signal to noise ratio. How these recent findings can be linked with the putative dimer band observed in this study is not very clear, since this band was stable even under treatment with strong reducing agents (200mM DTT).

Nonetheless, the nature of this high-molecular band cannot be clearly determined.

Taken together, both systems can be used in plants. Furthermore the data, obtained from the λN_{22} system seem to be more reliable than those obtained from the MS2 system. Not only is the smaller size of the lambda peptide more favorable over the quite large MS2CP (4 kDa vs. 16 kDa), since it is likely, that this has less influence on the whole protein composition, which assembles as the RNA transport and processing machinery. Additionally, the detected signal in the cytosol might be due to degradation of the fusion protein, as is indicated by the Western Blot, thus raising the background, which is undistinguishable from the signal. Finally, as fluorescence fluctuation spectroscopy data revealed, the MS2CP binds with only very low efficiency (40%) to the stem loops, due to its weak dimerization (Wu *et al.*, 2012). This would result in a non-reliable quantitative RNA visualization, which is not acceptable, mainly in regard to the egg cell project (see Chapter 2.2). This overall finding was further strengthened by the results obtained from the stable Arabidopsis lines, expressing MS2CP (see 2.2.3).

3.1.3. The position of the stem loops influences the capability of the RNA to be translated

The effect of the position of the loops was tested by cloning the stem-loops in 5' and in 3' position of the Gateway™ cassette. In animals Zip codes for RNA localization are often found in the 3' UTR of the RNA like for the beta-actin mRNA (Kislauskis *et al.,* 1994). Those zip code sequences often form secondary structures, which are even more important for the binding of trans acting localization machinery than the nucleotide sequence itself, as was shown before for *bicoid* RNA (Ferrandon *et al.,* 1997). Furthermore, as already mentioned above, the secondary structure seems to be even more crucial for the correct processing, export, localization and translational control of the mRNA than the primary sequence. The lack of a tight secondary structure for example facilitates the binding of a diverse set of proteins, which are necessary for function, localization and post-transcriptional regulation (Mauger *et al.,* 2010). Taken together, it could imply that the position of the loops in 3' position and the subsequent binding of the transport proteins could affect the recruitment of transport proteins and therefore the localization of RNA. Lange *et al* reported a case like this, where the positioning of boxB loops at the 3' end affected the transport of the fairly well examined *ash1* mRNA towards the bud tip (Lange *et al.,* 2008).

Nevertheless, there are also examples for a zip code located within the 5' UTR, e.g. *gurken* (Saunders *et al.,* 1999). In this case, the same objections mentioned above would apply. All those experiments, however, are derived from animal systems. Since there is no global analysis of the 3D structure of mRNA in plants available, it just can be hypothesized that similar mechanisms might play a role there.

In addition to that, the experiments in Figure 2-5 showed that upon infiltration of the RNA encoding for tagRFP, the position of the stem loops was crucial for the translation. Whilst the 3' position didn't affect translation, there was no protein detectable when the loops were in 5' position, although the RNA was detectable (see Figure 2-6). This observation could be made in both systems. Whether this is due to the several ATGs within the stem loop sequences or due to the binding of the BP-FP, thus blocking the ribosomal entry site, or even due to both, remains elusive. Nevertheless, it has been shown in a rabbit reticulocyte translation system that the presence of stem-loops with a high stability, which were placed in close proximity of the 5' cap blocked initiation of translation whereas the same stem-loop, placed 52 nt downstream had no effect. Obviously, those loops do not keep the 40S ribosomal subunit from binding to the mRNA but stops when facing this structure during scanning (Kozak

1989). Additionally, a motif like this can also be used for post-transcriptional gene regulation in the form of riboswitches. Those are *cis*-elements in the 5' UTR of an mRNA, which undergo a conformational shift upon response to an external clue, like temperature shifts or metal ions. When sensing this changed environment, the secondary structure alters, thus enabling or denying the formation of the translational complex (Smith *et al.*, 2010).
In context of the relation between translation and localization, however, it has been described that the protein product of *oskar* mRNA regulates its own RNA localization. In mutants lacking the Oskar protein, a reporter RNA, containing the oskar zip code cannot be localized correctly (Rongo *et al.*, 1995).
Summarizing the influence of the position of the loops reveals that both positions have to been seen with caution. Prevention of translation might have influences on the localization as well as a disturbed secondary structure at any position due to the introduction of stem loops. The subsequent binding of the marker proteins might also affect the assembly of the RNPs. Therefore it is recommendable to always work independently with loops at both positions to minimize any negative effects.

3.1.4. λN_{22} and MS2CP bind mRNA and form microscopically visible transport RNPs

When observing the different visualization systems, the appearance of cytoplasmic foci was evident. Those foci were observed independently from the type of RNA i.e. from tagRFP or endogenous RNA encoding for a secreted or nuclear localized protein and thus independent from translation at free or ER-associated ribosomes (Schönberger *et al.*, 2012).
The true size of a fluorescent particle is difficult to determine, due to the diffuse nature of a fluorescent signal (Barbarese *et al.*, 1995) and the multiple integration of RNA stem loops, thus leading to the binding of several BPs to a single molecule. Nevertheless, the observed diameter of the particles was rather uniform and can be estimated to a size between 800 and 1200 nm. This corresponds to reported RNP particles from rice endosperm cells (Hamada *et al.*, 2003) and the transport of movement particle RNA upon virus infection with TMV (Sambade *et al.*, 2008).
Another supporting evidence for the foci being mRNA transport granules is the way and speed of movement. The movement occurred in a stop-and-go fashion. Especially this alternation between a fast spanning of long distances and the pausing at a static position indicates the involvement of actin fibers in the movement. This pattern was already described for the movement of Golgi stack along actin within plant cells (Nebenfuhr *et al.*, 1999). The

origin of this stop-and-go mechanism is the switch of the motor proteins or the cargo between different actin cables. The involvement of the actin cytoskeleton in the transport of those mRNPs could further be tested by blocking either the motor proteins or disturbing the global integrity of the cytoskeleton. A study like this was done for an endogenous RBP in Chapter 2.3.2.

The directed movement of a foreign RNA like tagRFP along the cytoskeleton to a distinct point seems remarkable. Nevertheless, it has been reported, that diffusion alone wouldn't lead to an even distribution throughout the cell since nonbinding particles underlie a size-dependent diffusion resistance (Luby-Phelps *et al.*, 1987). Furthermore, the foreign *lacZ* RNA is transported in RNPs along the microtubules in mammalian cell culture (Fusco *et al.*, 2003). Additionally, it has been proposed recently that there is a complex interplay between different RNA-containing particles. The nascent RNA transcript is already bound by proteins, which facilitate export and splicing of the RNA, handing it over to stress granules, processing bodies or finally the translational active polysome. This suggests that any mRNA is always found in some form of RNP complex (Layana *et al.*, 2012). This could also give an explanation for the directional transport of *tagRFP* RNA.

When analyzing the speed of the putative RNPs, they were in good accordance with previously reported data from other organisms and tissues, which ranged from 0.4 µm s^{-1} for MS2CP up to 1.6 µm s^{-1} for λN_{22} (Bertrand *et al.*, 1998; Becht *et al.*, 2006; Lange *et al.*, 2008; Zimyanin *et al.*, 2008; Konig *et al.*, 2009). This is also consistent with the findings that e.g. stress granules travel at lower speed of 0.2 µm s^{-1} (Nadezhdina *et al.*, 2010) and the recently published movement of *β-actin* mRNA, monitored by the already mentioned Pumilio system, which estimated the velocity of the moving RNA with 1.78 ± 0.78 µm s^{-1} (Yamada *et al.*, 2011). These findings with the Pumilio system support the assumption that the observed granules of λN_{22} and MS2CP are RNA transport particles.

A third indication for RNPs is the translational control. When λN_{22} particles, harboring *tagRFP* mRNA, were examined more closely, it became obvious, that the co-localization of red and green fluorescence was not absolute. In the cytoplasmic foci the signal is derived from GFP solely, which is obvious in Figure 2-8. This indicates that there is no translational product present within the granules. This is in good accordance with the fact, that translational repression is a common feature of mRNPs. As already described in Chapter 1.3, *ash1* translation is delayed by the binding of the proteins Khd1 and Puf6 to specific *cis*-acting elements within the ORF of Ash1. Those factors are released, e.g. by the phosphorylation of

Khd1, only upon localization of *Ash1* to the bud tip of the cell and translation can occur (Gu *et al.*, 2004; Paquin *et al.*, 2007).

In cells, a wide number of RNPs, which not only transport but also store, process and degrade mRNA, are present. Next to the already mentioned stress granules the P-bodies are a well-characterized pool of foci. Those complexes harbor a wide variety of protein, which are mainly in charge of degrading and silencing mRNA. Therefore controls with DCP2, a known member of the decapping complex, were performed. This enzyme is an essential part of P-bodies (van Dijk *et al.*, 2002). Obviously, transient expression of a GFP-fusion revealed a different pattern. For one, the P-bodies remained static throughout the whole course of the experiment in contrast to the highly motile λN_{22} and MSCP2 particles. Additionally, the size of the putative mRNPs is rather uniform (Schönberger *et al.*, 2012), whereas the P-bodies show a broad size spectrum (200 – 600 µm, Figure 2-9), which fits with the previously reported data (Xu *et al.*, 2006).

In summary, all those finding support that RNA is transported within granules in plants. The movement of those granules can be monitored *in vivo* by applying the generated visualization system.

3.1.5. λN_{22} and MS2CP can be simultaneously used to monitor different pools of RNPs in planta

Due to the availability of the binding proteins in different colors a straightforward experiment was the simultaneous visualization of two distinct RNAs and RNPs. As it can be seen in Figure 2-11, this was possible. Nevertheless, it must be said that because of the "quick movement of the granules simultaneous tracking of two populations of granules requires patience and sophisticated equipment" (Schönberger *et al.*, 2012). Also the prerequisite of a quadruple transformed cell gives only a very low output. This obstacle could be overcome by cloning BP-FP and target RNA on one vector, thus reducing the necessary number of plasmids.

All those findings taken together, the reporter system MS2CP and λN_{22} work very well in transient assays for visualizing RNA. They could also be applied simultaneously and the monitoring of RNPs during their putative movement along the cytoskeleton is possible. With the generated vector series, we hold a versatile tool in hands, which allows us the quick analysis of any RNA. Further experiments like interaction studies of different proteins of the

RNP complexes via the quantification of FRET efficiencies or CLIP should also be possible. In the latter method, the RNA/protein complexes are **C**ovalently **L**inked and subsequently **I**mmuno-**P**recipitated (CLIP). Afterwards, the bound RNAs can be subjected to RNA sequencing whereas the identity of the proteins can be revealed via mass spectrometry. This would give a boost in the understanding of the assembly and constitution of mRNA transport particles in plant cells.

The vectors can also be applied if, beside the biochemical analysis of the RNPs, the visualization of localized RNA is desired. Positioning of the loops must be considered, since the localization elements of an unknown RNA cannot be predicted properly. Next to this and in accordance with data presented in Chapter 2.2.3, we found the λN_{22} system more reliable than the MS2CP system. This manifests itself mainly in a higher fluorescence background in the cytosol when using the latter one. We therefore recommend the use of the λN_{22} system together with RNA containing the stem loops in 5' and 3' position independently to give the best signal to noise ratio and to rule out any position effects of the attached stem loops.

3.2. The detection of an RNA gradient within the Arabidopsis egg cell

3.2.1. A versatile vector series for the high-throughput study of RNA visualization in the Arabidopsis egg cell

The use of the RNA detection systems λN_{22} and MS2 has already been extensively discussed in Chapter 3.1. In this chapter, only the different promoter of the vector series, which was built up for the high-throughput screen to monitor polarly distributed RNAs in the egg cell is highlighted. The egg cell specific promoter *EC1.1* (Sprunck *et al.*, accepted), which drives the expression of the second strongest gene within the egg cell (Šoljić et al, unpublished) was used for both parts of the systems, the markers and the stem-loop vectors. A risk, resulting from the use of such a strong promoter is the formation of artifacts by over-expression. Nevertheless, the accessibility of the egg cell within the embedding tissue requires a strong signal in order to visualize a putative gradient of RNA. Experiments with the RNAs of WOX2 and WOX8 under their endogenous promoters and the use of the MS2 system failed in detecting the presence of the RNAs in the egg cell (Thomas Laux, personal correspondence). *In situ* hybridization, however was sensitive enough for the detection in the embryo and showed the presence of *WOX2* to be exclusive to the apical cell, whereas *WOX8* could only be detected in the basal cell (Breuninger *et al.*, 2008). Yet, the egg cell itself is due to its size and position within the surrounding tissue technically not accessible to detect a potential RNA gradient with the *in situ* hybridization technique.

Another important feature of the *EC1.1* promoter is, that it shuts down directly after fertilization (Sprunck *et al.*, accepted). This ensures that the RNA was already present before fertilization and that it derives from the maternal side. Recent studies have shown the delivery of a paternal RNA into the egg cell, which then triggers a MAP kinase cascade. This SHORT SUSPENSOR (SSP) acts on YODA, which is supposed to be involved in the regulation of the differential expression of WOX 2, 8 and 9 (Zhang *et al.*, 2011). While this is a single example for a paternal influence on embryo development, it is widely believed, that maternal factors are the driving force in early embryo development. It has been shown that the RNA polymerase II is less active in the zygote and early embryo compared with the endosperm, which would indicate a less active transcriptional level (Pillot *et al.*, 2010). Thus, the maternally delivered RNA would be translated in the early phase of the plant embryo. Supported by findings like this, and the fact, that in animals most transcripts in the zygote are derived from the maternal side, the egg cell specific promoter is considered to be a versatile

tool in unraveling the distribution of maternally derived RNAs within the early development of the Arabidopsis plant.

In addition to the tissue specificity of the expression, the choice, which RNA form of the candidate genes should be investigated is a crucial part of the experiment. It was already mentioned, that especially the UTRs of an mRNA are important for regulation by recruiting *trans*-acting factors. The influence of the stem loops, which are adjacent to either the 5' or the 3' UTR of the RNA has been extensively discussed in Chapter 3.1.3. But not only those non-translated regions are important for the localization of the RNA, as they contain the zip codes in most of the cases. It has also been shown, that splicing processes can be essential for the correct localization of the RNA. As was introduced in Chapter 1.4, *oskar* RNA in the Drosophila egg cell is located to the posterior pole but it requires at least one intron for this localization (Hachet *et al.,* 2004). Furthermore, all four core proteins of the exon junction complex, which are essential for splicing, colocalize with the RNA at the posterior pole (Palacios *et al.*, 2004). Due to those findings and the knowledge of the importance of the UTRs for the correct localization of RNA the genomic regions of all candidate genes were cloned, including UTRs and introns. This should rule out the possibility to experimentally alter the correct distribution of the investigated RNA.

3.2.2. A candidate list of putative polar RNA candidates was generated based on single cell microarray studies from the female gametophytes of Arabidopsis and Maize

Based on microarray data from Arabidopsis egg cells (Šoljić et al, unpublished) and embryonic apical and basal cells from maize (Krohn et al., unpublished) a list of candidate RNAs was generated, which is under investigation. The genes were primarily sorted for high abundance in the egg cell. A second criterion was a potential unequal distribution of the ortholog in the maize data set. Finally the data were compared with the data set available on the eFP browser published by Casson *et al* (Casson *et al.,* 2005). Nevertheless, the latter data have to be handled with care. For this approach, single cells were obtained by laser capture microdissection. Maybe due to the technical limitations of this method, the standard error of a large number of expression values is very high. With this in mind, the sometimes contradicting distribution between apical and basal cell, e.g. for the gene with the accession number At2g20130 could be explained. Another reason for this could be that while capturing

the basal cell of the globular embryo cells from the suspensor were also captured, thus adding also a transcriptional level of genes of the pro-embryo to the basal data set.

The list of putatively polarized RNAs is divided into four major subgroups. The first one is the group of transcription factors. This is not surprising, since the temporal and spatial regulation of gene expression is a pivotal element of every developmental process. A prominent example for a transcription factor, whose mRNA is localized, is *bicoid.* The RNA localizes to the anterior side of the egg cell. The translated protein thus forms a anterior-posterior gradient, which leads to the distinct activation of the gap class genes (Driever *et al.,* 1988), which triggers the activation of further genes which are essential for the development of the mature fruit fly.

The second class of RNAs, which is investigated, is the group of RNA binding proteins (RBPs). RBPs can be important in the correct localization of mRNA, e.g. Staufen is essential for *oskar* mRNA locality determination. But also RNA of such RBPs can be distributed unequally, e.g. nanos in Drosophila. The RNA of *nanos* is accumulated at the posterior pole of the early embryo. When it gets translated it binds to the 3' UTR of *hunchback* thus keeping it at a repressional state (Sonoda *et al.,* 1999). Through the gradient, the translation of hunchback is facilitated at the anterior pole, where it is not suppressed by Nanos, thus leading to an inverse gradient.

The third fraction of candidate RNAs was literature derived. The role of WOX2, WOX8 and auxin, with PIN1 being an auxin transporter, has already been introduced in Chapter 1.2.

The auxin response factor *monopteros* (*mp*) and its repressor *bodenlos* (*bdl*) both work antagonistically in the same pathway. It was shown, that both genes are expressed in the hypophysis of the early embryo and are involved in the formation of the root meristem (Hamann *et al.,* 2002). Furthermore, mutations in either of the genes resulted in abnormal embryo formation. This manifests itself in a disorientation of the division plane of the apical daughter, which leads to double-octant proembryos (Berleth *et al.,* 1993; Hamann *et al.,* 1999). Due to the crucial role of those genes in early embryogenesis they were taken up in the list.

The last subgroup on the list is very diverse and has no common motif. These genes were picked because of their high expression values in the egg cell microarray and their, in some cases, unequal expression after the first cell division according to the dataset from the eFP browser or the maize microarray. A potentially interesting candidate, due to its protein product being involved in a metabolic pathway, is the gene with the accession number At4g17770, which encodes for the Trehalose phosphate synthase 5 (TPS5). The class of TPS

proteins phosphorylates trehalose to form trehalose-6-phosphate. Normally it interacts with a trehalose phosphatase (TPP) in an antagonistic fashion. The Arabidopsis genome encodes for eleven TPSs but so far, the catalytic function could only be shown for TPS1. Nevertheless, the other genes of this family are supposed to posses regulatory next to their catalytic functions (Schluepmann *et al.*, 2009). Furthermore, Arabidopsis tps1 mutants are embryo lethal, linking the metabolic pathway very close with early embryonic development (Eastmond *et al.*, 2002).
Taken all those elements together, the candidate list, presented in Table 2-1 shows a broad spectrum of genes, which might have a polar RNA localization and thus this list is a good starting point for the high-throughput study.

3.2.3. λN_{22} exhibits a reliable expression pattern and subcellular localization under egg cell specific expression

When the RBP markers were introduced into Arabidopsis wild type plants, they showed a clear difference between the λN_{22} and the MS2 system. Although extensively tested in transient assays (Schönberger *et al.*, 2012), the MS2CP showed cytosolic background. As was observed in the transient experiments (see Chapter 2.1.2), this might be the result from proteolytic cleavage of the fusion protein. Furthermore, the promoter was leaky and showed signals in the synergids in several plants examined. A reason could be positional effects of the integrations. None of this was the case for the λN_{22}, which showed an exclusive nuclear localization and no expression in the synergids.
Together with the findings obtained from the transient experiments (see Chapter 2.1.2) the λN_{22} was the first choice for the further experiments.
After obtaining a homozygous line, this was crossed with several candidates, with the boxB stem loops attached to the 3' UTR. So far, none of the candidates tested showed a polar localization in the egg cell. Obviously, the system itself works, since there is a clear relocalization of signal into the cytosol, although this is very weak. Nevertheless, a gradient could not be observed. Since the Arabidopsis egg cell contains a very large vacuole only a little part of the cell is comprised of cytosol. This might impede the visibility of a gradient, if there is one. For this purpose, a working positive control would be essential but is so far unavailable, since also *WOX2* and *WOX8* showed no polar distribution according to the data obtained from the λN_{22} system.

3.2.4. Subcellular localization studies of translational products of all candidate RNAs provide supporting information for subsequent biological studies of polarly distributed transcripts

The subcellular localization studies of the proteins, which are encoded by the candidate RNAs didn't reveal any surprising insights. The data were consistent with the predictions made by databases (www.arabidopsis.org). Nevertheless, the information gained might be useful for subsequent experiments. If one of the RNAs turns out to be unequally distributed between the apical and basal cell of the first cell division, the knowledge of the protein localization linked with its putative function might ease the access to further studies. Furthermore the proteins fused to GFP under the control of their endogenous promoters are currently under investigation.

3.3. Characterization of an endogenous RNA binding protein

3.3.1. RBP1 (At4g17520) forms cytoplasmic foci resembling RNPs

When RBP1 (At4g17520) was analyzed for subcellular localization, the visible granules resembled very closely the pattern, which is typical for known RNA binding proteins (RNPs) such as the transport protein from tobacco mosaic virus or λN_{22} (Sambade *et al.,* 2008; Schönberger *et al.,* 2012).

This was the initiation for a further analysis of RBP1 and its homologs in Arabidopsis, At4g16830, named RGGA, and At5g47210, named RBPX.

In addition to the bioinformatical data introduced in Chapter 2.3.1, the subcellular localization of RBP1, RGGA and RBPX is a strong indicator that those proteins really function as RNA binding proteins since they localized to granules, which are transport through the cell via the actin cytoskeleton as described for other RNPs. In the case of RBP1 the observed foci have the same size as the RNA bound λN_{22} and MS2CP granules and the same velocity as the λN_{22} particles described in Chapter 2.1.4 (800 – 1200 nm).

The expression profile of RBP1 showed an expression in all tissues examined at a rather similar level with the highest value in open flowers. This showed a significant increase about two-fold compared to the other tissues. This indicates RBP1 to be rather an unspecific RNA binding housekeeping gene. Nevertheless, due to elevated expression level in young flowers it might play a more specific role in the formation of the gametophytes but this can only be speculated.

With RBP1, however, we hold a valuable tool in hands to combine an endogenous RNA binding protein with the artificial λN_{22} system, which was described in Chapter 2.1.1. After co-expression of RBP1-GFP, λN_{22}-mCherry-NLS, and an endogenous RNA, green granules were observed most frequently. Those consisted only of RBP1-GFP. Foci, which were comprised exclusively of red λN_{22}-mCherry, however, were less abundant. This is not surprising, since RBP1 is an endogenous RNA binding protein with a low specificity for RNAs compared to the highly specific binding of λN_{22}. Intriguingly, a lot of granules contained both distinct red and green fluorescent protein. Those granules moved insignificantly slower than the granules, which only contained one sort of binding protein (0.5 ± 0.1 µm s^{-1} vs. 0.9 ± 0.1 µm s^{-1} (red) and 1.4 ± 0.5 µm s^{-1} (green), respectively) (Schönberger *et al.,* 2012). What is more interesting is the fact, that both fluorescent signals could be distinguished within the higher order complex. Nevertheless, those two adjacent granules

moved together presumably along the cytoskeleton, since they also showed the typical stop-and-go movement (Schönberger *et al.*, 2012). Besides that, the movement of those "tandem" particles resembled the movement of a Slinky toy. A similar movement could be monitored for the transport of prolamine RNA in rice (Hamada *et al.*, 2003). The formation of large RNPs, which contain a lot of different and structurally not-related proteins, has already been shown in yeast, where *Ash1* is transported in such a heterogeneous RNP (Muller *et al.*, 2011). The "tandem" particle, which is described above is also a large complex, which probably consists of several more RNAs and RBPs. Whether in this case a protein or even an RNA molecule work as a scaffold remains elusive.

3.3.2. RBP1 containing RNPs are transported along the cytoskeleton

When RNPs are transported through the cell they are moving along the cytoskeleton in a process mediated by motor proteins. Transport along microtubules together with dyneins or kinesins has been reported for most transported mRNAs described so far in yeast and Drosophila probably due to the high polarity of microtubules, resulting in an efficient and direct transport of the cargo RNA. Nevertheless, the myosin-driven motion along the actin cytoskeleton has also been described (Gagnon *et al.*, 2011). Therefore, an experiment to investigate the interaction between RBP1 and the cytoskeleton was designed. Recently, Lifeact, a 17-amino-acid peptide binding F-actin has become a widely used *in vivo* actin marker (Riedl *et al.*, 2008). Co-infiltration of RBP1-GFP with Lifeact-tagRFP revealed no clear indication for an interaction. From Figure 2-25 no clear co-localization can be concluded. This might be due to the high dynamics of actin fibers in combination with the technical limitations of using the LSM510 confocal microscope. Since a cross talk between GFP and RFP should be excluded from co-localization experiments, a sequential scan of the two channels must be applied. Due to the hardware, filters have to be switched in the hardware, which takes some milliseconds, thus resulting in a short time gap between the capture of the two frames. This is time enough for the cytoskeleton to rearrange. Therefore, the microscope pictures cannot give a final answer. Yet, what is more intriguing is the reduced dynamics of RBP1 granules when co-infiltrated with Lifeact-tagRFP. In those experiments, only a slight shivering of the granules instead of directed movement could be detected. Controls under the same conditions, without the actin marker, showed the typical behavior. This lead to the conclusion, that RBP1 is somehow associated with the actin cytoskeleton. It has been shown, that Lifeact doesn't affect the dynamics of the actin skeleton

and associated motor proteins (Era *et al.,* 2009), although some data suggest, that under strong overexpression of Lifeact, the actin dynamics can be disturbed through the excessive binding of Lifeact to the F-actin molecules (van der Honing *et al.,* 2011). The binding of a lot of Lifeact molecules to the actin potentially acts like the isolation of an electric wire, thus preventing the binding of normally associated proteins, like kinesins. A similar observation has been described for the actin binding domain of mouse talin, which had been used as an actin marker before the introduction of Lifeact (Holweg 2007). This expression-level derived influence might be the case, when expressing Lifeact-tagRFP under the control of the *UBQ10* promoter, which is quite strong in transient assays (Grefen *et al.,* 2010). For further analysis, the myosin ATPase inhibitor 2, 3-Butanedione monoxime (BDM) was applied to RBP1 expressing leaf sections. This lead to a quantitative abortion of RBP1 granule movement. In plants, several transport mechanisms have been linked to myosins, like organelle movement or the transport of viral particles (Sparkes 2010). Higher plants only posses two classes of myosins, type VIII and XI, respectively. Interestingly, the myosin type XI in plants is structurally related to type V myosins in yeast. The motor protein, which is responsible for *Ash1* localization is a Myo4p a class V myosin motor (Jansen *et al.,* 1996). Taken this together, the disturbance of the plant myosins by BDM could disturb the movement of RBP1 granules along the actin cytoskeleton. However, the specificity of BDM for solely affecting myosin is questioned (McCurdy 1999). The combined results from those experiments strongly indicate a movement of RBP1 containing granules along the actin cytoskeleton via myosin motor proteins. Nevertheless, further experiments have to be done to support this hypothesis. One is the co-immunoprecipitation of RBP1 and myosin. Another is immunostaining for RBP1 and components of the actin cytoskeleton in a fixed tissue to show a clear colocalization.

3.3.3. RBP1 can be purified from E. coli

To further deepen the knowledge about RBP1 and the composition of its putative RNPs, the protein should be heterologously expressed in *E. coli*. As the Chitin Tag, provided by the IMPACT™ system from NEB®, worked very well for the purification of GFP in our lab before (Data not shown), this was the first choice for the purification of RBP1. As a second tag, GFP was chosen, to have an antigen for subsequent co-immunoprecipitation experiments. A reproducible procedure with satisfying protein yields could finally be established. Obviously, a deep-freezing of the induced *E. coli* cells in liquid nitrogen leads to a

conformational shift within the three-dimensional structure of the protein, thus releasing the hitherto hidden tag, which enabled the binding of the protein to an affinity matrix. So far, the necessity of a cold shock for “activation” of an affinity tag has not been described. It remains elusive, however, whether this rapid freezing really leads to the exposure of the tag or if another reaction is triggered.

With the successful purification of the protein, the experiments mentioned above can be performed for a further characterization. Furthermore, the purification should be repeated without a GFP tag to be able to obtain antibodies against RBP1, which will be necessary for further experiments as well as validation of previously obtained ones.

4. Summary

Polar cell division is a key mechanism for the development of any multicellular organism throughout all kingdoms of life. In order to cope with the challenge of how to establish a differential cell fate for daughter cells, which share a common mother, nature had come up with several solutions. One mechanism, which is found in all species from yeast to mammals, is the polar localization of mRNA to a distinct pole of the cell. While several pathways of unequal RNA distribution have been uncovered over the past few years in animals the kingdom of plants remains a "terra incognita" for this mechanism, although polar cell divisions occur frequently in plants. For example, the egg cell of *Arabidopsis thaliana*, is already a highly polarized cell and subsequent division of the zygote results in a small apical and a large basal cell. This knowledge led to the hypothesis, that this first very asymmetric cell division might be regulated by the distinct localization of mRNA within the egg cell.

To address this issue, two systems for RNA visualization were used, λN_{22} and MS2 respectively, which take advantage of the binding of virus-derived RNA binding proteins (RBP). These are fused to a fluorescent protein for visualization, to specific RNA stem loops. A vector series for both systems to be used in plants could be generated. For the first time, the functionality of the λN_{22} system in plants was shown. Furthermore the monitoring of the transport of mRNA in high-molecular ribonucleoprotein (RNP) particles in plant cells could be established for both systems. Intriguingly, the simultaneous use of both systems facilitated the parallel monitoring of two distinct RNPs, carrying two distinct RNAs. Holding this tool in hands, which include the binding proteins fused to CFP, GFP, mVenus or mCherry, respectively, and a Gateway™ based stem loop series, which enable high-throughput studies, is a great step forward in the elucidation of general processes of RNA transport within plant cells.

After establishing the RNA visualization in plants, the system was adopted for the monitoring of RNAs in the Arabidopsis egg cell. For this purpose, the egg cell specific promoter *EC1.1* was used to drive expression of the detection systems. A special feature of this promoter is the immediate shutdown of expression after fertilization. This ensures the mRNA being of maternal origin. As subject of study, a list of genes was generated, of which the RNAs were investigated upon their localization in the egg cell by fusing them to the corresponding stem loops. This list was based on single cell array data from Arabidopsis and Maize egg cells and embryos, respectively, and includes transcription factors, RNA binding proteins and various other functions. The cloned RNA-loop constructs were crossed into a line, stably expressing

the corresponding binding protein. The use of the system in the egg cell could be shown but so far, however, no candidate RNA showed a polar distribution in the egg cell.

Additionally, during the course of all experiments, λN_{22} showed a clear superiority over the MS2 system in terms of stability and reliability, thus promoting the preferential use of the first one.

In addition to the investigation of the RNA distribution in the egg cell, an endogenous RNA binding protein, RBP1, was examined more closely. RBP1 showed a similar behavior as the heterologous λN_{22} and MS2 systems respectively, as the formation of microscopically visible RNPs and their transport properties. Additionally, the transport of labeled RNA together with endogenous RBPs could be shown by the simultaneous use of the endogenous RBP and λN_{22}. Further studies on this protein suggested association and transport of the formed RNPs with the actin cytoskeleton. Finally, RBP1 was expressed in the heterologous *E. coli* system. A method for purification could be established which enables subsequent experiments like binding assays, Co-IP and CLIPs, which will give a further insight into the nature of plant RNPs.

All those data together lay the groundwork for extensive studies of RNA distribution, transport, localization as well as RNP formation in plants, which will help to uncover the central role of mRNA.

5. Zusammenfassung

Polare Zellteilung ist ein Schlüsselmechanismus bei der Entwicklung sämtlicher vielzelliger Organismen in allen Königreichen des Lebens. Um mit der Herausforderung, unterschiedliche Zellschicksale von Tochterzellen, welche von einer gemeinsamen Mutter abstammen, zu etablieren, kam die Natur auf mehrere Lösungen. Ein Mechanismus, welcher von der Hefe bis hin zum Menschen beschrieben wurde, ist die polare Verteilung von mRNA zu einem bestimmten Pol der Zelle. Während in Tieren einige dieser Prozesse in den letzten Jahren aufgeklärt werden konnten, bleibt das Königreich der Pflanzen eine Art „Terra incognita" für diesen Mechanismus, obwohl auch in Pflanzen eine Reihe höchst polarer Zellteilungen stattfindet. Die Eizelle von *Arabidopsis thaliana* zum Beispiel ist bereits eine stark polare Zelle und die folgende erste Zellteilung der Zygote führt zur Entstehung einer kleinen Apikal- und einer großen Basalzelle. Mit diesem Wissen als Grundlage wurde die Hypothese aufgestellt, dass diese erste asymmetrische Zellteilung durch die spezifische Lokalisierung von mRNA innerhalb der Eizelle gesteuert wird.

Um diese Frage zu beantworten wurden zwei Systeme zur RNA-Visualisierung, das λN_{22} und das MS2, verwendet. Diese nutzen die Eigenschaft viraler RNA Bindeproteine (RBP), welche zur Visualisierung mit Fluoreszenzproteinen fusioniert sind, an sequenzspezifische RNA-Strukturen zu binden. Es gelang, eine Vektorserie beider Systeme für den Gebrauch in Pflanzen zu generieren. Die Funktionalität des λN_{22} System konnte zum ersten Mal überhaupt in Pflanzen gezeigt werden. Zusätzlich konnte die Beobachtung des Transports von mRNA in hochmolekularen Ribonucleoproteinpartikeln (RNP) in Pflanzenzellen etabliert werden. Durch die parallele Anwendung beider Systeme war es zudem möglich, zwei unterschiedliche RNPs, welche unterschiedliche RNAs enthielten, zeitgleich zu detektieren. Somit wurde ein Werkzeug geschaffen, welches RBPs fusioniert mit CFP, GFP, mVenus und mCherry ebenso beinhaltet wie eine Gateway™ basierte Vektorserie für die Fusion mit den spezifischen RNA-Schleifen, und dadurch Hochdurchsatzanalyse von RNAs ermöglicht. Dies ist ein großer Schritt vorwärts bei den Bemühungen die allgemeinen Prozesse des RNA Transports in Pflanzenzellen zu verstehen.

Nachdem das Visualisierungssystem in Pflanzen etabliert werden konnte wurde es für die Beobachtung von mRNA in der Arabidopsis Eizelle adaptiert. Zu diesem Zweck wurde der eizellspezifische Promotor *EC1.1* verwendet um die Expression beide Teile des Detektionssystems zu steuern. Eine besondere Eigenschaft dieses Promotors ist es, sofort nach der Befruchtung abgeschaltet zu werden. Dies stellt sicher, dass die untersuchte RNA

maternalen Ursprungs ist. Es wurde eine Liste von Genen erstellt, deren RNAs auf eine polare Lokalisierung in der Eizelle hin untersucht werden sollen, indem sie mit den spezifischen RNA-Schleifen fusioniert werden. Diese Liste basiert auf den Microarray-Daten isolierter Arabidopsis Eizellen, den apikalen und basalen Zellen des frühen Maisembryos sowie Zellen des weiterentwickelten Embryos. Sie beinhaltet Transkriptionsfaktoren, RNA Bindeproteine sowie Transkripte unterschiedlichster Funktion. Die so klonierten RNA-Schleifen-Fusionen wurden in eine Pflanzenlinie gekreuzt, welche das entsprechende Bindeprotein stabil exprimiert. Die Funktionalität des Systems in der Eizelle konnte gezeigt werden, jedoch zeigte bisher keine der untersuchten RNAs eine polare Verteilung innerhalb der Eizelle.

Zusätzlich zeigte sich während sämtlicher Experimente eine klare Vorteilhaftigkeit des λN_{22} Systems gegenüber dem MS2 System in Bezug auf Stabilität und Zuverlässigkeit, weswegen es nun dauerhaft als Einziges zum Einsatz kommt.

Neben der Untersuchung der RNA Verteilung in der Eizelle wurde ein endogenes RNA Bindeprotein, nämlich RBP1 genauer charakterisiert. RBP1 zeigt ein ähnliches Verhalten wie die heterologen Systeme λN_{22} und MS2, wie die Bildung von mikroskopisch sichtbaren RNPs. Zusätzlich konnte durch die simultane Expression von RBP1 und λN_{22} der Transport von markierter RNA mittels eines endogenen RBPs gezeigt werden. Weiterführende Experimente deuten auf eine Assoziation des Transports von RBP1 Partikeln mit dem Aktin Cytoskelett hin. Abschließend wurde RBP1 heterolog in *E. coli* exprimiert. Eine Methode zur erfolgreichen Aufreinigung konnte etabliert werden, was in der Folge weitere Experiment wie die Untersuchung der Bindeeigenschaft, Co-Immunopräzipitation oder CLIP ermöglicht. Dies wird helfen die Natur von RBPs besser zu verstehen.

All diese Daten zusammengenommen haben das Fundament für extensive Untersuchungen der RNA Verteilung, Lokalisierung, des Transports und der Zusammensetzung von RNPs in Pflanzen gelegt, welche helfen werden, die zentrale Rolle von mRNA besser zu verstehen.

6. Material and methods

For all reactions and experiments, only molecular grade and p.a. (per analysis) chemical reagents have been used. Molecular biological work was mainly based on protocols, published by Sambrook *et al* (Sambrook *et al.*, 1989).

6.1. Cultivation of bacteria

The Cultivation of *E. coli* in liquid culture was performed in LB media at 37 ºC. Agrobacteria were cultured in LB at 30 °C. The Antibiotics were added after autoclaving to the following final concentrations:

Ampicillin	100 µg/ml
Chloramphenicol	50 µg/ml
Kanamycin	50 µg/ml
Spectinomycin	50 µg/ml
Streptomycin	10 µg/ml

LB media

1.0 % Bacto Tryptone (w/v)
0.5 % Yeast Extract (w/v)
1.0 % NaCl (w/v)
Optional
1.8 % Bacto Agar (w/v)

6.2. Molecularbiological Methods

6.2.1. Polymerase chain reaction (PCR)

6.2.1.1. Phusion™ DNA-Polymerase

Reactions (Phusion™)

5 µl	5x Phusion™ HF-buffer
0.5 µl	dNTP (10 mM)
0.5 µl	Primer Forward (10 µM)
0.5 µl	Primer Reverse (10 µM)
x µl	DNA Template
0.3 µl	Phusion™ DNA-Polymerase
0.6 µl	DMSO
ad 20 µl	ddH_2O

Program

98 °C	60 sec	
98 °C	15 sec	} 30x
53 °C	15 sec	
72 °C	t_E	
72 °C	10 min	
10 °C	hold	

The amount of DNA used as a template was dependant on the nature of the DNA. Of plasmid DNA 0.1 µl was used, while 1 µl were used from a preparation of genomic DNA.
The extension time t_E was calculated upon the lengths of the amplicon, given an amplification rate of the Phusion™-Polymerase of 2 kb/min.

6.2.1.2. Taq DNA-Polymerase

Reactions

2 µl	10x Taq-Buffer
2 µl	50 mM $MgCl_2$
1 µl	dNTP (2 mM)
1 µl	Primer Forward (10 µM)
1 µl	Primer Reverse (10 µM)
x µl	DNA Template
0.3 µl	Taq DNA-polymerase
ad 20 µl	H_2O

Program

98 °C	3 min	
98 °C	1 min	30x
53 °C	1 min	
72 °C	t_E	
72 °C	10 min	
10 °C	hold	

The extension time t_E was calculated upon the lengths of the amplicon, given an amplification rate of the Taq-Polymerase of 1 kb/min.

6.2.2. Isolation of highly pure genomic DNA from Arabidopsis thaliana

For the amplification of genes, a highly pure genomic DNA was used. For this purpose, fresh plant material is frozen and ground to a fine powder in liquid nitrogen. 5 ml of prewarmed (60 °C) extraction buffer are added per 3 g of fresh plant material and incubated at 60 °C in a water bath. Afterwards, the same volume of a mixture of chloroform and isoamylalcohol (24:1) is added and gently mixed, followed by a centrifugation step at 1 600 g at for 5 min at

room temperature. Subsequently, the aqueous phase is mixed with a corresponding two-third volume of ice-cold isopropanol and rocked gently for 30 min or overnight at room temperature until precipitation is visible. The mixture is spinned for 2 min at 500 g and the pellet is washed for 20 min with a solution of 76 % EtOH and 10 mM Ammoniumacetate. This is followed by a 10 min spin at 1 600 g. After air-drying the pellet it is resuspended in 2 ml of TE buffer (10 mM Tris, 1 mM EDTA, pH 8.0) and subsequently treated with 2 µl RNase A (DNase free, 10 mg/ml) for 30 min at 37 °C. Afterwards, the DNA and proteins are separated by chloroform-phenol extraction as was previously described (Chomczynski *et al.*, 1987). The aqueous phase is mixed with 3 ml TE, 1 ml of a 1 M NaCl solution and 4 ml cold isopropanol, followed by a 10 min spin at 1 600 g. Finally the pellet is again washed with 70 % EtOH and air dried before being resuspended in 100 µl Tris pH 8.0. The genomic DNA is stored at -20 °C.

Extraction Buffer (High Pure)

2 % (w/v)	CTAB
1.4 M	NaCl
20 mM	EDTA
100 mM	Tris pH 8.0
0.2 % (v/v)	EtSH

6.2.3. Quick preparation of genomic DNA from Arabidopsis thaliana

For genotyping a quick-prep genomic DNA was used. A little piece of an Arabidopsis leaf (3 x 3 mm) is cut out and ground with a pistil in an Eppendorf cup for 15 seconds. Afterwards, 400 µl of extraction buffer is added and the cup is vortexed for 5 seconds with full speed. Subsequently, the probe is centrifuged for 1 minute at 14 000 g. 300 µl of the supernatant is mixed with 300 µl of isopropanol in a new cup and vortexed. After leaving the sample at room temperature for 2 minutes, it is centrifuged for 5 min at 14 000 g. The pellet is dried at room temperature for 20 min before taken up in 100 µl TE buffer.

Extraction Buffer (Quick prep)

200 mM	Tris-Cl pH 7.5
250 mM	NaCl
25 mM	EDTA
0.5 % (w/v)	SDS

6.2.4. Agarose gelelectrophoresis

For analysis of DNA fragments, gel electrophoresis according to Sambrock *et al.* (Sambrook *et al.*, 1989), was performed. 0.8 g of Agarose was boiled in 100 ml TAE buffer, 3 µl Ethidium bromide were added and the mixture was poured in the gel apparatus.
The Samples were mixed with 6x Loading Buffer prior to running. The runs were performed at 130 V in TAE buffer.
For size assignment, either the 100 bp or 1 kb ladder from NEB was co-run with the samples.

6.2.5. Restriction digests

Restriction digests were performed with NEB enzymes exclusively according to the manufacturer's manual and separated on an agarose gel (see Chapter 6.2.4)

Restriction digest

app. 500 ng	DNA
2 µl	10x Buffer
0.3 µl	Restriction enzyme I
Opt. 0.3 µl	Restriction enzyme II
0.2 µl	BSA (where recommended)
ad 20 µl	ddH_2O

6.2.6. DNA ligation

Ligations where performed with the T4 DNA ligase from NEB. The reactions were set at room temperature for 30min. Vector and insert were always used in a molar ratio of 1:5.

Ligation	
50 ng	Vector
x ng	Insert
2 µl	Ligase buffer
1 µl	T4 Ligase
ad 20 µl	ddH_2O

6.2.7. Subcloning with Zero Blunt® TOPO® PCR Cloning Kit

PCR fragments were subcloned into the pCR®-Blunt II-TOPO Vector for later restriction digests according to the manufacturer's (Invitrogen™) manual and cloned into One Shot® TOP10 Chemically Competent *E. coli* cells, supplied with the kit.

6.2.8. Subcloning with pENTR™/D-TOPO® Cloning Kit

Gateway® compatible PCR fragments were subcloned into the pENTR™/D-TOPO® Vector for later Gateway® reactions according to the manufacturer's (Invitrogen™) manual and cloned into One Shot® TOP10 Chemically Competent *E. coli* cells, supplied with the kit. The primers for directed TOPO cloning were designed with a CACC sequence at the 5' end of each forward primer.

6.2.9. Generation of chemically competent E. coli cells

The protocol was adopted from Inoue *et al (Inoue et al., 1990).*
A single colony of an E. coli strain (see Table below) was grown in LB_0 overnight at 37 °C. The culture was diluted the next day in 250 ml SOB to about 1:100. This culture was grown at 18 °C until an OD_{600} of about 0.6 could be measured. Afterwards, the cells were cooled quickly in an ice water bath for ten minutes before harvested at 4 °C. The pellet was

resuspended in ice-cold TB buffer and kept on ice for ten minutes. Following an additional harvesting step (30', 4 000 g, 4 °C), the pellet was gently taken up in 20 ml ice-cold TB buffer. Afterwards DMSO was added to a final concentration of 7 % (v/v). The cells are then aliquoted, immediately frozen in liquid nitrogen and stored at -80 °C.

***E. coli* strain**	**Used for**
DH5alpha	Standard cloning, LR cloning
DB3.1	Propagation of Gateway™ vectors
BL21 gold	Heterologous expression

TB Buffer

10 mM	Pipes
55 mM	$MnCl_2$
15 mM	$CaCl_2$
250 mM	KCl

Everything is mixed, except $MnCl_2$ and titrated with KOH to pH 6.7. Subsequently MnCl2 is added and solution is filter-sterilized

SOB Media

2 % (w/v)	Tryptone
0.5 % (w/v)	Yeast extract
10 mM	NaCl
2.5 mM	KCl

After autoclaving the necessary amount of 50x SOC, which is filter-sterilized, is added:

1 M	Glucose
0.5 M	$MgCl_2$
0.5 M	$MgSO_4$

6.2.10. Transformation of E. coli

100 µl of chemical competent cells (see 6.2.9) are thawed on ice and mixed with the DNA, which is used for transformation. After 15 min of incubation on ice, the cells are heat shocked at 42 ºC, mixed with one milliliter of LB and incubated at 37 ºC under constant shaking for approximately 45 min. Finally, the cells are plated on LB plates, containing the demanded antibiotic.

6.2.11. Generation of competent Agrobacteria cells

The agrobacteria strain C58C1 was incubated in LB without antibiotics overnight. Next morning, 2 ml of the well-grown culture are added to 200 ml LB and incubated at 30 °C for approximately six hours until the OD is between 0.5 and 1. Cells are harvested by a 20 min spin at 4 °C at 5 000 g and washed with cold TE buffer. Subsequently, the cells are again pelleted by a 20 min spin at 4 °C and 5 000 g and finally resuspended in 20 ml cold LB medium. The cells are aliquoted (500 µl) and immediately frozen in liquid nitrogen.

6.2.12. Transformation of Agrobacteria

An aliquot of competent C58C1 agrobacteria (see 6.2.11) was thawed on ice. Afterwards, about 2 µg of plasmid DNA was added to cells and vortexed vigorously. This was followed by a five minutes incubation each on ice, in liquid nitrogen and at 37 °C. Subsequently, 1 ml of LB media was added to the cells before they were incubated at 30 °C under constant shaking. Finally, an aliquot of the cells was plated on LB plates containing the correct antibiotics.

6.2.13. Minipreparation with Invitrogen™ PureLink® Quick Plasmid Miniprep Kit

For Minipreparation of Plasmid DNA, 5 ml of LB media, containing the necessary antibiotic, was inoculated with a colony of cells and incubated at 37 ºC over night.
The Plasmid was then purified according to the manufacturer's instructions. The amount of DNA was measured with a NanoDrop ND1000.

6.2.14. Midipreparation with Invitrogen™ PureLink® HiPure Plasmid Midiprep Kit

Plasmid preparation was performed according to the manufacturer's instructions.

6.2.15. mRNA isolation and reverse transcriptase (RT)-PCR

For general expression analysis of genes in various tissues, mRNA was extracted directly and reversely transcribed into cDNA. For mRNA isolation, the Dynabeads® mRNA DIRECT™ Micro Kit (Invitrogen®) was used and the extraction was carried out following the manufacturer's instructions. Directly after isolation, mRNA was treated with DNase I, Amplification Grade (Invitrogen). Briefly, 8 µl DEPC-treated water, 1 µl 10 x DNase I Reaction Buffer, 1 µl DNase I together with the mRNA attached to Oligo(dT)$_{25}$ Dynabeads® were incubated for 15 min at RT. For inactivation of DNase I, 1 µl of 25 mM EDTA was added and the sample was incubated at 65°C for 10 min.
First-strand synthesis of cDNA was carried out using Oligo(dT)$_{18}$ primers and Superscript™ Reverse Transcriptase according to the manufacturer's instructions (Invitrogen®). For following PCR reactions, 1 µl of cDNA was used as template.

6.2.16. Quantitative real-time PCR

For analyzing expression profile of genes, the KAPA™ SYBR® FAST kit from Peqlab (Erlangen, Germany) was used according to the manufacturer's instructions. The cDNA of tissues of interest (see Chapter 6.2.15) was used at concentrations between 5 and 10 ng/µl. qRT-PCR runs were performed and analyzed with the Mastercycler® ep realplex from Eppendorf (Hamburg, Germany) according to the manufacturer's instructions.

6.2.17. Gel extraction of DNA fragments

DNA fragments were isolated from 0.8% Agarose gels with the „Gel Extraction Kit" from Qiagen® according to the manufacturer's instructions.

6.2.18. Sequencing

Sequencing was performed either by 4base lab (Reutlingen) or GATC Biotech (Konstanz). Plasmids were prepared as described in 6.2.13 and sent in the concentrations demanded.

6.3. Biochemical Methods

6.3.1. SDS-PAGE

In order to separate proteins, SDS-PAGE according to Laemmli (Laemmli 1970) was performed with a *Protean Cell III* (BioRad). Samples were separated at currents between 150 and 210 V until the front of the loading dye reached the lower end of the gel. Depending on the size of the proteins, the concentration of acryl amide was varying between 8 and 12%. Prior to sample loading, they were mixed with either 2x (containing DTT) or 6x (containing EtSH) SDS loading dye and boiled at 95 °C for 5 min when protein extract was used. The incubation time was extended to 15 min when intact *E. coli* cells were used.

Resolving gel	
0.375 M	Tris-Cl pH 8.8
X %	30 % Acrylamide/ 0.8 % Bisacrylamide
0.1 %	SDS (w/v)
0.05 %	TEMED (v/v)
300 µg/ml	APS

Stacking gel	
0.125 M	Tris-Cl pH 6.8
5 %	30 % Acrylamide / 0.8% Bisacrylamide
0.1 %	SDS (w/v)
0.04 %	TEMED (v/v)
450 µg/ml	APS

2x Sample buffer	
100 mM	Tris-Cl pH 6.8
4 %	SDS (w/v)
20 %	Glycerol (v/v)
200 mM	DTT
0.2 %	Bromphenolblue (w/v)

SDS running buffer	
25 mM	Tris-Base
192 mM	Glycine
0.1 %	SDS (w/v)

6.3.2. Coomassie Staining

For visualization of proteins in a SDS-Polyacrylamide gel, the gels were incubated in a solution of colloidal coomassie brilliant blue until the bands were clearly visible. Destaining was not necessary. Instead, the gels were washed several times with sufficient amounts of water.

Colloidal Coomassie Staining Solution

0.02 % (w/v)	Coomassie Brilliant Blue (CBB-G250)
5 % (w/v)	Aluminiumsulfate-(14-18)-hydrate
10 % (v/v)	Ethanol
2 % (v/v)	Orthophosphoric acid

For preparing the staining solution, the order of mixing is crucial: First, aluminiumsulfate is dissolved in water. Afterwards, ethanol is added and the solution is homogenized. Subsequently, CBB-250 is added. Finally the phosophoric acid is added and water is added, until the necessary volume is achieved.

6.3.3. Wet Blot

Through a Wet Blot procedure, proteins were transferred onto a nitrocellulose membrane in a Protean Cell III apparatus (BioRad) after separation via SDS-PAGE. The blot was assembled according to the manufacturer's instructions. The transfer was done for 30 min at 360 mA or 90 min at 150 mA. After finishing, the membrane was shortly stained with Ponceau S in order to mark the lanes. Afterwards the membrane was shortly destained with water. To saturate unspecific binding sites, the membrane was incubated in blocking solution (TBS, 0.2 % Tween (v/v), 5 % milk powder (w/v)) for at least 60 min. After washing the membrane in TBS three times for ten minutes, it was incubated with the primary antibody with the necessary dilution in 5 ml TBS + 1 % milk powder (w/v) over night at 4 °C. The next day, the blot was washed three times in TBS-T (TBS, 0.2 % Tween (v/v)). Afterwards, the membrane was incubated with the secondary antibody for 60 min. Finally the blot was washed for 15 min with washing solution (TBS, 0.2 % Tween (v/v), 1 % milk powder (w/v)), followed by a

10 min wash each with TBS-T and TBS respectively. For detection of the antigen-antibody-HRP complexes, the Enhancer solution from PJK (Kleinblittersdorf) was used.

Summary of used antibodies

Used antibodies		Dilution
anti-GFP	Roche, IgG1, clone 7.1	1: 1 000 to 1: 2 500
anti-mCherry	Clontech, Lot-Nr. 1011301A	1: 7 000
anti-mouse IgG	Goat anti-mouse IgG-HRP, Santa Cruz, Lot-Nr. L1008	1: 5 000 to 1: 10 000
Anti-CBD	NEB, IgG1, Lot-Nr.0061202	1: 1 000
Anti-MBP	NEB, IgG2a, Lot-Nr. 0081202	1: 2 000

Transfer buffer	
48 mM	Tris
39 mM	Glycine
20 %	Methanol (v/v)
0.037%	SDS (w/v)

TBS	
50 mM	Tris-Cl pH 7.5
150 mM	NaCl

6.3.4. Crude Protein Extract from plants

Fresh plant material was weighed and frozen in liquid nitrogen. Afterwards, the material was ground in a cooled mortar, and cooled grinding buffer was added in a ratio of buffer to fresh plant material of 3 to 1. The fine powder was transferred into an Eppendorf tube and thawed on ice. Subsequently, the material is centrifuged at 2 000 g and 4 °C for 5 minutes and the

supernatant is collected, whereas the cell debris is discarded. This procedure is repeated, until the supernatant is totally clear and free of debris.

Grinding Buffer

20 mM	HEPES, pH 7.5
100 mM	NaCl
5 mM	MgCl2
1 mM	DTT
1x	Complete Plus® Protease Inhibitor (Roche)

6.3.5. Heterologous Expression of RBP1 in E. coli

The constructs from Table 2-3 in Chapter 2.3.3 were used to transform competent BL21 gold cells. A single colony was incubated overnight in LB at 37 °C with the corresponding antibiotic and 1 % (w/v) glucose in order to repress the expression. The next day, cells were diluted 1:100 in LB and grown at 20 °C for 24 hours. After cooling the cells in an ice-water bath for 15 minutes, they were harvested by a 30 min spin at 3500 g and 4 °C. The pellet was frozen in liquid nitrogen and stored at -80 °C overnight. The next day, the cells were thawed on ice and subsequently washed with ice-cold lysis buffer and pelleted again, as on the previous day. Afterwards, the cells were taken up in lysis buffer (about 1/10 of culture volume) and broken through three rounds in a French Press, applying 10 000 psi. Cell debris was removed by a 30 min spin at 20 000 g and 4 °C. The supernatant was then loaded on a column, filled with the corresponding affinity matrix. This was all done at 4 °C. The flow-through was loaded twice and left on the column for 24 h the second time. Afterwards, the matrix was washed with 100 ml washing buffer. In the case of a Chitin binding column, it was subsequently incubated with 5 ml elution buffer. This was left on the column and in the dark for 48 to 72 hours for on column cleavage before draining the column and flushing with additional 5 ml elution buffer. In the case of MBP, the protein was eluted with 100 ml elution buffer with only a short incubation time preceding the drain.

Basic Buffers

HEPES
20 mM Hepes, 1 mM EDTA, 1 µM PMSF

Tris
50 mM Tris, 1mM EDTA, 1 µM PMSF

Variations

Purpose	pH range	Salt	Detergents/Additives
Lysis	7.5 – 9.5	50 mM NaCl	0.01 - 0.1 % Triton X-100 0.01 - 0.1 % Tween20
Washing	7.5 – 9.5	0.1 – 1 M NaCl	0.01 - 0.1 % Triton X-100 0.01 - 0.1 % Tween20
Elution	7.5 – 9.5	50 mM NaCl	20 mM DTT (for CBD) 10 mM Maltose (for MBP)

6.4. Cell Biological and Plant Work

6.4.1. Plant material and growth conditions

The *Arabidopsis thaliana* Columbia accession (Col-0) was used as wild type and for transformation. Seeds were put on soil (mixture of 65 % substrate, 25 % sand and 10 % expanded clay), stratified at 4 °C in the dark for two days and subsequently transferred into plant growth chambers under long day conditions (16 hours light / 8 hours dark). Transformation of *Arabidopsis thaliana* plants was carried out using the floral dip method as previously described by Clough *et al.* (Clough *et al.*, 1998).
Plants transformed with the *bar* or *pat* gene (Phosphinotricin-Acetyltransferase) as a selection marker conferring BASTA® resistance, were sprayed with BASTA® (Bayer Crop Science) with a concentration of 200 mg/l glufosinate ammonium supplemented with 0.1 % Tween-20 three days after germination. Spraying was repeated two more times with an interval of two days. For growing plants under sterile conditions, seeds had to be surface sterilized. For this

purpose the seed were dispersed on an empty petri dish and incubated in an exsiccator filled with chloric gas overnight. The gas was generated by mixing 50 ml hypochloric acid solution (12.5 %) with 2 ml concentrated HCl followed by immediate closing of the exsiccator.
The sterile seeds were dispersed in a sterile 0.1 % agarose solution and sowed out on solid 1/2 x MS medium containing vitamins and MES buffer (Murashige & Skoog, Duchefa) prepared with 0.8 % Phytagar (Duchefa). For selection of plants carrying the *nptII* gene (neomycin Phosphotransferase II) as a selection marker, the medium was supplemented with 50 µg/ml kanamycin. Seeds were stratified for two days at 4 °C in the dark and then transferred to long day for 6 h to induce germination. Afterwards, plants were put in the dark at 22 °C for two days before being transferred into a long day growth chamber.

6.4.2. Dissection of ovules

For microscopy analysis, ovules and developing seeds had to be dissected using a stereomicroscope. First, the pistil was freed by removing all other floral organs. Afterwards, the pistil was cut along the septum at both sides using a hypodermic needle (0.4 x 20 mm, Braun) so that the carpels could be detached. For fluorescence microscopy, the pistil was then transferred into 50 mM sodium phosphate buffer pH 7.5, the placenta was separated lengthwise into two halves using two hypodermic needles and directly analyzed at the confocal microscope with the respective filter set.

6.4.3. Infiltration of N. benthamiana

Agrobacteria were transformed as described in 6.2.12 and fresh colonies were picked and grown overnight in LB with the corresponding antibiotic at 30 °C. The OD_{600} was measured next day and it should be in a range between 1.0 and 2.0. Cells were harvested by a 5 min spin at 4 000 g and set to an OD_{600} of 1.0 with infiltration buffer. The mixture was left at room temperature for about one hour and then it was infiltrated into the leafs of *Nicotiana benthamiana* by the use of a 1 ml syringe. After two days, the leaf sections were cut out and further analyzed.

6.4.4. Confocal Microscopy

All microscopic studies were performed with a LSM510 or LSM710 from Zeiss®. The following table depicts the used excitation wavelengths and filters, depending on the fluorescent protein. The pictures were analyzed by the confocal software LSM Imager and ZEN™, respectively.

Fluorescent protein	Excitation wavelength	MBS (Main Beam Splitter)	Emission filter
CFP	458 nm	458/514 nm	475 – 525 nm
GFP	488 nm	488/543 nm	505 – 530 nm
mVenus	514 nm	458/514 nm	530 – 600 nm
mCherry	543 nm	488/543 nm	585 – 615 nm

7. Bibliography

Ackermann, M., L. Chao, C. T. Bergstrom und M. Doebeli (2007). "On the evolutionary origin of aging." Aging Cell **6**(2): 235-44.

Anderson, P. und N. Kedersha (2008). "Stress granules: the Tao of RNA triage." Trends in biochemical sciences **33**(3): 141-50.

Barbarese, E., D. E. Koppel, M. P. Deutscher, C. L. Smith, K. Ainger, F. Morgan und J. H. Carson (1995). "Protein translation components are colocalized in granules in oligodendrocytes." Journal of Cell Science **108 (Pt 8)**: 2781-90.

Bayer, M., T. Nawy, C. Giglione, M. Galli, T. Meinnel und W. Lukowitz (2009). "Paternal control of embryonic patterning in Arabidopsis thaliana." Science (Washington D C) **323**(5920): 1485-8.

Becht, P., J. Konig und M. Feldbrugge (2006). "The RNA-binding protein Rrm4 is essential for polarity in Ustilago maydis and shuttles along microtubules." Journal of Cell Science **119**(Pt 23): 4964-73.

Benfey, P. N. und N. H. Chua (1989). "Regulated genes in transgenic plants." Science **244**(4901): 174-81.

Bergmann, D. C., W. Lukowitz und C. R. Somerville (2004). "Stomatal development and pattern controlled by a MAPKK kinase." Science **304**(5676): 1494-7.

Berleth, T. und G. Jürgens (1993). "The role of the monopteros gene in organising the basal body region of the Arabidopsis embryo." Development **118**(2): 575-587.

Bertrand, E., P. Chartrand, M. Schaefer, S. M. Shenoy, R. H. Singer und R. M. Long (1998). "Localization of ASH1 mRNA particles in living yeast." Molecular cell **2**(4): 437-45.

Bressan, G. C. und J. Kobarg (2010). "From protein interaction profile to functional assignment: the human protein Ki-1/57 is associated with pre-mRNA splicing events." RNA biology **7**(3): 268-71.

Breuninger, H., E. Rikirsch, M. Hermann, M. Ueda und T. Laux (2008). "Differential expression of WOX genes mediates apical-basal axis formation in the Arabidopsis embryo." Developmental Cell **14**(6): 867-76.

Casson, S., M. Spencer, K. Walker und K. Lindsey (2005). "Laser capture microdissection for the analysis of gene expression during embryogenesis of Arabidopsis." The Plant journal : for cell and molecular biology **42**(1): 111-23.

Chandler, J., J. Nardmann und W. Werr (2008). "Plant development revolves around axes." Trends in plant science **13**(2): 78-84.

Cheong, C. G. und T. M. Hall (2006). "Engineering RNA sequence specificity of Pumilio repeats." Proceedings of the National Academy of Sciences of the United States of America **103**(37): 13635-9.

Chomczynski, P. und N. Sacchi (1987). "Single-step method of RNA isolation by acid guanidinium thiocyanate-phenol-chloroform extraction." Analytical biochemistry **162**(1): 156-9.

Christensen, N., J. Tilsner, K. Bell, P. Hammann, R. Parton, C. Lacomme und K. Oparka (2009). "The 5' cap of tobacco mosaic virus (TMV) is required for virion attachment to the actin/endoplasmic reticulum network during early infection." Traffic **10**(5): 536-51.

Christensen, N. M., K. J. Oparka und J. Tilsner (2010). "Advances in imaging RNA in plants." Trends in Plant Science **15**(4): 196-203.

Clough, S. J. und A. F. Bent (1998). "Floral dip: a simplified method for Agrobacterium-mediated transformation of Arabidopsis thaliana." The Plant journal : for cell and molecular biology **16**(6): 735-43.

Corley, S. M. und J. E. Gready (2008). "Identification of the RGG box motif in Shadoo: RNA-binding and signaling roles?" Bioinformatics and biology insights **2**: 383-400.

Czechowski, T., M. Stitt, T. Altmann, M. K. Udvardi und W. R. Scheible (2005). "Genome-wide identification and testing of superior reference genes for transcript normalization in Arabidopsis." Plant physiology **139**(1): 5-17.

Daigle, N. und J. Ellenberg (2007). "λN-GFP: an RNA reporter system for live-cell imaging." Nature Methods **4**(8): 633-6.

Dong, J., C. A. MacAlister und D. C. Bergmann (2009). "BASL controls asymmetric cell division in Arabidopsis." Cell **137**(7): 1320-30.

Driever, W. und C. Nusslein-Volhard (1988). "The bicoid protein determines position in the Drosophila embryo in a concentration-dependent manner." Cell **54**(1): 95-104.

Eastmond, P. J., A. J. van Dijken, M. Spielman, A. Kerr, A. F. Tissier, H. G. Dickinson, J. D. Jones, S. C. Smeekens und I. A. Graham (2002). "Trehalose-6-phosphate synthase 1, which catalyses the first step in trehalose synthesis, is essential for Arabidopsis embryo maturation." The Plant journal : for cell and molecular biology **29**(2): 225-35.

Era, A., M. Tominaga, K. Ebine, C. Awai, C. Saito, K. Ishizaki, K. T. Yamato, T. Kohchi, A. Nakano und T. Ueda (2009). "Application of Lifeact reveals F-actin dynamics in Arabidopsis thaliana and the liverwort, Marchantia polymorpha." Plant & cell physiology **50**(6): 1041-8.

Faure, J. E., N. Rotman, P. Fortune und C. Dumas (2002). "Fertilization in Arabidopsis thaliana wild type: developmental stages and time course." The Plant journal : for cell and molecular biology **30**(4): 481-8.

Feng, W., H. Wu, L. N. Chan und M. Zhang (2007). "The Par-3 NTD adopts a PB1-like structure required for Par-3 oligomerization and membrane localization." EMBO J **26**(11): 2786-96.

Ferrandon, D., I. Koch, E. Westhof und C. Nusslein-Volhard (1997). "RNA-RNA interaction is required for the formation of specific bicoid mRNA 3' UTR-STAUFEN ribonucleoprotein particles." EMBO J **16**(7): 1751-8.

Fletcher, J. C., U. Brand, M. P. Running, R. Simon und E. M. Meyerowitz (1999). "Signaling of cell fate decisions by CLAVATA3 in Arabidopsis shoot meristems." Science **283**(5409): 1911-4.

Forrest, K. M. und E. R. Gavis (2003). "Live imaging of endogenous RNA reveals a diffusion and entrapment mechanism for nanos mRNA localization in Drosophila." Current biology : CB **13**(14): 1159-68.

Friml, J., A. Vieten, M. Sauer, D. Weijers, H. Schwarz, T. Hamann, R. Offringa und G. Jurgens (2003). "Efflux-dependent auxin gradients establish the apical-basal axis of Arabidopsis." Nature **426**(6963): 147-53.

Fusco, D., N. Accornero, B. Lavoie, S. M. Shenoy, J. M. Blanchard, R. H. Singer und E. Bertrand (2003). "Single mRNA molecules demonstrate probabilistic movement in living mammalian cells." Current biology : CB **13**(2): 161-7.

Gagnon, J. A. und K. L. Mowry (2011). "Molecular motors: directing traffic during RNA localization." Critical reviews in biochemistry and molecular biology **46**(3): 229-39.

Galweiler, L., C. Guan, A. Muller, E. Wisman, K. Mendgen, A. Yephremov und K. Palme (1998). "Regulation of polar auxin transport by AtPIN1 in Arabidopsis vascular tissue." Science **282**(5397): 2226-30.

Ghosh, S., V. Marchand, I. Gaspar und A. Ephrussi (2012). "Control of RNP motility and localization by a splicing-dependent structure in oskar mRNA." Nature structural & molecular biology **19**(4): 441-9.

Giorgi, C. und M. J. Moore (2007). "The nuclear nurture and cytoplasmic nature of localized mRNPs." Seminars in Cell & Developmental Biology **18**(2): 186-93.

Goldstein, B. und I. G. Macara (2007). "The PAR proteins: fundamental players in animal cell polarization." Dev Cell **13**(5): 609-22.

Grefen, C., N. Donald, K. Hashimoto, J. Kudla, K. Schumacher und M. R. Blatt (2010). "A ubiquitin-10 promoter-based vector set for fluorescent protein tagging facilitates temporal stability and native protein distribution in transient and stable expression studies." Plant Journal **64**(2): 355-65.

Gu, W., Y. Deng, D. Zenklusen und R. H. Singer (2004). "A new yeast PUF family protein, Puf6p, represses ASH1 mRNA translation and is required for its localization." Genes & development **18**(12): 1452-65.

Hachet, O. und A. Ephrussi (2004). "Splicing of oskar RNA in the nucleus is coupled to its cytoplasmic localization." Nature **428**(6986): 959-63.

Haecker, A., R. Gross-Hardt, B. Geiges, A. Sarkar, H. Breuninger, M. Herrmann und T. Laux (2004). "Expression dynamics of WOX genes mark cell fate decisions during early embryonic patterning in Arabidopsis thaliana." Development **131**(3): 657-68.

Hamada, S., K. Ishiyama, S. B. Choi, C. Wang, S. Singh, N. Kawai, V. R. Franceschi und T. W. Okita (2003). "The transport of prolamine RNAs to prolamine protein bodies in living rice endosperm cells." Plant Cell **15**(10): 2253-64.

Hamann, T., E. Benkova, I. Baurle, M. Kientz und G. Jurgens (2002). "The Arabidopsis BODENLOS gene encodes an auxin response protein inhibiting MONOPTEROS-mediated embryo patterning." Genes & development **16**(13): 1610-5.

Hamann, T., U. Mayer und G. Jurgens (1999). "The auxin-insensitive bodenlos mutation affects primary root formation and apical-basal patterning in the Arabidopsis embryo." Development **126**(7): 1387-95.

Hardtke, C. S. und T. Berleth (1998). "The Arabidopsis gene MONOPTEROS encodes a transcription factor mediating embryo axis formation and vascular development." The EMBO journal **17**(5): 1405-11.

Heaton, J. H., W. M. Dlakic, M. Dlakic und T. D. Gelehrter (2001). "Identification and cDNA cloning of a novel RNA-binding protein that interacts with the cyclic nucleotide-responsive sequence in the Type-1 plasminogen activator inhibitor mRNA." The Journal of biological chemistry **276**(5): 3341-7.

Hirokawa, N., R. Nitta und Y. Okada (2009). "The mechanisms of kinesin motor motility: lessons from the monomeric motor KIF1A." Nature reviews. Molecular cell biology **10**(12): 877-84.

Holweg, C. L. (2007). "Living markers for actin block myosin-dependent motility of plant organelles and auxin." Cell motility and the cytoskeleton **64**(2): 69-81.

Huang, L., N. Grammatikakis, M. Yoneda, S. D. Banerjee und B. P. Toole (2000). "Molecular characterization of a novel intracellular hyaluronan-binding protein." The Journal of biological chemistry **275**(38): 29829-39.

Inoue, H., H. Nojima und H. Okayama (1990). "High efficiency transformation of Escherichia coli with plasmids." Gene **96**(1): 23-8.

Jansen, R. P., C. Dowzer, C. Michaelis, M. Galova und K. Nasmyth (1996). "Mother cell-specific HO expression in budding yeast depends on the unconventional myosin myo4p and other cytoplasmic proteins." Cell **84**(5): 687-97.

Jellbauer, S. und R. P. Jansen (2008). "A putative function of the nucleolus in the assembly or maturation of specialized messenger ribonucleoprotein complexes." RNA biology **5**(4): 225-9.

Jeong, S., M. Bayer und W. Lukowitz (2011). "Taking the very first steps: from polarity to axial domains in the early Arabidopsis embryo." Journal of experimental botany **62**(5): 1687-97.

Kalderon, D., B. L. Roberts, W. D. Richardson und A. E. Smith (1984). "A short amino acid sequence able to specify nuclear location." Cell **39**(3 Pt 2): 499-509.

Karimi, M., B. De Meyer und P. Hilson (2005). "Modular cloning in plant cells." Trends in plant science **10**(3): 103-5.

Kedersha, N., G. Stoecklin, M. Ayodele, P. Yacono, J. Lykke-Andersen, M. J. Fritzler, D. Scheuner, R. J. Kaufman, D. E. Golan und P. Anderson (2005). "Stress granules and processing bodies are dynamically linked sites of mRNP remodeling." The Journal of cell biology **169**(6): 871-84.

Kertesz, M., Y. Wan, E. Mazor, J. L. Rinn, R. C. Nutter, H. Y. Chang und E. Segal (2010). "Genome-wide measurement of RNA secondary structure in yeast." Nature **467**(7311): 103-7.

Kislauskis, E. H., X. Zhu und R. H. Singer (1994). "Sequences responsible for intracellular localization of beta-actin messenger RNA also affect cell phenotype." The Journal of cell biology **127**(2): 441-51.

Knoblich, J. A. (2008). "Mechanisms of asymmetric stem cell division." Cell **132**(4): 583-97.

Konig, J., S. Baumann, J. Koepke, T. Pohlmann, K. Zarnack und M. Feldbrugge (2009). "The fungal RNA-binding protein Rrm4 mediates long-distance transport of ubi1 and rho3 mRNAs." The EMBO journal **28**(13): 1855-66.

Kozak, M. (1989). "Circumstances and mechanisms of inhibition of translation by secondary structure in eucaryotic mRNAs." Molecular and cellular biology **9**(11): 5134-42.

Laemmli, U. K. (1970). "Cleavage of structural proteins during the assembly of the head of bacteriophage T4." Nature **227**(5259): 680-5.

Lamesch, P., K. Dreher, D. Swarbreck, R. Sasidharan, L. Reiser und E. Huala (2010). "Using the Arabidopsis information resource (TAIR) to find information about Arabidopsis genes." Current protocols in bioinformatics / editoral board, Andreas D. Baxevanis ... [et al.] **Chapter 1**: Unit1 11.

Lange, S., Y. Katayama, M. Schmid, O. Burkacky, C. Brauchle, D. C. Lamb und R. P. Jansen (2008). "Simultaneous transport of different localized mRNA species revealed by live-cell imaging." Traffic **9**(8): 1256-67.

Laux, T., K. F. Mayer, J. Berger und G. Jurgens (1996). "The WUSCHEL gene is required for shoot and floral meristem integrity in Arabidopsis." Development **122**(1): 87-96.

Layana, C., P. Ferrero und R. Rivera-Pomar (2012). "Cytoplasmic Ribonucleoprotein Foci in Eukaryotes: Hotspots of Bio(chemical)Diversity." Comparative and functional genomics **2012**: 504292.

Lecuyer, E., H. Yoshida, N. Parthasarathy, C. Alm, T. Babak, T. Cerovina, T. R. Hughes, P. Tomancak und H. M. Krause (2007). "Global analysis of mRNA localization reveals a prominent role in organizing cellular architecture and function." Cell **131**(1): 174-87.

LeCuyer, K. A., L. S. Behlen und O. C. Uhlenbeck (1995). "Mutants of the bacteriophage MS2 coat protein that alter its cooperative binding to RNA." Biochemistry **34**(33): 10600-6.

Lenhard, M. und T. Laux (1999). "Shoot meristem formation and maintenance." Current Opinion in Plant Biology **2**(1): 44-50.

Lindner, A. B., R. Madden, A. Demarez, E. J. Stewart und F. Taddei (2008). "Asymmetric segregation of protein aggregates is associated with cellular aging and rejuvenation." Proc Natl Acad Sci U S A **105**(8): 3076-81.

Lorkovic, Z. J. und A. Barta (2002). "Genome analysis: RNA recognition motif (RRM) and K homology (KH) domain RNA-binding proteins from the flowering plant Arabidopsis thaliana." Nucleic acids research **30**(3): 623-35.

Luby-Phelps, K., P. E. Castle, D. L. Taylor und F. Lanni (1987). "Hindered diffusion of inert tracer particles in the cytoplasm of mouse 3T3 cells." Proceedings of the National Academy of Sciences of the United States of America **84**(14): 4910-3.

Lukowitz, W., A. Roeder, D. Parmenter und C. Somerville (2004). "A MAPKK kinase gene regulates extra-embryonic cell fate in Arabidopsis." Cell **116**(1): 109-19.

Macdonald, P. M., K. Kerr, J. L. Smith und A. Leask (1993). "RNA regulatory element BLE1 directs the early steps of bicoid mRNA localization." Development **118**(4): 1233-43.

Macdonald, P. M. und G. Struhl (1988). "cis-acting sequences responsible for anterior localization of bicoid mRNA in Drosophila embryos." Nature **336**(6199): 595-8.

Martin, K. C. und A. Ephrussi (2009). "mRNA localization: gene expression in the spatial dimension." Cell **136**(4): 719-30.

Mauger, D. M. und K. M. Weeks (2010). "Toward global RNA structure analysis." Nature biotechnology **28**(11): 1178-9.

McCurdy, D. W. (1999). "Is 2,3-butanedione monoxime an effective inhibitor of myosin-based activities in plant cells?" Protoplasma **209**(1-2): 120-5.

Medioni, C., K. Mowry und F. Besse (2012). "Principles and roles of mRNA localization in animal development." Development **139**(18): 3263-76.

Menke, F. L. und B. Scheres (2009). "Plant asymmetric cell division, vive la difference!" Cell **137**(7): 1189-92.

Moser, J. J. und M. J. Fritzler (2010). "Cytoplasmic ribonucleoprotein (RNP) bodies and their relationship to GW/P bodies." The international journal of biochemistry & cell biology **42**(6): 828-43.

Muller, M., R. G. Heym, A. Mayer, K. Kramer, M. Schmid, P. Cramer, H. Urlaub, R. P. Jansen und D. Niessing (2011). "A cytoplasmic complex mediates specific mRNA recognition and localization in yeast." PLoS Biol **9**(4): e1000611.

Munchow, S., C. Sauter und R. P. Jansen (1999). "Association of the class V myosin Myo4p with a localised messenger RNA in budding yeast depends on She proteins." Journal of Cell Science **112 (Pt 10)**: 1511-8.

Nadezhdina, E. S., A. J. Lomakin, A. A. Shpilman, E. M. Chudinova und P. A. Ivanov (2010). "Microtubules govern stress granule mobility and dynamics." Biochimica et biophysica acta **1803**(3): 361-71.

Nebenfuhr, A., L. A. Gallagher, T. G. Dunahay, J. A. Frohlick, A. M. Mazurkiewicz, J. B. Meehl und L. A. Staehelin (1999). "Stop-and-go movements of plant Golgi stacks are mediated by the acto-myosin system." Plant physiology **121**(4): 1127-42.

Nery, F. C., D. O. Passos, V. S. Garcia und J. Kobarg (2004). "Ki-1/57 interacts with RACK1 and is a substrate for the phosphorylation by phorbol 12-myristate 13-acetate-activated protein kinase C." The Journal of biological chemistry **279**(12): 11444-55.

Nevo-Dinur, K., A. Nussbaum-Shochat, S. Ben-Yehuda und O. Amster-Choder (2011). "Translation-Independent Localization of mRNA in E. coli." Science **331**(6020): 1081-1084.

Ozawa, T., Y. Natori, M. Sato und Y. Umezawa (2007). "Imaging dynamics of endogenous mitochondrial RNA in single living cells." Nature methods **4**(5): 413-9.

Paige, J. S., K. Y. Wu und S. R. Jaffrey (2011). "RNA Mimics of Green Fluorescent Protein." Science **333**(6042): 642-646.

Palacios, I. M., D. Gatfield, D. St Johnston und E. Izaurralde (2004). "An eIF4AIII-containing complex required for mRNA localization and nonsense-mediated mRNA decay." Nature **427**(6976): 753-7.

Paquin, N. und P. Chartrand (2008). "Local regulation of mRNA translation: new insights from the bud." Trends Cell Biol **18**(3): 105-11.

Paquin, N., M. Menade, G. Poirier, D. Donato, E. Drouet und P. Chartrand (2007). "Local activation of yeast ASH1 mRNA translation through phosphorylation of Khd1p by the casein kinase Yck1p." Molecular cell **26**(6): 795-809.

Petricka, J. J., J. M. Van Norman und P. N. Benfey (2009). "Symmetry breaking in plants: molecular mechanisms regulating asymmetric cell divisions in Arabidopsis." Cold Spring Harbor perspectives in biology **1**(5): a000497.

Pillot, M., C. Baroux, M. A. Vazquez, D. Autran, O. Leblanc, J. P. Vielle-Calzada, U. Grossniklaus und D. Grimanelli (2010). "Embryo and endosperm inherit distinct chromatin and transcriptional states from the female gametes in Arabidopsis." The Plant cell **22**(2): 307-20.

Riedl, J., A. H. Crevenna, K. Kessenbrock, J. H. Yu, D. Neukirchen, M. Bista, F. Bradke, D. Jenne, T. A. Holak, Z. Werb, M. Sixt und R. Wedlich-Soldner (2008). "Lifeact: a versatile marker to visualize F-actin." Nature Methods **5**(7): 605-7.

Rongo, C., E. R. Gavis und R. Lehmann (1995). "Localization of oskar RNA regulates oskar translation and requires Oskar protein." Development **121**(9): 2737-46.

Sambade, A., K. Brandner, C. Hofmann, M. Seemanpillai, J. Mutterer und M. Heinlein (2008). "Transport of TMV movement protein particles associated with the targeting of RNA to plasmodesmata." Traffic **9**(12): 2073-88.

Sambrook, J., E. F. Fritsch und T. Maniatis (1989). Molecular cloning : a laboratory manual. Cold Spring Harbor, N.Y., Cold Spring Harbor Laboratory Press.

Saunders, C. und R. S. Cohen (1999). "The role of oocyte transcription, the 5'UTR, and translation repression and derepression in Drosophila gurken mRNA and protein localization." Molecular cell **3**(1): 43-54.

Schluepmann, H. und M. Paul (2009). "Trehalose Metabolites in Arabidopsis-elusive, active and central." The Arabidopsis book / American Society of Plant Biologists **7**: e0122.

Schönberger, J., U. Z. Hammes und T. Dresselhaus (2012). "In vivo visualization of RNA in plants cells using the lambdaN22 system and a GATEWAY-compatible vector series for candidate RNAs." The Plant journal : for cell and molecular biology **71**(1): 173-81.

Shav-Tal, Y. und R. H. Singer (2005). "RNA localization." J Cell Sci **118**(Pt 18): 4077-81.

Shepard, K. A., A. P. Gerber, A. Jambhekar, P. A. Takizawa, P. O. Brown, D. Herschlag, J. L. DeRisi und R. D. Vale (2003). "Widespread cytoplasmic mRNA transport in yeast: identification of 22 bud-localized transcripts using DNA microarray analysis." Proc Natl Acad Sci U S A **100**(20): 11429-34.

Smith, A. M., R. T. Fuchs, F. J. Grundy und T. M. Henkin (2010). "Riboswitch RNAs: regulation of gene expression by direct monitoring of a physiological signal." RNA biology **7**(1): 104-10.

Sonoda, J. und R. P. Wharton (1999). "Recruitment of Nanos to hunchback mRNA by Pumilio." Genes & development **13**(20): 2704-12.

Sparkes, I. A. (2010). "Motoring around the plant cell: insights from plant myosins." Biochemical Society transactions **38**(3): 833-8.

Sprunck, S. und R. Gross-Hardt (2011). "Nuclear behavior, cell polarity, and cell specification in the female gametophyte." Sexual plant reproduction **24**(2): 123-36.

Sprunck, S., Rademacher, S., Vogler, F., Gheyselinck, J., Grossniklaus, U., Dresselhaus, T., "Egg cell-secreted EC1 triggers sperm cell activation during double fertilization." Science, accepted

Stewart, E. J., R. Madden, G. Paul und F. Taddei (2005). "Aging and death in an organism that reproduces by morphologically symmetric division." PLoS Biol **3**(2): e45.

Thomas, M. G., M. Loschi, M. A. Desbats und G. L. Boccaccio (2011). "RNA granules: the good, the bad and the ugly." Cellular signalling **23**(2): 324-34.

Tilsner, J., O. Linnik, N. M. Christensen, K. Bell, I. M. Roberts, C. Lacomme und K. J. Oparka (2009). "Live-cell imaging of viral RNA genomes using a Pumilio-based reporter." The Plant journal : for cell and molecular biology **57**(4): 758-70.

Valegard, K., J. B. Murray, P. G. Stockley, N. J. Stonehouse und L. Liljas (1994). "Crystal structure of an RNA bacteriophage coat protein-operator complex." Nature **371**(6498): 623-6.

Vallee, R. B., J. C. Williams, D. Varma und L. E. Barnhart (2004). "Dynein: An ancient motor protein involved in multiple modes of transport." Journal of neurobiology **58**(2): 189-200.

van der Honing, H. S., L. S. van Bezouwen, A. M. Emons und T. Ketelaar (2011). "High expression of Lifeact in Arabidopsis thaliana reduces dynamic reorganization of actin filaments but does not affect plant development." Cytoskeleton **68**(10): 578-87.

van Dijk, E., N. Cougot, S. Meyer, S. Babajko, E. Wahle und B. Seraphin (2002). "Human Dcp2: a catalytically active mRNA decapping enzyme located in specific cytoplasmic structures." The EMBO journal **21**(24): 6915-24.

Winter, D., B. Vinegar, H. Nahal, R. Ammar, G. V. Wilson und N. J. Provart (2007). "An "Electronic Fluorescent Pictograph" browser for exploring and analyzing large-scale biological data sets." PloS one **2**(8): e718.

Wu, B., J. A. Chao und R. H. Singer (2012). "Fluorescence fluctuation spectroscopy enables quantitative imaging of single mRNAs in living cells." Biophysical journal **102**(12): 2936-44.

Wu, X., J. Chory und D. Weigel (2007). "Combinations of WOX activities regulate tissue proliferation during Arabidopsis embryonic development." Developmental Biology **309**(2): 306-16.

Xu, J., J. Y. Yang, Q. W. Niu und N. H. Chua (2006). "Arabidopsis DCP2, DCP1, and VARICOSE form a decapping complex required for postembryonic development." The Plant cell **18**(12): 3386-98.

Yamada, T., H. Yoshimura, A. Inaguma und T. Ozawa (2011). "Visualization of nonengineered single mRNAs in living cells using genetically encoded fluorescent probes." Analytical chemistry **83**(14): 5708-14.

Yamashita, Y. M. und M. T. Fuller (2008). "Asymmetric centrosome behavior and the mechanisms of stem cell division." J Cell Biol **180**(2): 261-6.

Zaessinger, S., I. Busseau und M. Simonelig (2006). "Oskar allows nanos mRNA translation in Drosophila embryos by preventing its deadenylation by Smaug/CCR4." Development **133**(22): 4573-83.

Zhang, F. und A. E. Simon (2003). "A novel procedure for the localization of viral RNAs in protoplasts and whole plants." Plant Journal **35**(5): 665-73.

Zhang, Z. und T. Laux (2011). "The asymmetric division of the Arabidopsis zygote: from cell polarity to an embryo axis." Sexual plant reproduction **24**(2): 161-9.

Zimyanin, V. L., K. Belaya, J. Pecreaux, M. J. Gilchrist, A. Clark, I. Davis und D. St Johnston (2008). "In vivo imaging of oskar mRNA transport reveals the mechanism of posterior localization." Cell **134**(5): 843-53.

8. Appendix

8.1. Oligos

Name/Length	SCJ001 DNA; 30 BP
Description	At1g31450 Aspartyl Protease FWD
Sequence	CACCATGGCAACCAAAACTTTTCTCTACTG
Name/Length	SCJ002 DNA; 28 BP
Description	At1g31450 Rev
Sequence	GGATCMTAAGTTCCCGGAGCAATCCATG
Name/Length	SCJ003 DNA; 28 BP
Description	At2g21740 unknown FWD
Sequence	CACCATGGCTTCTAACACAAGTTTCCTC
Name/Length	SCJ004 DNA; 32 BP
Description	At2g21740 unknown REV
Sequence	GGATCMAAGTTTCACAGAGGAAGGCGCCGGAG
Name/Length	SCJ005 DNA; 30 BP
Description	At5g59120 FWD
Sequence	CACCATGGCGACGCTAGCAGCTTCCTCTAG
Name/Length	SCJ006 DNA; 27 BP
Description	At5g59120 Subtilase REV
Sequence	GGATCMGTAATCACTAGTATAAACAAC
Name/Length	SCJ007 DNA; 28 BP
Description	At1g24510 T-complex protein FWD
Sequence	CACCATGGCGCTGGCGTTCGATGAGTTC
Name/Length	SCJ008 DNA; 30 BP
Description	At1g24510 T-complex protein REV
Sequence	GGATCMGTATTCAGAATTGGAGATGACATC
Name/Length	SCJ009 DNA; 27 BP
Description	At5g65620 Peptidase M3 FWD
Sequence	CACCATGTTAATGGCGACTCCAACGTC

Name/Length	SCJ010 DNA; 28 BP
Description	At5g65620 Peptidase M3 REV
Sequence	GGATCMAGCAGAAGCAGAGGCAGCCAAG
Name/Length	SCJ011 DNA; 29 BP
Description	At5g04340 Zink Finger C2H2 FWD
Sequence	CACCATGGCACTTGAAACTCTTACTTCTC
Name/Length	SCJ012 DNA; 28 BP
Description	At5g04340 Zink Finger C2H2 REV
Sequence	GGATCMGGGTTTCTCCGGGAAGTCAAAC
Name/Length	SCJ013 DNA; 30 BP
Description	At2g17410 DNA binding protein FWD
Sequence	CACCATGGAGAATTTGACGGAAATAGAATC
Name/Length	SCJ014 DNA; 27 BP
Description	At2g17410 DNA binding protein REV
Sequence	GGATCMCTCCAATTGCTCCAGAGGCAC
Name/Length	SCJ015 DNA; 29 BP
Description	At3g61830 ARF18 FWD
Sequence	CACCATGGCGAGTGTTGAAGGTGATGATG
Name/Length	SCJ016 DNA; 29 BP
Description	At3g61830 ARF18 REV
Sequence	GGATCMCCCCCTACTACGATTTTCGAATG
Name/Length	SCJ017 DNA; 26 BP
Description	At1g60030 Xanthin/Uracil Permease FWD
Sequence	CACCATGGCCGGTGGTGGTGGAGGAG
Name/Length	SCJ018 DNA; 30 BP
Description	At1g60030 Xanthin/Uracil Permease REV
Sequence	GGATCMCACAGAGGGAAAATACTTGTTGAG
Name/Length	SCJ019 DNA; 29 BP
Description	At1g63010 SPX domain protein FWD
Sequence	CACCATGGTGGCTTTTGGGAAATACTTGC
Name/Length	SCJ020 DNA; 29 BP
Description	At1g63010 SPX domain protein REV
Sequence	GGATCMATAGAGTGAGTTATAAGTACAAC

Name/Length	SCJ021 DNA; 29 BP
Description	At4g17770 Trehalose-Phosphat Synthase Homolog FWD
Sequence	CACCATGGTATCAAGATCTTATTCAAACC
Name/Length	SCJ022 DNA; 29 BP
Description	At4g17770 Trehalose-Phosphat Synthase Homolog REV
Sequence	GGATCMAAACAGATCTTTAGTTGGAACAG
Name/Length	SCJ023 DNA; 26 BP
Description	Aspartyl Protease Sequencing Primer
Sequence	GTCTTTGGTTGCGGCTACAACAACGG
Name/Length	SCJ024 DNA; 30 BP
Description	Aspartylprotease At1g31450 Promotor FWD
Sequence	CACCAATTCCAAGTCTTTCCTAAGAATTTG
Name/Length	SCJ025 DNA; 28 BP
Description	Aspartylprotease At1g31450 Promotor REV
Sequence	TTTTGGATGATTTGGTAAGTTTGTGGTG
Name/Length	SCJ026 DNA; 30 BP
Description	Subtilase At5g59120 Promotor FWD
Sequence	CACCTAGAACTTTGGAATCCCAAAGAATTG
Name/Length	SCJ027 DNA; 31 BP
Description	Subtilase At5g59120 Promotor REV
Sequence	TTGCTTGAAAGAAAATTACTGTAATGTTTAG
Name/Length	SCJ028 DNA; 29 BP
Description	T complex protein At1g24510 Promoter FWD
Sequence	CACCGATTTCCGAAGATGAGTTTGATATG
Name/Length	SCJ029 DNA; 25 BP
Description	T complex protein At1g24510 Promoter REV
Sequence	TTTCGAGCTTCTCTCGATCCGATCG
Name/Length	SCJ030 DNA; 28 BP
Description	Peptidase M3 At5g65620 Promoter FWD
Sequence	CACCTATGGGGTTTATAATCGACGAAAG
Name/Length	SCJ031 DNA; 26 BP
Description	Peptidase M3 At5g65620 Promoter REV
Sequence	GTTTGCTATTACAAGCGTTGCCATTA

Name/Length	SCJ032 DNA; 30 BP
Description	Zink Finger C2H2 At5g04340 Promoter FWD
Sequence	CACCCATACTTGACTTGTAAGCTATAAACG
Name/Length	SCJ033 DNA; 28 BP
Description	Zink Finger C2H2 At5g04340 Promoter REV
Sequence	TATCTTGAAGACTAGCTACTAAGTTCTA
Name/Length	SCJ034 DNA; 32 BP
Description	ARID DNA Bdg Protein At2g17410 Promoter FWD
Sequence	CACCCTCAAAATTGAGGTTACTTCAATTTAAC
Name/Length	SCJ035 DNA; 26 BP
Description	ARID DNA Bdg Protein At2g17410 Promoter REV
Sequence	TGTTGATTCCAATTAAACAGCATTCC
Name/Length	SCJ036 DNA; 30 BP
Description	ARF18 At3g61830 Promotor FWD
Sequence	CACCTTATTTATTACTATCGTCTTGATCGG
Name/Length	SCJ037 DNA; 25 BP
Description	ARF18 At3g61830 Promotor REV
Sequence	TGAAGAACCCAGATGAGAACTGGAG
Name/Length	SCJ038 DNA; 28 BP
Description	Xanthin/uracil Permease At1g60030 Promoter FWD
Sequence	CACCCAATTAGCGACTGCTAGTACTGTC
Name/Length	SCJ039 DNA; 29 BP
Description	Xanthin/uracil Permease At1g60030 Promoter REV
Sequence	TTCCTTTAACTTCTGATGAAACCCAAAAG
Name/Length	SCJ040 DNA; 28 BP
Description	SPX Domain protein Promoter FWD
Sequence	CACCTTCTTCACCTTTTTACCAATTTCC
Name/Length	SCJ041 DNA; 29 BP
Description	SPX Domain protein Promoter REV
Sequence	CTTTTAATCGCAGAAAGCAGAGAGCAAAG
Name/Length	SCJ042 DNA; 28 BP
Description	TrehalosePSynthase At4g17770 Promotor FWD
Sequence	CACCCAATGACATCATTAGTTCAATTGC

Name/Length	SCJ043 DNA; 30 BP
Description	TrehalosePSynthase At4g17770 Promotor REV
Sequence	ATCTCTACAGCAAGTGAAGTAGATACAATG
Name/Length	SCJ044 DNA; 30 BP
Description	Subtilase At5g59120 UTR FWD
Sequence	CACCAACATTACAGTAATTTTCTTTCAAGC
Name/Length	SCJ045 DNA; 29 BP
Description	Subtilase At5g59120 UTR REV
Sequence	AAACAAAGCATCTCGATTATCCAATTAGC
Name/Length	SCJ046 DNA; 27 BP
Description	T-complex protein At1g24510 UTR FWD
Sequence	CACCTCTTCCAGACATTCTTCTTCTCG
Name/Length	SCJ047 DNA; 28 BP
Description	T-complex protein At1g24510 UTR REV
Sequence	AGATCTGACGATGTTCTTAAATAGAAGG
Name/Length	SCJ048 DNA; 29 BP
Description	Peptidase M3 At5g65620 UTR FWD
Sequence	CACCGCTTGTAATAGCAAACATGTTAATG
Name/Length	SCJ049 DNA; 27 BP
Description	Peptidase M3 At5g65620 UTR REV
Sequence	CATTTGGGAATTTAACCGTTGATTCTG
Name/Length	SCJ050 DNA; 32 BP
Description	Zink Finger C2H2 At5g04340 UTR FWD
Sequence	CACCCAAATCTTTTCATTTACAATTATCTTTC
Name/Length	SCJ051 DNA; 27 BP
Description	Zink Finger C2H2 At5g04340 UTR REV
Sequence	TGATGTATCCAAGCAAATTTTGATACG
Name/Length	SCJ052 DNA; 30 BP
Description	ARID Bright DNA Bdg protein At2g17410 UTR FWD
Sequence	CACCTCGATAGACGCTGGGTAAAAAAATTC
Name/Length	SCJ053 DNA; 29 BP
Description	ARID Bright DNA Bdg protein At2g17410 UTR REV
Sequence	GGTTGTAGATTTGTGTGTTCTTAATAGAA

Name/Length	SCJ054 DNA; 26 BP
Description	ARF18 At3g61830 UTR FWD
Sequence	CACCGTGGCTGACGGAAAAAAAAAGG
Name/Length	SCJ055 DNA; 29 BP
Description	ARF18 At3g61830 UTR REV
Sequence	AATCTTTGAACCCATAACTAATTGAATGT
Name/Length	SCJ056 DNA; 27 BP
Description	Xanthin/uracil Permease At1g60030 UTR FWD
Sequence	CACCCATCTTCGTCTTCTTTCACTTTC
Name/Length	SCJ057 DNA; 26 BP
Description	Xanthin/uracil Permease At1g60030 UTR REV
Sequence	GAAAACAGGCACACACCACAAAGAAG
Name/Length	SCJ058 DNA; 33 BP
Description	SPX Domain protein At1g63010 UTR FWD
Sequence	CACCCTAGTATTTATATAATATTTTGTGTAGGC
Name/Length	SCJ059 DNA; 30 BP
Description	SPX Domain protein At1g63010 UTR REV
Sequence	CAATACTTCAGAAAAAGAATCTCACAAAAC
Name/Length	SCJ060 DNA; 33 BP
Description	TrehalosePSynthase At4g17770 UTR FWD
Sequence	CACCAGAAGAGAATCTTCCAAAAATGTTAAATC
Name/Length	SCJ061 DNA; 34 BP
Description	TrehalosePSynthase At4g17770 UTR REV
Sequence	CATCTTAATATATAAGATTTATTTTGCTAACTCC
Name/Length	SCJ062 DNA; 27 BP
Description	WOX2 UTR FWD
Sequence	CACCCATGCAAACCATCGTCTTAAAAC
Name/Length	SCJ063 DNA; 29 BP
Description	WOX2 UTR REV
Sequence	TTCGTTACAACCCATTACCATTACTATCG
Name/Length	SCJ064 DNA; 27 BP
Description	WOX8 UTR FWD
Sequence	CACCTACACCATCATCATGTCCTCCTC

Name/Length	SCJ065 DNA; 34 BP
Description	WOX8 UTR REV
Sequence	GTCCTGTAAATTGTTCATAAATTTAAAAGATAAG
Name/Length	SCJ066 DNA; 29 BP
Description	OtsA FWD
Sequence	CACCCTCGAGATGAGTCGTTTAGTCGTAG
Name/Length	SCJ067 DNA; 27 BP
Description	OtsA REV
Sequence	GGATCMCGCAAGCTTTGGAAAGGTAGC
Name/Length	SCJ068 DNA; 29 BP
Description	OtsB FWD
Sequence	CACCCTCGAGCAATGACAGAACCGTTAAC
Name/Length	SCJ069 DNA; 29 BP
Description	OtsB REV
Sequence	GGATCMGATACTACGACTAAACGACTCAT
Name/Length	SCJ070 DNA; 27 BP
Description	DD65 CC Promotor FWD
Sequence	CACCAGTCAGCAAAATCAAAATTTAAC
Name/Length	SCJ071 DNA; 37 BP
Description	DD65 CC Promotor REV
Sequence	CTCGAGATCCTTTTCTACTTTGTTTTTGTTTTTGTGC
Name/Length	SCJ072 DNA; 28 BP
Description	PIN1 UTR FWD
Sequence	CACCAACACTCACTTTACTCTTTTTTCC
Name/Length	SCJ073 DNA; 29 BP
Description	PIN1 UTR REV
Sequence	TGATATTTTCCTTAACGTTTTTAATTCAC
Name/Length	SCJ074 DNA; 28 BP
Description	RBP1 UTR FWD
Sequence	CACCTATTATCTTCTTCTCTCTCTAACC
Name/Length	SCJ075 DNA; 30 BP
Description	RBP1 UTR REV lang
Sequence	TTCGCTTTGGTAACACTTAACCATATTATG

Name/Length	SCJ076 DNA; 26 BP
Description	RBP1 UTR REV kurz
Sequence	CTTAAAACTCCCAAAATTGGGTTCGC
Name/Length	SCJ077 DNA; 24 BP
Description	RBP2 UTR FWD
Sequence	CACCACCCGCCTCCATTGTTACCG
Name/Length	SCJ078 DNA; 30 BP
Description	RBP2 UTR REV
Sequence	ACTTTTTTTGAATATAAAGAAGATTTCCGG
Name/Length	SCJ079 DNA; 27 BP
Description	RBP3 UTR FWD
Sequence	CACCAATCCTCTGCAGTTATTTCATTG
Name/Length	SCJ080 DNA; 30 BP
Description	RBP3 UTR REV
Sequence	AGGATCATAAGAACATAACTTTTTTACTGC
Name/Length	SCJ081 DNA; 27 BP
Description	Kinesin UTR FWD
Sequence	CACCCTTCATAAACAAATCACTGCCAC
Name/Length	SCJ082 DNA; 31 BP
Description	Kinesin UTR REV
Sequence	AAATTTTGAATATTTTTCCTTTATTATAAGC
Name/Length	SCJ083 DNA; 28 BP
Description	LCV1 UTR FWD
Sequence	CACCAAAAATCAATTTCATCGTCTTCTC
Name/Length	SCJ084 DNA; 26 BP
Description	LCV1 UTR REV
Sequence	CAATGCGACAGTAATATGAAAGACAC
Name/Length	SCJ085 DNA; 29 BP
Description	WRKY UTR FWD
Sequence	CACCGAAAAAATCTATTTTCTTCTCTTTC
Name/Length	SCJ086 DNA; 28 BP
Description	WRKY UTR REV
Sequence	TTTGCCATCTTTAGTGTCATGATGTATC

Name/Length	SCJ087 DNA; 28 BP
Description	ZF-HD Homeobox UTR FWD
Sequence	CACCATTTATTATTCACATTTATTAACA
Name/Length	SCJ088 DNA; 30 BP
Description	ZF-HD homeobox UTR REV
Sequence	AAAAAAGAGCTAAAAGAGTTTAATTAATAT
Name/Length	SCJ089 DNA; 27 BP
Description	NAM UTR FWD
Sequence	CACCATGAAAGTTGAAGACGAAGCAAC
Name/Length	SCJ090 DNA; 25 BP
Description	NAM UTR REV
Sequence	TTACCTTTGGTTGAGTGGGATTAAG
Name/Length	SCJ091 DNA; 23 BP
Description	ABI4 UTR FWD
Sequence	CACCATGGACCCTTTAGCTTCCC
Name/Length	SCJ092 DNA; 27 BP
Description	ABI4 UTR REV
Sequence	TTAATAGAATTCCCCCAAGATGGGATC
Name/Length	SCJ093 DNA; 27 BP
Description	ZF C3HC4 UTR FWD
Sequence	CACCAAGTCAACAACTAAGATGAGAAG
Name/Length	SCJ094 DNA; 25 BP
Description	ZF C3HC4 UTR REV
Sequence	GAACTATGAAGTCTTCCGATTTTTG
Name/Length	SCJ095 DNA; 27 BP
Description	RNA Recogn Motif UTR FWD
Sequence	CACCAAAAAAAACTTATCTTATGAATC
Name/Length	SCJ096 DNA; 30 BP
Description	RNA Recogn Motif UTR REV
Sequence	GTGCTGATCATTTTGCTTAATTATGCAATC
Name/Length	SCJ097 DNA; 25 BP
Description	Myb Family TF UTR FWD
Sequence	CACCCCTGCAAAAAAGTTGAAGAAG

Name/Length	SCJ098 DNA; 31 BP
Description	Myb Family TF UTR REV lang
Sequence	AGCTGAGATTGGGGATCAAAATATTTAATTC
Name/Length	SCJ099 DNA; 29 BP
Description	Myb Family TF UTR REV
Sequence	CTTAACAATACAACAAACTCTTCCTTCTG
Name/Length	SCJ100 DNA; 53 BP
Description	T-compl Protein BP-Prim FWD
Sequence	GGGGACAAGTTTGTACAAAAAAGCAGGCTCAAATCTTCCAGACATTCTTCTTC
Name/Length	SCJ101 DNA; 57 BP
Description	T-compl Protein BP-Prim REV
Sequence	GGGGACCACTTTGTACAAGAAAGCTGGGTAGATCTGACGATGTTCTTAAATAGAAGG
Name/Length	SCJ102 DNA; 54 BP
Description	Wox8 UTR BP-Prim FWD
Sequence	GGGGACAAGTTTGTACAAAAAAGCAGGCTTCATTACACCATCATCATGTCCTCC
Name/Length	SCJ103 DNA; 58 BP
Description	Wox8 UTR BP-Prim REV
Sequence	GGGGACCACTTTGTACAAGAAAGCTGGGTGTCCTGTAAATTGTTCATAAATTTAAAAG
Name/Length	SCJ104 DNA; 23 BP
Description	At3g04610 RBP2 ORF FWD
Sequence	CACCATGGCTGAAGCTGAAGATC
Name/Length	SCJ105 DNA; 22 BP
Description	At3g04610 RBP2 ORF REV
Sequence	TCAGTAACCGTAGCCTGAGCTG
Name/Length	SCJ108 DNA; 56 BP
Description	BP Cloning NAM At1g60280
Sequence	GGGGACAAGTTTGTACAAAAAAGCAGGCTACCAATGAAAGTTGAAGACGAAGCAAC
Name/Length	SCJ109 DNA; 54 BP
Description	BP Cloning NAM At1g60280
Sequence	GGGGACCACTTTGTACAAGAAAGCTGGGTTTACCTTTGGTTGAGTGGGATTAAG
Name/Length	SCJ110 DNA; 28 BP
Description	MSCP-mVENUS TOPO
Sequence	CACCATGGCTTCTAACTTTACTCAGTTC

Name/Length	SCJ111 DNA; 29 BP
Description	MSCP-mVENUS TOPO
Sequence	CTCAGACCTTTCTCTTCTTTTTTGGAGGC
Name/Length	SCJ112 DNA; 25 BP
Description	LamdaN TOPO
Sequence	CACCATGGCCAGATCTGACGCCCAG
Name/Length	SCJ113 DNA; 27 BP
Description	LamdaN TOPO
Sequence	CTTTACGCTTTTTCGACCTTTCTCTTC
Name/Length	SCJ114 DNA; 29 BP
Description	p35S Xho FWD
Sequence	CTCGAGAATTCCAATCCCACAAAAATCTG
Name/Length	SCJ115 DNA; 31 BP
Description	p35S Pac Rev
Sequence	TTAATTAAGCGTGTCCTCTCCAAATGAAATG
Name/Length	SCJ118 DNA; 25 BP
Description	boxB FWD
Sequence	CACTATCACTAGTGCGGCCTAATTC
Name/Length	SCJ119 DNA; 27 BP
Description	boxB REV
Sequence	CCTTAATTAAGCATCGATGTCGACTAG
Name/Length	SCJ122 DNA; 31 BP
Description	Gateway FWD SpeI
Sequence	ACTAGTACAAGTTTGTACAAAAAAGCTGAAC
Name/Length	SCJ123 DNA; 31 BP
Description	GW REV SpeI
Sequence	ACTAGTACCACTTTGTACAAGAAAGCTGAAC
Name/Length	SCJ124 DNA; 27 BP
Description	MS2 FWD
Sequence	CAAGCTAGCTGAGGATCCTAAGGTACC
Name/Length	SCJ125 DNA; 25 BP
Description	MS2 Rev
Sequence	GTACAAACTTGTGATCTCGAAGCTC

Name/Length	SCJ126 DNA; 33 BP
Description	MS2 Fwd Xho
Sequence	CTCGAGCAAGCTAGCTGAGGATCCTAAGGTACC
Name/Length	SCJ127 DNA; 31 BP
Description	MS2 Rev Xho
Sequence	CTCGAGGTACAAACTTGTGATCTCGAAGCTC
Name/Length	SCJ128 DNA; 35 BP
Description	MS2 Fwd Pac
Sequence	TTAATTAACAAGCTAGCTGAGGATCCTAAGGTACC
Name/Length	SCJ129 DNA; 33 BP
Description	MS2 Rev Pac
Sequence	TTAATTAAGTACAAACTTGTGATCTCGAAGCTC
Name/Length	SCJ130 DNA; 33 BP
Description	boxB Rev Xho
Sequence	CTCGAGCCTTAATTAAGCATCGATGTCGACTAG
Name/Length	SCJ131 DNA; 33 BP
Description	boxB Fwd Pac
Sequence	TTAATTAACACTATCACTAGTGCGGCCTAATTC
Name/Length	SCJ132 DNA; 27 BP
Description	MSCP NotI FWD
Sequence	GCGGCCGCATGGCTTCTAACTTTACTC
Name/Length	SCJ133 DNA; 26 BP
Description	MSCP NotI Rev inFrame
Sequence	GCGGCCGCCGTAGATGCCGGAGTTTG
Name/Length	SCJ134 DNA; 24 BP
Description	GFP TOPO Fwd
Sequence	CACCATGGTGAGCAAGGGCGAGGA
Name/Length	SCJ135 DNA; 24 BP
Description	GFP TOPO Rev
Sequence	TTACTTGTACAGCTCGTCCATGCC
Name/Length	SCJ136 DNA; 28 BP
Description	Gateway Xho Fwd
Sequence	CTCGAGACAAGTTTGTACAAAAAAGCTG

Name/Length	SCJ137 DNA; 28 BP
Description	Gateway BglII Rev
Sequence	AGATCTACCACTTTGTACAAGAAAGCTG
Name/Length	SCJ138 DNA; 25 BP
Description	PIN1 CDS Fwd
Sequence	CACCATGATTACGGCGGCGGACTTC
Name/Length	SCJ139 DNA; 28 BP
Description	PIN1 CDS Rev
Sequence	GGATCMTAGACCCAAGAGAATGTAGTAG
Name/Length	SCJ140 DNA; 26 BP
Description	RBP1 CDS Fwd
Sequence	CACCATGGCGTCTGTGAACCCTTTCG
Name/Length	SCJ141 DNA; 25 BP
Description	RBP1 CDS Rev
Sequence	GGATCMCTTACCCAAAGTAGGGAAC
Name/Length	SCJ142 DNA; 26 BP
Description	RBP2 CDS Fwd
Sequence	CACCATGGCTGAAGCTGAAGATCAGC
Name/Length	SCJ143 DNA; 30 BP
Description	RBP2 CDS Rev
Sequence	GGATCMGTAACCGTAGCCTGAGCTGTAATC
Name/Length	SCJ144 DNA; 27 BP
Description	RBP3 CDS Fwd
Sequence	CACCATGAAAGATAGAGAAAACGATGG
Name/Length	SCJ145 DNA; 29 BP
Description	RBP3 CDS Rev
Sequence	GGATCMCCAACGTTCATATGATGAAGGTC
Name/Length	SCJ146 DNA; 28 BP
Description	Kinesin CDS Fwd
Sequence	CACCATGGCTATCATCGCAAGCACGTTC
Name/Length	SCJ147 DNA; 30 BP
Description	Kinsesin CDS Rev
Sequence	GGATCMCTGTTTCTTGAGAAGAAGAGGGCC

Name/Length	SCJ148 DNA; 27 BP
Description	LCV1 CDS Fwd
Sequence	CACCATGGCCAATCGAGAAAGAGATCG
Name/Length	SCJ149 DNA; 28 BP
Description	LCV1 CDS Rev
Sequence	GGATCMAGATTCATTTCCAATCGAGGCC
Name/Length	SCJ150 DNA; 28 BP
Description	WRKY CDS Fwd
Sequence	CACCATGGATTCGAATAGTAACAACACG
Name/Length	SCJ151 DNA; 30 BP
Description	WRKY CDS Rev
Sequence	GGATCMCATAGCACTTGTTCTTTCATAATC
Name/Length	SCJ152 DNA; 31 BP
Description	ZF-HD CDS Fwd
Sequence	CACCATGCTTGAAGTTAGATCAATGGATATG
Name/Length	SCJ153 DNA; 30 BP
Description	ZF-HD CDS Rev
Sequence	GGATCMCGACGAAGACGACGAGGCGTTTAC
Name/Length	SCJ154 DNA; 27 BP
Description	NAM CDS Fwd
Sequence	CACCATGAAAGTTGAAGACGAAGCAAC
Name/Length	SCJ155 DNA; 28 BP
Description	NAM CDS Rev
Sequence	GGATCMCCTTTGGTTGAGTGGGATTAAG
Name/Length	SCJ156 DNA; 23 BP
Description	ABI4 CDS Fwd
Sequence	CACCATGGACCCTTTAGCTTCCC
Name/Length	SCJ157 DNA; 27 BP
Description	ABI4 CDS Rev
Sequence	GGATCMATAGAATTCCCCCAAGATGGG
Name/Length	SCJ158 DNA; 24 BP
Description	ZF C3HC4 CDS Fwd
Sequence	CACCATGGCGAGGAAGAAGCATCG

Name/Length	SCJ159 DNA; 26 BP
Description	ZF C3HC4 CDS Rev
Sequence	GGATCMCAGCGGAAAAACCGAACTCT
Name/Length	SCJ160 DNA; 22 BP
Description	RRM CDS Fwd
Sequence	CACCATGGCGGGAGGAATAGGG
Name/Length	SCJ161 DNA; 30 BP
Description	RRM CDS Rev
Sequence	GGATCMGCAATATCTCTCAAAGAGAAACCC
Name/Length	SCJ162 DNA; 28 BP
Description	MYB124 CDS Fwd
Sequence	CACCATGGAAGATACGAAGAAGAAAAAG
Name/Length	SCJ163 DNA; 32 BP
Description	MYB124 CDS Rev
Sequence	GGATCMCAAGCTATGGAGAAGGACTCTTTTGC
Name/Length	SCJ164 DNA; 23 BP
Description	LambdaN NotI inFrame FWD
Sequence	GCGGCCGCATGGCCAGATCTGAC
Name/Length	SCJ165 DNA; 22 BP
Description	LambdaN NotI inFrame REV
Sequence	GCGGCCGCCACCGTTGGCGGCC
Name/Length	SCJ166 DNA; 25 BP
Description	mCherry BamHI Fwd
Sequence	GGATCCATGTTAGTGAGCAAGGGCG
Name/Length	SCJ167 DNA; 24 BP
Description	mCherry Asc Rev
Sequence	GGCGCGCCTCAGACCTTTCTCTTC
Name/Length	SCJ168 DNA; 23 BP
Description	mCherry Asc für C-terminal Fusion in 275 FWD
Sequence	GGCGCGCCATGTTAGTGAGCAAG
Name/Length	SCJ169 DNA; 22 BP
Description	mCherry Asc für C-terminal Fusion in 275 REV
Sequence	GGCGCGCCTAGTACAGCTCGTC

Name/Length	SCJ170 DNA; 23 BP
Description	mCherry Not für N-terminal Fusion in 276 FWD
Sequence	GCGGCCGCATGTTAGTGAGCAAG
Name/Length	SCJ171 DNA; 21 BP
Description	mCherry Not für N-terminal Fusion in 276 REV
Sequence	GCGGCCGCCTTGTACAGCTCG
Name/Length	SCJ172 DNA; 25 BP
Description	mCherry Xho für N-terminal Fusion in 279 FWD
Sequence	CTCGAGATGTTAGTGAGCAAGGGCG
Name/Length	SCJ173 DNA; 25 BP
Description	mCherry Xho für N-terminal Fusion in 279 REV
Sequence	CTCGAGCTTGTACAGCTCGTCCATG
Name/Length	SCJ174 DNA; 32 BP
Description	Pac Primer für 207 FWD
Sequence	TTAATTAATCGGATCCACTAGTAACGGCCGCC
Name/Length	SCJ175 DNA; 25 BP
Description	Pac Primer für 207 REV
Sequence	TTAATTAAGCTCGAGCGGCCGCCAG
Name/Length	SCJ176 DNA; 27 BP
Description	Sara 1 At3g43230 Fwd
Sequence	CACCATGGCTACTCTCAACGGAAAAGC
Name/Length	SCJ177 DNA; 25 BP
Description	Sara 1 At3g43230 Rev
Sequence	GGATCMCGGGCGCAAACGAGCATAG
Name/Length	SCJ178 DNA; 33 BP
Description	Sara 2 At1g29800 Fwd
Sequence	CACCATGGATGAAAGAGATCGAGAAATTCGTGC
Name/Length	SCJ179 DNA; 31 BP
Description	Sara 2 At1g29800 Rev
Sequence	GGATCMGTCTTCAGACAATGGAGAAATTGCC
Name/Length	SCJ180 DNA; 31 BP
Description	Sara 3 At1g20110 Fwd
Sequence	CACCATGCAACAGGGAGATTACAATTCGTAC

Name/Length	SCJ181 DNA; 28 BP
Description	Sara 3 At1g20110 Rev
Sequence	GGATCMATGTGCGCTAACGAGGAAAGGG
Name/Length	SCJ182 DNA; 27 BP
Description	Sara 4 At4g33240 Fwd
Sequence	CACCATGGACTCACAAGATCACAAAGC
Name/Length	SCJ183 DNA; 30 BP
Description	Sara 4 At4g33240 Rev
Sequence	GGATCMGGACTTGTTACCAACAGCTTGAGG
Name/Length	SCJ184 DNA; 30 BP
Description	CAT6 Promoter KpnI Fwd UliCloning
Sequence	GGTACCCTCGAGGTCGACGGTATCGATAAG
Name/Length	SCJ185 DNA; 34 BP
Description	CAT6 Promoter SacI Rev UliCloning
Sequence	GAGCTCTTGAAATATGACTAACGAATATACCTGC
Name/Length	SCJ186 DNA; 30 BP
Description	GFP Fwd Not für pSCJ280
Sequence	GCGGCCGCATGGTAGATCTGACTAGTAAAG
Name/Length	SCJ187 DNA; 29 BP
Description	GFP Rev Not ohne Stop für pSCJ280
Sequence	GCGGCCGCGCTAGCTTTGTATAGTTCATC
Name/Length	SCJ188 DNA; 21 BP
Description	Ubi10 FW HindIII
Sequence	AAGCTTGGCGCGCCGAGCTCG
Name/Length	SCJ189 DNA; 25 BP
Description	Ubi10 Rev SpeI
Sequence	ACTAGTGGCGCGCCCTGTTAATCAG
Name/Length	SCJ190 DNA; 32 BP
Description	UliCat6 Fwd Asc
Sequence	GGCGCGCCCTCGAGGTCGACGGTATCGATAAG
Name/Length	SCJ191 DNA; 33 BP
Description	UliCat6 Rev Asc
Sequence	GGCGCGCCTTGAAATATGACTAACGAATATACC

Name/Length	SCJ192 DNA; 25 BP
Description	CFP-inFrame FWD für pSCJ288
Sequence	CACCCCATGGTGAGCAAGGGCGAGG
Name/Length	SCJ193 DNA; 53 BP
Description	CFP Rev mit NLS für pSCJ288
Sequence	TCAGACCTTTCTCTTCTTTTTTGGAGGCGCTTTCTTGTACAGCTCGTCCATGC
Name/Length	SCJ194 DNA; 24 BP
Description	CFP Fwd BamHI
Sequence	GGATCCATGGTGAGCAAGGGCGAG
Name/Length	SCJ195 DNA; 24 BP
Description	DCP2 TOPO FWD
Sequence	CACCATGTCGGGCCTCCATCGATC
Name/Length	SCJ196 DNA; 25 BP
Description	DCP2 Rev
Sequence	GGATCMAGCTGAATTACCAGATTCC
Name/Length	SCJ197 DNA; 22 BP
Description	mVenus Fwd BamHI inFrame 201
Sequence	GGATCCATGGTGAGCAAGGGCG
Name/Length	SCJ198 DNA; 23 BP
Description	Inverse PCR binding Fwd in MCS
Sequence	CGCGCCTTAATTAAGCGGCCGCG
Name/Length	SCJ199 DNA; 25 BP
Description	Inverse PCR binding Rev in LB
Sequence	CAGCTCGGCACAAAATCACCACTCG
Name/Length	SCJ200 DNA; 28 BP
Description	RBP1 Fwd XhoI Het Express
Sequence	CTCGAGATGGCGTCTGTGAACCCTTTCG
Name/Length	SCJ201 DNA; 28 BP
Description	eGFP Rev XhoI Het Express
Sequence	CTCGAGCTTGTACAGCTCGTCCATGCCG
Name/Length	SCJ202 DNA; 25 BP
Description	eGFP Fwd XhoI Het Express
Sequence	CTCGAGATGGTGAGCAAGGGCGAGG

Name/Length	SCJ203 DNA; 30 BP
Description	RBP1 Rev XhoI Het Express
Sequence	CTCGAGCTTACCCAAAGTAGGGAACTGTGC
Name/Length	SCJ204 DNA; 26 BP
Description	RGGA At4g16830 Fwd CDS
Sequence	CACCATGGCAACTTTGAACCCTTTTG
Name/Length	SCJ205 DNA; 23 BP
Description	RGGA At4g16830 CDS Rev
Sequence	GGATCMCTTGCCCCCAAGAGATG
Name/Length	SCJ206 DNA; 26 BP
Description	RBPX At5g47210 CDS Fwd
Sequence	CACCATGGCGTCTTTGAACCCTTTCG
Name/Length	SCJ207 DNA; 24 BP
Description	RBPX At5g47210 CDS Rev
Sequence	GGATCMGCCCAACGAAGGGAACTG
Name/Length	SCJ208 DNA; 29 BP
Description	pTYB Sequencing 01
Sequence	CTCGATCCCGCGAAATTAATACGACTCAC
Name/Length	SCJ209 DNA; 26 BP
Description	pTYB Sequencing 02
Sequence	GCTGACTTTTCTGCACGACGCTGTAC
Name/Length	SCJ210 DNA; 23 BP
Description	GS-TAP Tag Fwd SmaI
Sequence	CCCGGGGAGCAGAAGCTTATCTC
Name/Length	SCJ211 DNA; 28 BP
Description	GS-TAP Tag Rev PstI
Sequence	CTGCAGCTATTCAGTGACAGTGAAAGTC
Name/Length	SCJ212 DNA; 27 BP
Description	GFP-RBP1 Fwd SacI f pTYB21
Sequence	GAGCTCATATGGTGAGCAAGGGCGAGG
Name/Length	SCJ213 DNA; 30 BP
Description	GFP-RBP1 Rev EcoRI STOP f pTYB21
Sequence	GAATTCTCACTTACCCAAAGTAGGGAACTG

Name/Length	SCJ214 DNA; 49 BP
Description	GFP Fwd with Factor Xa Cleavage Site
Sequence	CACCATCGAGGGAAGGGCGGCAATGGTGAGCAAGGGCGAGGAGCTGTTC
Name/Length	SCJ215 DNA; 25 BP
Description	RBP1 realtime FWD
Sequence	ACAGAGAAGGACAAGCGCATTACTG
Name/Length	SCJ216 DNA; 24 BP
Description	RBP1 realtime REV
Sequence	TTCCACCTTGGTAACCACCTCTTG
Name/Length	HAU73 DNA; 27 BP
Description	UBQ10 realtime FWD
Sequence	GGCCTTGTATAATCCCTGATGAATAAG
Name/Length	HAU74 DNA; 28 BP
Description	UBQ10 realtime REV
Sequence	AAAGAGATAACAGGAACGGAAACATAGT

8.2. Plasmid Sequences

All Plasmids cloned and used during this thesis can be viewed either as Vector NTI™ or genbank files on the attached CD.

Due to the great number of cloned plasmids, only important vectors are depicted below.

8.2.1. Vectors used for transient assay

For the vectors, which contain either the MS2CP or the λN_{22}, a representative fluorescent protein (FP) stands for CFP, GFP, mVenus and mCherry, respectively.

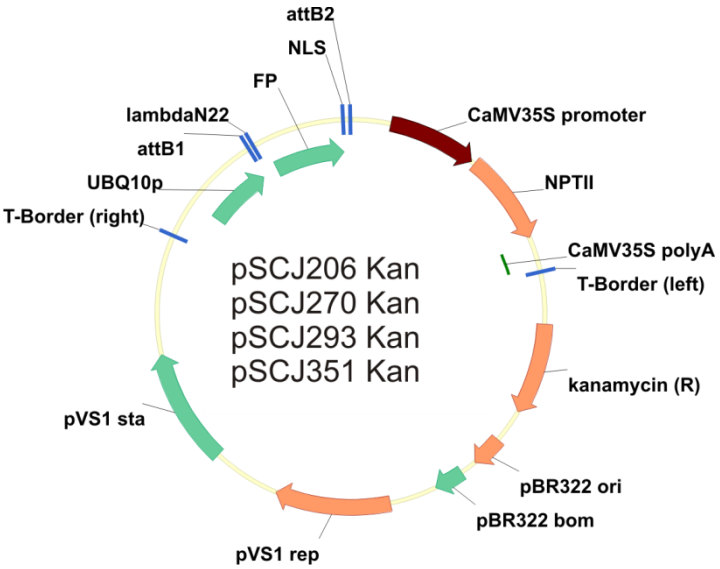

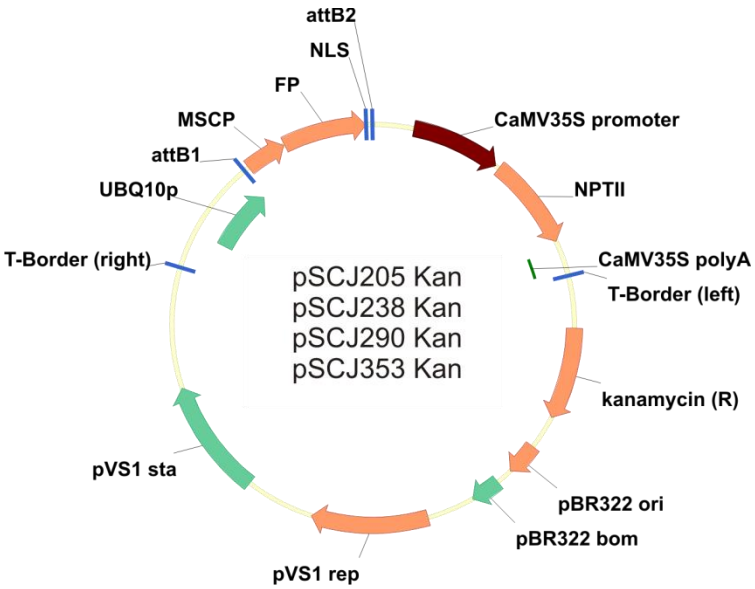

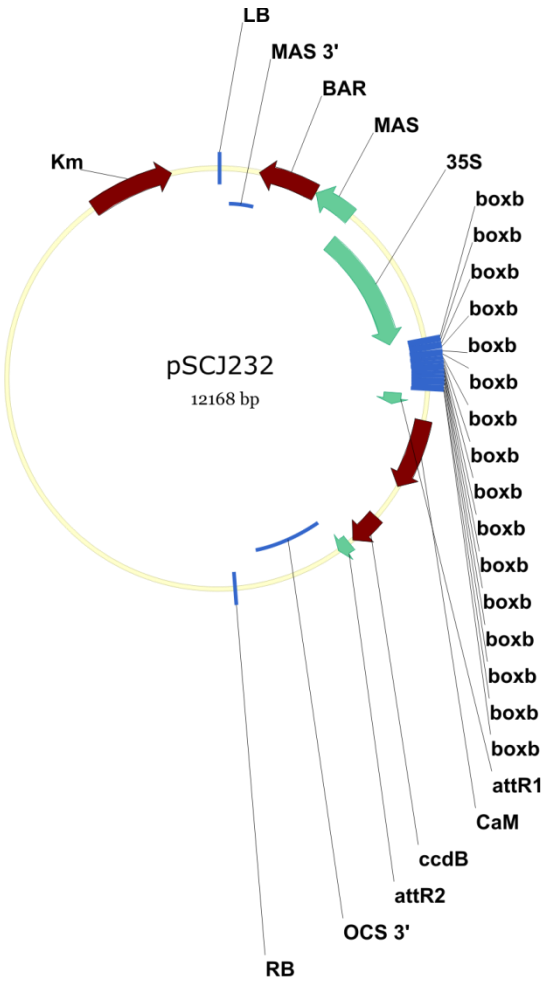
LB
MAS 3'
BAR
MAS
35S
Km
boxb
boxb
boxb
boxb
boxb
boxb
boxb
boxb
boxb
boxb
boxb
boxb
boxb
attR1
CaM
ccdB
attR2
OCS 3'
RB
pSCJ232
12168 bp

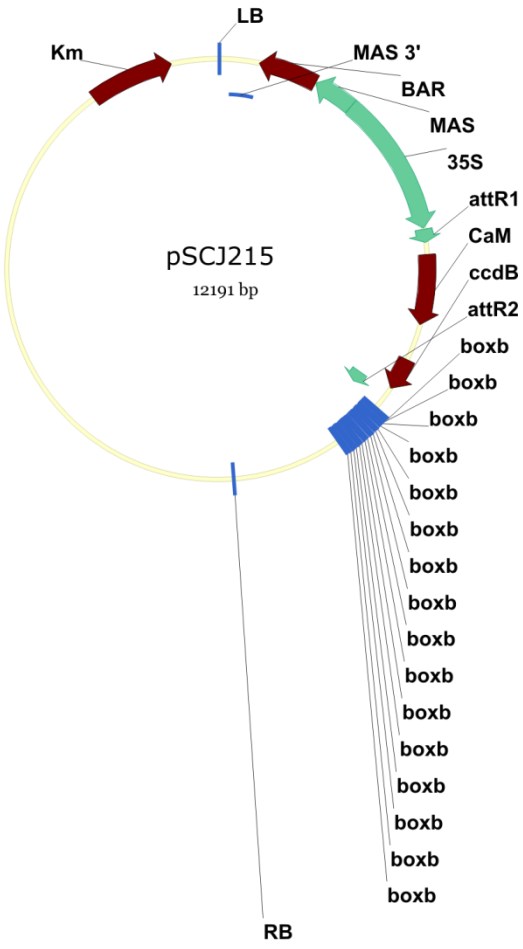
LB
Km
MAS 3'
BAR
MAS
35S
attR1
CaM
ccdB
attR2
boxb
boxb
boxb
boxb
boxb
boxb
boxb
boxb
boxb
boxb
boxb
boxb
boxb
boxb
boxb
boxb
boxb
boxb
RB
pSCJ215
12191 bp

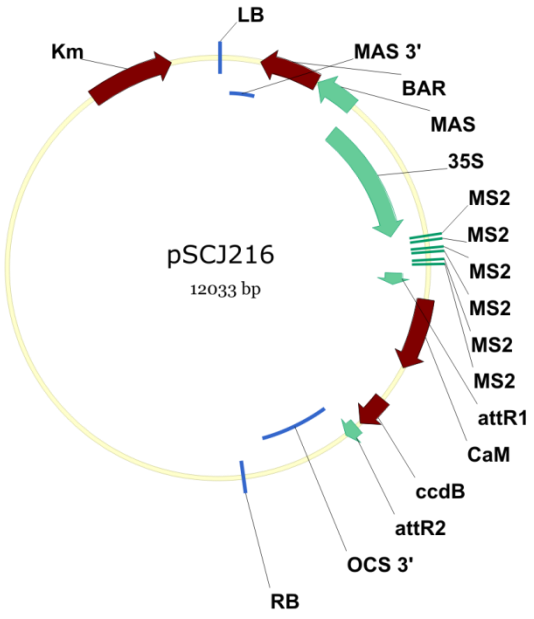
LB
Km
MAS 3'
BAR
MAS
35S
MS2
MS2
MS2
MS2
MS2
MS2
attR1
CaM
ccdB
attR2
OCS 3'
RB
pSCJ216
12033 bp

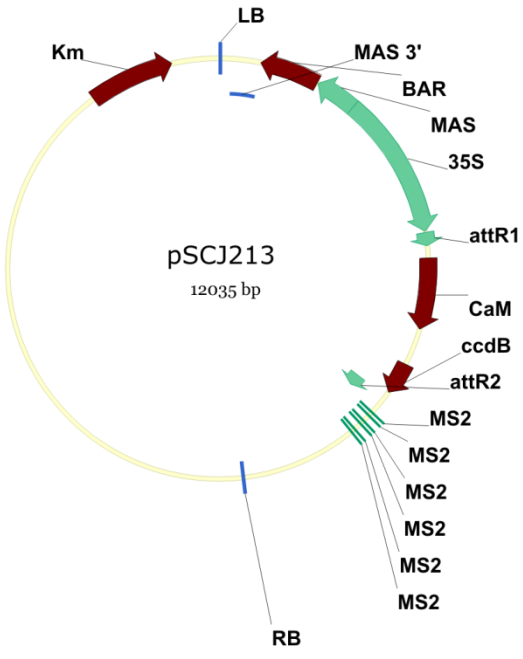
LB
Km
MAS 3'
BAR
MAS
35S
attR1
CaM
ccdB
attR2
MS2
MS2
MS2
MS2
MS2
MS2
RB
pSCJ213
12035 bp

8.2.2. Vectors used for stable transformation of Arabidopsis thaliana

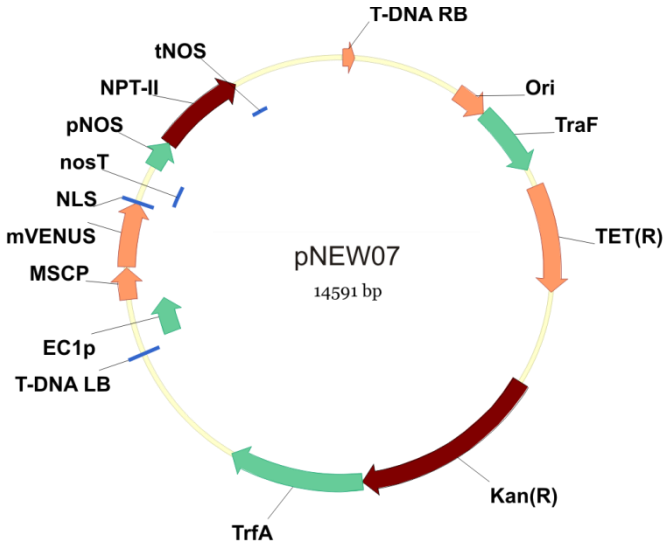

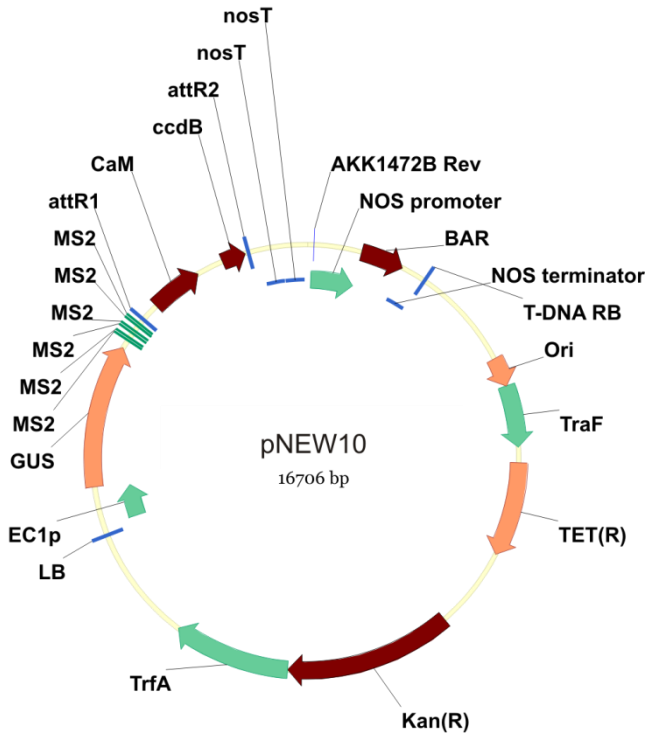

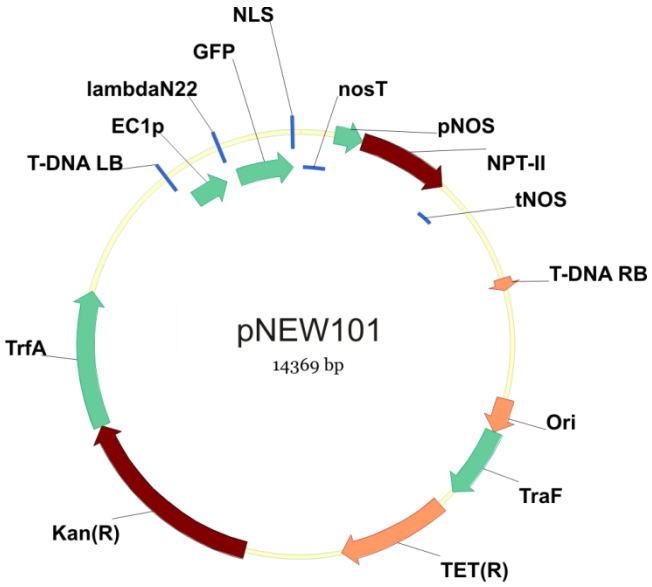
NLS
GFP
lambdaN22
EC1p
T-DNA LB
nosT
pNOS
NPT-II
tNOS
T-DNA RB
pNEW101
14369 bp
TrfA
Ori
TraF
Kan(R)
TET(R)

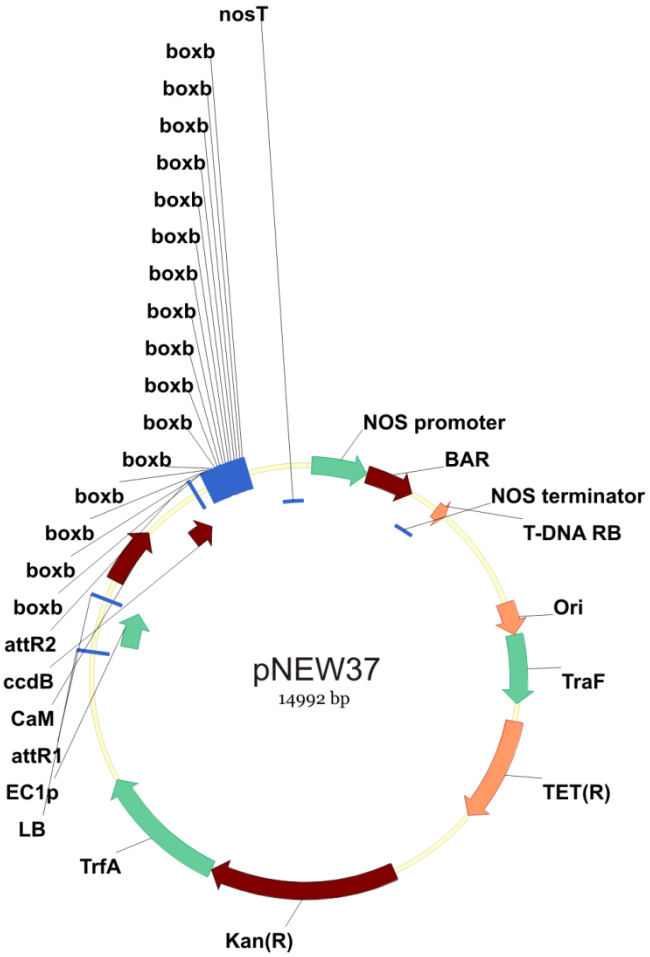
nosT
boxb
boxb
boxb
boxb
boxb
boxb
boxb
boxb
boxb
boxb
boxb
boxb
boxb
boxb
attR2
ccdB
CaM
attR1
EC1p
LB
NOS promoter
BAR
NOS terminator
T-DNA RB
Ori
TraF
TET(R)
pNEW37
14992 bp
TrfA
Kan(R)

8.2.3. Vector for heterologous expression of CBD-GFP-RBP1

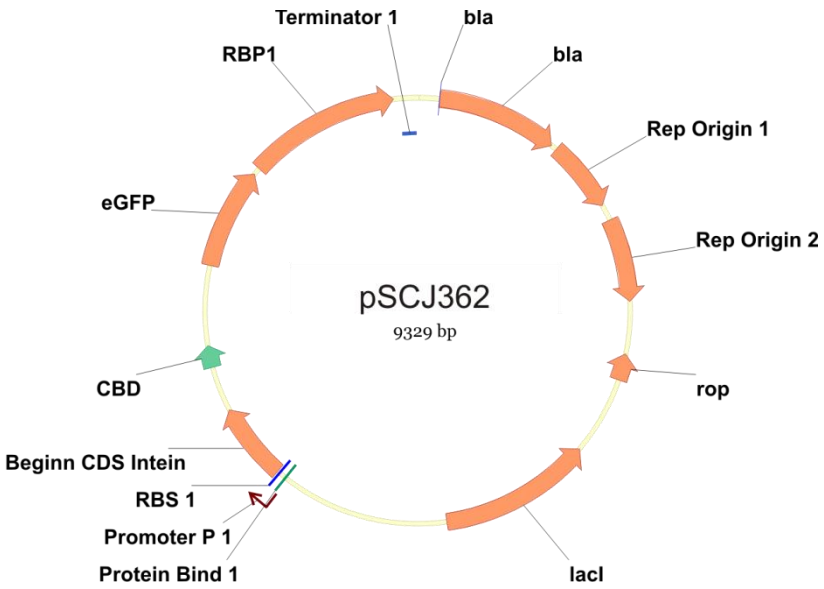

8.3. Subcellular localizations

Scale bars represent 20 µm each. Given is the Accession Number, assigned name and observed localization (see Chapter 2.2.5).

At5g04340
Cold Induced Zinc Finger (C2H2 type)
Nucleus

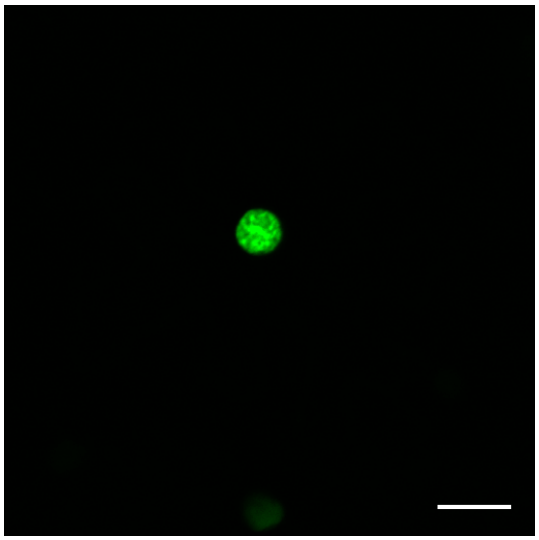

At2g17410
ARID/BRIGHT DNA-binding Protein;
Nucleus

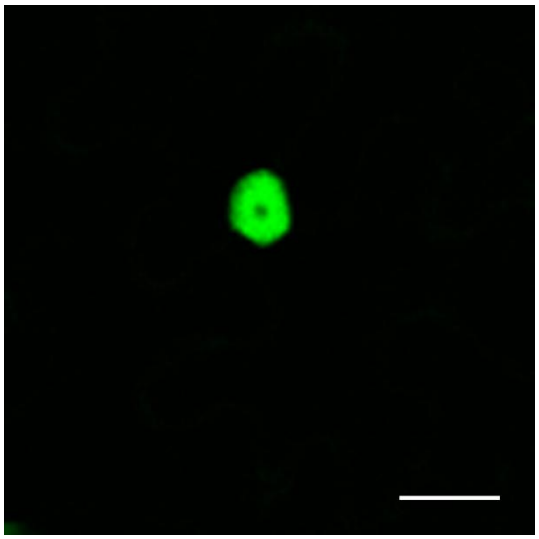

At3g61830
ARF18
Nucleus

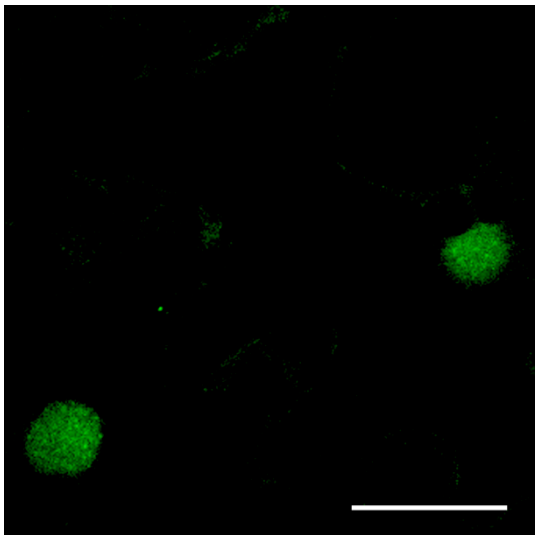

At2g20130
LCV1 (LIKE COV 1)
Cytosol/Granules

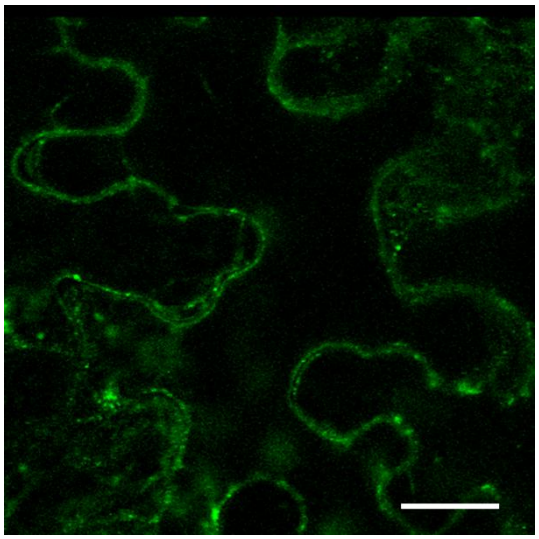

At2g40750
WRKY 54
Nucleus

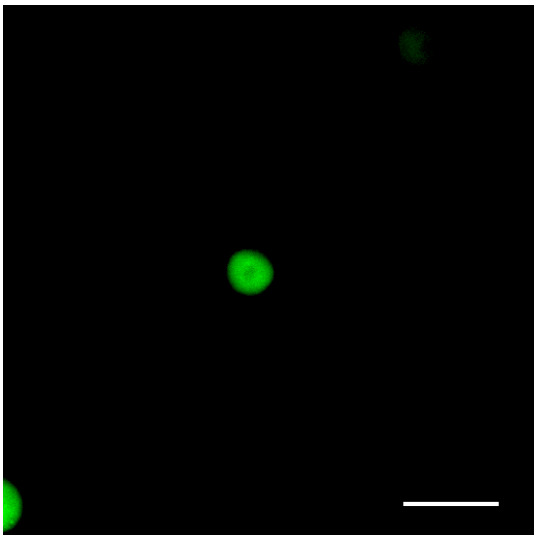

At3g28920
Zinc Finger Homeodomain 9
Nucleus

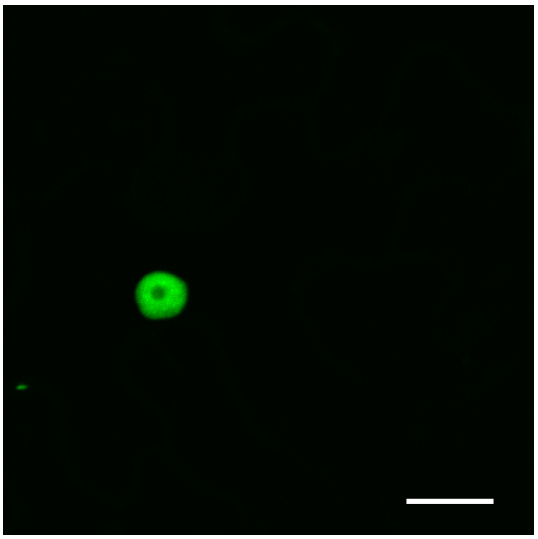

At2g40220
ABI4
Nucleus

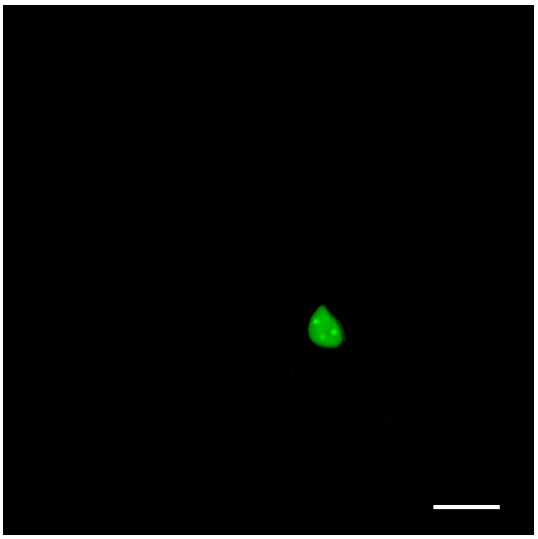

At1g14350
MYB124
Nucleus

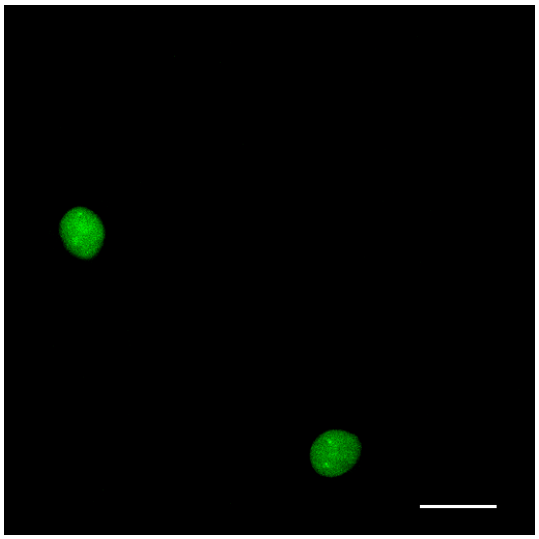

At3g04610
Flowering Locus KH Domain
Nucleus

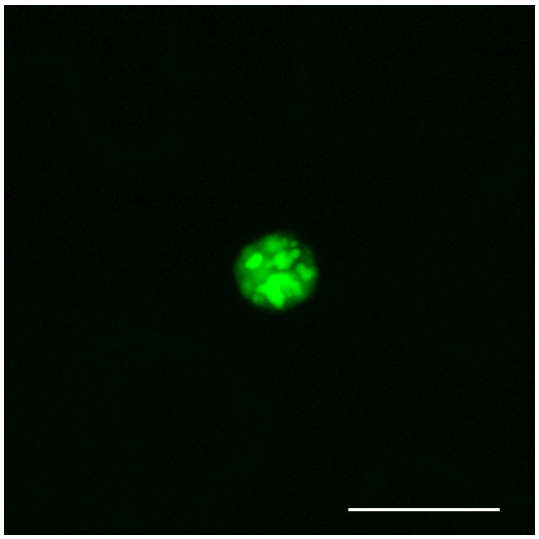

At1g60650
Zinc Finger-containing Glycine-rich RNA-binding Proteins
Nucleus

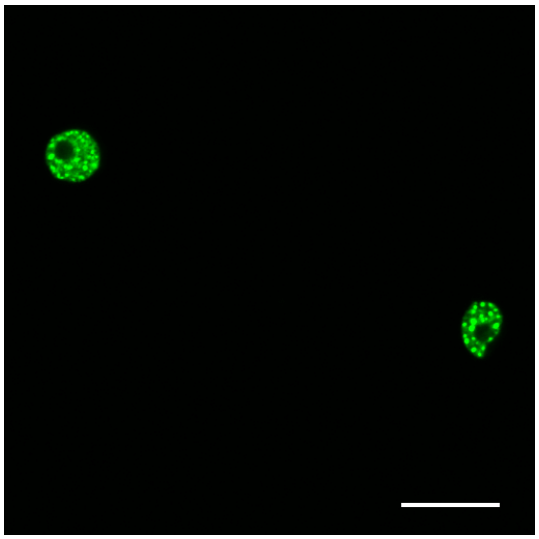

At1g31450
Aspartylprotease
ER

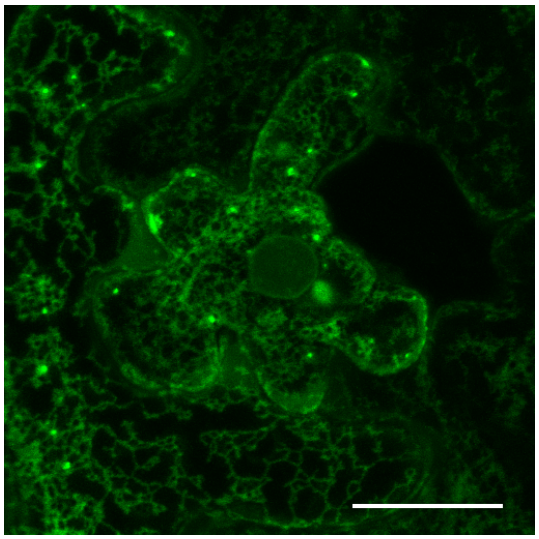

At1g24510
TCP-1/cpn60 Chaperonin Family Protein
Cytosol

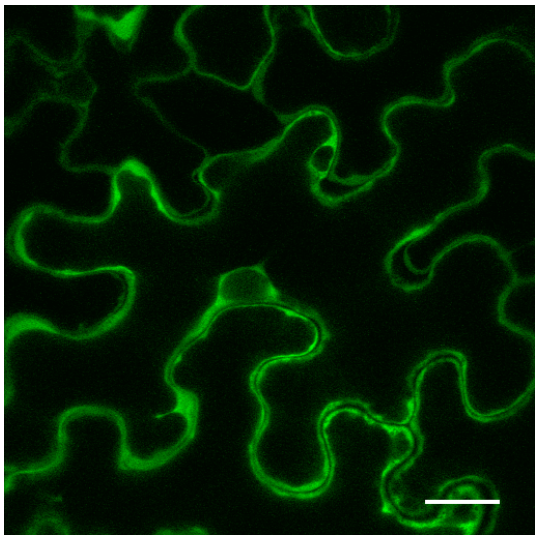

At5g65620
Zincin-like Metalloproteases Family Protein
Chloroplasts and Mitochondria

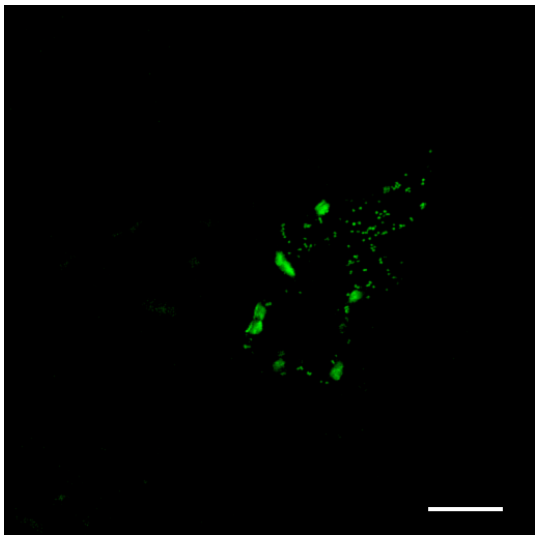

At1g63010
SPX domain-containing protein
Vacuole

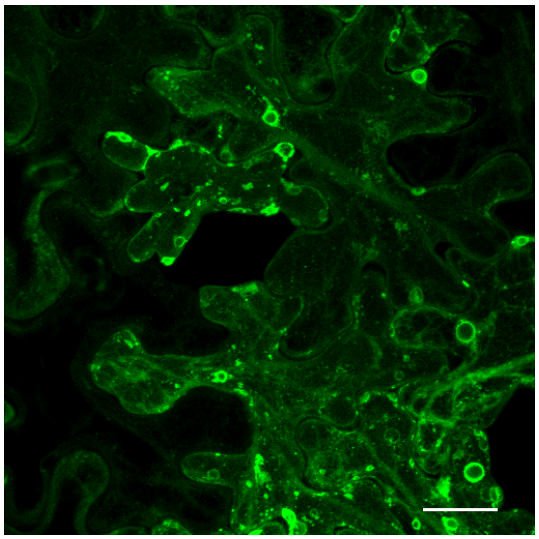

At4g17770
TPS5
ER

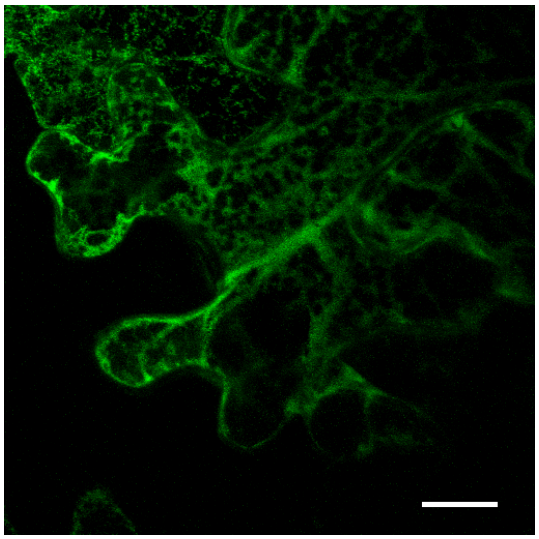

At5g51720
AT-NEET
Chloroplasts

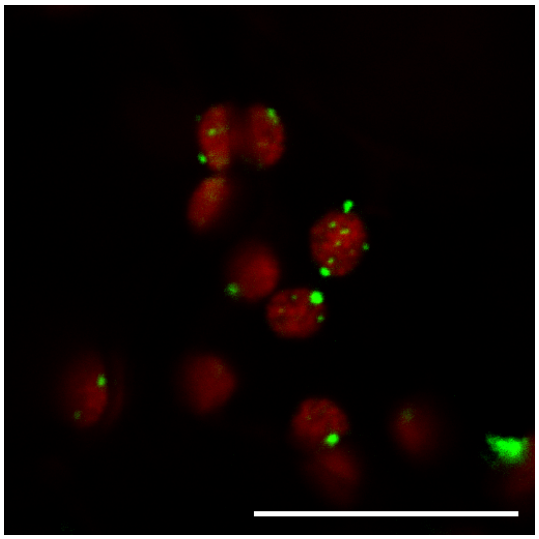

At5g59120
Subtilase 4. 13
ER/Golgi

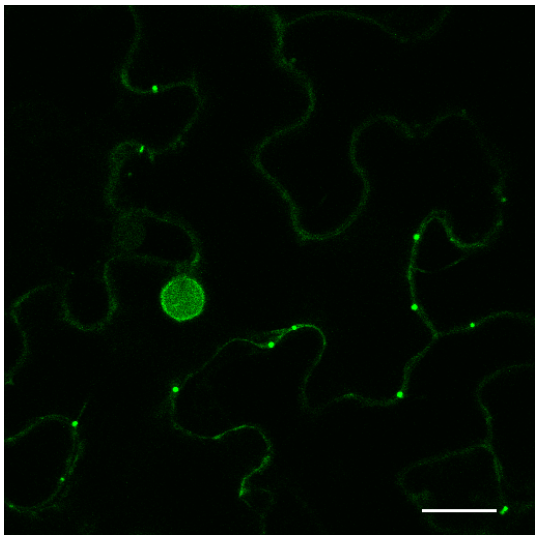

Acknowledgements

I would like to thank Professor Thomas Dresselhaus for giving me the chance to work on this interesting project, for scientific discussion as well as for his open door policy concerning any issue and last but not least for funding me during my work.

Furthermore, I'm very grateful to my supervisor and friend Dr. Ulrich Hammes for his scientific advice and the atmosphere we always had in our working group. It was great to work in such a friendly environment, especially when scientific issues were no reason for happiness. Moreover I appreciate the discussions on my thesis as well as correcting.

I am much obliged to Professor Widmar Tanner for giving me the chance to be part of the amazing experience *Roche Continents 2010* and for all the other support and interest he showed for my work.

Many thanks of course shall go to my long-time lab-buddy Birgit. Our relationship has been quite rollercoaster over the last years. Anywho, I really enjoyed working with you!

I'm very thankful to Dr. Andrea Bleckmann who supported me on my project during the last year with valuable input and for correcting my thesis.

I'm obliged to all the supportive people from our department, namely JD (who turned out to be a good colleague and flat mate), Philipp A. and D., Martin, Andi, Svenja and all the others I might have forgotten for always have an open ear, when suggesting a roof-top beer or a Schafkopf.

I further wanted to thank all the student assistants, we guided through our labs during all those years for their supportive work: Astrid, Tina, Hanna and Nina.

Moreover I wanted to thank Vroni for any administrative help and of course Günther, for his indefatigable dedication for successful plant growth and support in sowing and picking.

Finally I wanted to thank my girlfriend Claudia, who supported me in whatever situation and who finally proof-read the manuscript although it was all Greek to her. Thank you!!!

And last but not least, I wanted to thank my parents for the support, they gave me through all of my life. Thanks for letting me find my own way!

Eidesstattliche Erklärung

Ich erkläre hiermit an Eides statt, dass ich die vorliegende Arbeit ohne unzulässige Hilfe Dritter und ohne Benutzung anderer als der angegebenen Hilfsmittel angefertigt habe;

die aus anderen Quellen direkt oder indirekt übernommenen Daten und Konzepte sind unter Angabe des Literaturzitats gekennzeichnet.

Johannes Schönberger

Regensburg, den 22.10.2012